# CDF STUDY REPORT

# ELRR

## EUROPA LOW RESOURCE RADAR

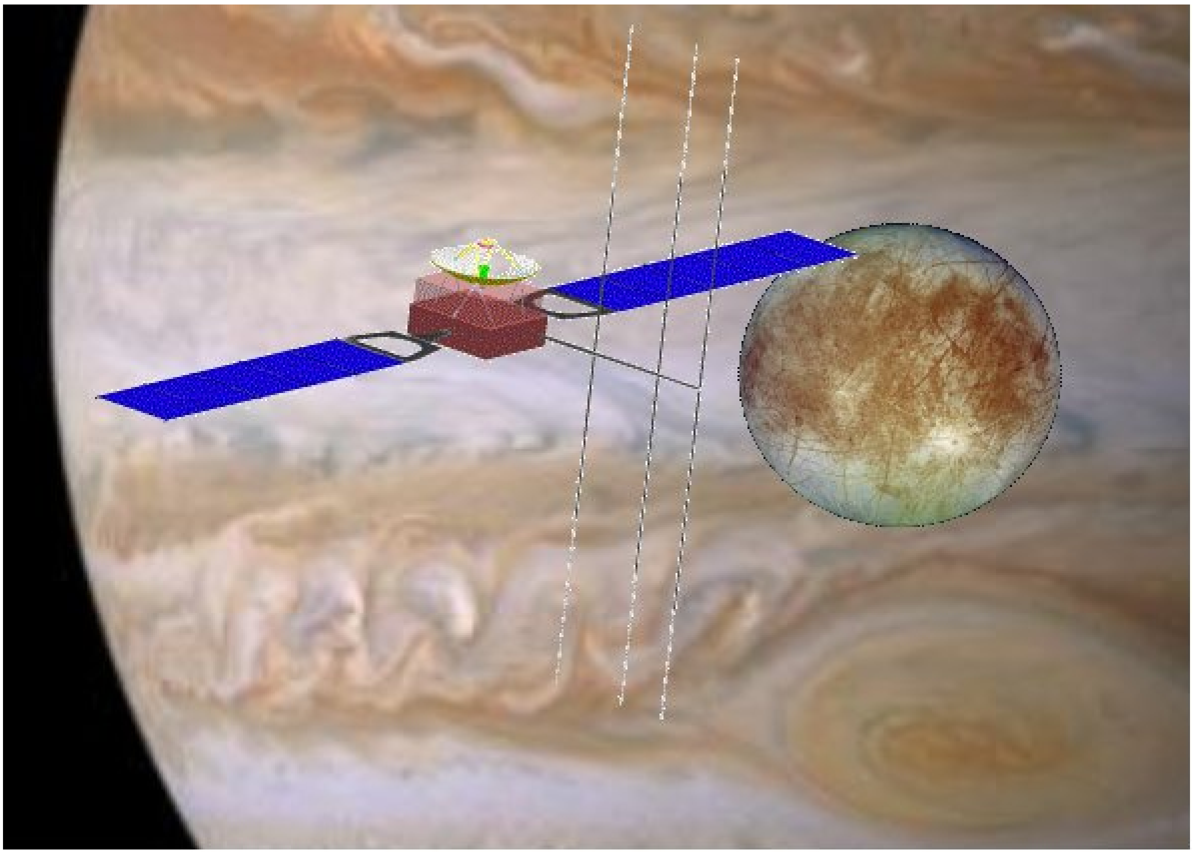

**This is an edited version of the Final Report of the Europa Low Resource Radar study, performed by the Concurrent Design Facility (CDF) at ESA ESTEC for the Science Directorate (SCI-A), in the frame of the Jupiter Minisat Explorer Technology Reference Study.**

**Some sections of the report have been removed from this version of the report and this is indicated where appropriate.**

**The results must be seen in the context of the feasibility study and are not intended as a final design of a low resource radar for Europa, but rather as a starting point.**

**The mentioned spacecraft budgets reflect the status of the studies in 2004 and are therefore not in-line with the later studies performed up to now.**

FRONT COVER

Jupiter Europa Orbiter spacecraft showing the deployed Europa Low Resource Radar with the Jovian moon Europa in the background

(Spacecraft configuration courtesy EADS Astrium)

# TABLE OF CONTENTS

1 INTRODUCTION ........ 7
1.1 Background ........ 7
1.2 Scope ........ 7
2 EXECUTIVE SUMMARY ........ 9
2.1 Study flow ........ 9
2.2 Requirements and design drivers ........ 9
2.3 Design strategy ........ 10
2.4 Instrument design ........ 10
2.5 JEO mission, spacecraft design ........ 11
2.6 Critical issues and conclusions ........ 12
3 SYSTEM REQUIREMENTS AND COMPLIANCE ........ 15
3.1 Science requirements ........ 15
3.2 System requirements ........ 16
*3.2.1 Planetary protection ........ 16*
3.3 Radar sounder requirements/goals ........ 16
3.4 Compliance matrix ........ 17
4 WAVE INTERACTION ANALYSIS ........ 19
4.1 Requirements ........ 19
4.2 Knowledge of the structure of Europa ........ 19
*4.2.1 Outer structure – surface topography and roughness ........ 19*
*4.2.2 Inner structure ........ 20*
4.3 Characterisation of the medium: assumptions and trades ........ 21
*4.3.1 Parameters influencing the propagation within the ice ........ 21*
*4.3.2 Atmosphere-ice interface on surface of Europa ........ 23*
*4.3.3 Basal interface ........ 25*
*4.3.4 Summary ........ 25*
4.4 Interaction model – assumptions and trades ........ 26
*4.4.1 Scattering components ........ 26*
*4.4.2 Attenuation ........ 27*
4.5 Simulation results ........ 28
*4.5.1 Model output – sensitivity to descriptive parameters ........ 29*
*4.5.2 Standard case – Case A ........ 30*
*4.5.3 High concentration of dust – Case E ........ 30*
*4.5.4 Smooth atmosphere-ice interface – Case F ........ 31*
*4.5.5 Other test sites ........ 32*
*4.5.6 Other cases of surface roughness ........ 33*
*4.5.7 Conclusions of the geophysical sensitivity study ........ 34*
*4.5.8 Alternative system configurations ........ 35*
*4.5.9 Other simulations ........ 36*
4.6 Radio noise ........ 36
4.7 Critical issues and conclusion ........ 38
5 INSTRUMENT SYSTEM DESIGN ........ 39
5.1 Purpose and objectives ........ 39
5.2 Scientific requirements and design drivers ........ 39
5.3 System analysis ........ 39
*5.3.1 Assumptions and trade-offs ........ 39*
*5.3.2 System trade-off and performance ........ 43*
*5.3.3 Baseline design ........ 50*
5.4 Conclusions ........ 51
6 INSTRUMENT ELECTRONICS ........ 53
6.1 Requirements and design drivers ........ 53
6.2 Assumptions, design calculations and trades ........ 54

*6.2.1 Stepped Frequency Radar* ........ *54*
*6.2.2 Chirped Doppler Radar* ........ *56*
*6.2.3 HPA Assembly sizing, power consumption and dissipation* ........ *57*
*6.2.4 Number of bits required for analogue-to-digital conversion* ........ *59*
*6.2.5 On-board data compression* ........ *59*
6.3 Baseline design ........ 61
*6.3.1 Radar electronics* ........ *62*
*6.3.2 High-Power Amplifier Assembly* ........ *63*
6.4 Budgets ........ 64
*6.4.1 Power* ........ *64*
*6.4.2 Data rates* ........ *64*
6.5 Critical issues and conclusions ........ 64
**7 ANTENNAS ........ 65**
7.1 Requirements and design drivers ........ 65
7.2 Assumptions, design calculations and trades ........ 65
*7.2.1 Basic antenna trade-off* ........ *65*
*7.2.2 Optimisation of selected antenna* ........ *66*
*7.2.3 Frequency bandwidth* ........ *68*
*7.2.4 Influence of satellite body and solar panels* ........ *68*
*7.2.5 Mechanical stability requirement* ........ *69*
*7.2.6 Tapering of the dipole elements* ........ *70*
*7.2.7 Conductivity of interconnecting tubes* ........ *70*
7.3 Baseline design ........ 72
*7.3.1 Geometry* ........ *72*
*7.3.2 Antenna performance* ........ *73*
7.4 Critical issues and conclusions ........ 73
*7.4.1 Critical issues* ........ *73*
*7.4.2 Conclusions* ........ *73*
*7.4.3 Future activities* ........ *74*
**8 CONFIGURATION ........ 75**
8.1 Requirements and design drivers ........ 75
8.2 Assumptions and trades ........ 75
8.3 Baseline design ........ 75
8.4 Overall dimensions ........ 76
**9 MECHANISMS ........ 79**
9.1 Requirements specification ........ 79
9.2 Design drivers / objectives ........ 79
9.3 Trade-offs ........ 80
*9.3.1 Structural frame architecture* ........ *80*
*9.3.2 Materials* ........ *82*
9.4 Mechanical and structural design baseline description ........ 83
*9.4.1 Parts list and materials* ........ *83*
*9.4.2 Hinges* ........ *84*
*9.4.3 Synchronisation and stiffening mechanisms* ........ *85*
*9.4.4 Hold-Down and Release Mechanisms* ........ *86*
9.5 Stiffness, strength and stability analyses ........ 88
*9.5.1 Stiffness* ........ *88*
*9.5.2 Strength* ........ *89*
*9.5.3 Structural stability* ........ *89*
*9.5.4 Deployed shape stability* ........ *90*
9.6 Deployment configuration/sequence ........ 90
9.7 Options ........ 93
9.8 Critical issues and development needs ........ 93
*9.8.1 Mass drivers* ........ *93*
*9.8.2 Development critical issues* ........ *93*

*9.8.3 Specific development needs / investigations ........ 94*
*9.8.4 ELRR design requirements ........ 94*
9.9 Conclusions ........ 95
**10 THERMAL ........ 97**
10.1 Requirements and design drivers ........ 97
10.2 Assumptions and baseline ........ 98
10.3 Thermal predictions ........ 98
*10.3.1 Europa orbit ........ 98*
*10.3.2 Venus fly-by ........ 105*
10.4 Budget ........ 106
10.5 Critical issues and conclusions ........ 106
**11 SIMULATION AND VISUALISATION ........ 109**
11.1 Introduction ........ 109
11.2 Simulation requirements ........ 109
11.3 Assumptions ........ 109
11.4 Simulation results ........ 109
**12 PLATFORM DESIGN REVIEW ........ 113**
12.1 Platform systems ........ 113
*12.1.1 Design review ........ 113*
*12.1.2 Requirements and design drivers ........ 113*
*12.1.3 JEO design baseline ........ 113*
*12.1.4 Baseline design summary ........ 115*
*12.1.5 Budgets ........ 117*
*12.1.6 Critical issues and conclusions ........ 118*
12.2 AOCS ........ 118
*12.2.1 Introduction ........ 118*
*12.2.2 JEO – radar antenna design impact on the AOCS ........ 119*
*12.2.3 RCS-based control modes ........ 121*
*12.2.4 Antenna deployment ........ 122*
*12.2.5 Antenna nadir-pointing requirement ........ 123*
*12.2.6 Effect of Europa radiation environment on AOCS ........ 123*
*12.2.7 JEO – Europa orbit characteristics ........ 124*
12.3 Power constraints: orbital altitude selection trade ........ 128
*12.3.1 Introduction ........ 128*
*12.3.2 Inputs and assumptions ........ 128*
*12.3.3 Mission inputs ........ 128*
*12.3.4 Power inputs ........ 130*
*12.3.5 Power architecture inputs ........ 130*
*12.3.6 Results ........ 131*
12.4 Telecommunications ........ 132
*12.4.1 Assumptions and trades ........ 132*
*12.4.2 Conclusions ........ 134*
**13 PROGRAMMATICS ........ 135**
**14 TECHNICAL RISK ASSESSMENT ........ 137**
**15 COST ........ 139**
**16 CONCLUSIONS ........ 141**
16.1 Key conclusions ........ 141
16.2 Critical areas ........ 142
**17 REFERENCES ........ 145**
**18 ACRONYMS ........ 147**

# 1 INTRODUCTION

## 1.1 Background

This is an edited version of the Final Report of the Europa Low Resource Radar study, performed by the Concurrent Design Facility (CDF) at ESA ESTEC for the Science Directorate (SCI-A), in the frame of the Jupiter Minisat Explorer Technology Reference Study.

Some sections of the report have been removed from this version of the report and this is indicated where appropriate.

The results must be seen in the context of the feasibility study and are not intended as a final design of a low resource radar for Europa, but rather as a starting point.

The mentioned spacecraft budgets reflect the status of the studies in 2004 and are therefore not in-line with the later studies performed up to now.

## 1.2 Scope

The objectives of the study were to perform instrument conceptual design and trades, prepare a preliminary instrument design including budgets and subsystem designs with required performance, show science requirements compliance, define critical design issues requiring further analysis and assess and analyse programme, risk and costs. Further the constraints imposed by the chosen spacecraft platform and orbit were analysed and described where appropriate. This document reports on the analysis performed and conclusions for a Europa Low Resource Radar (ELRR) conceptual design.

# 2 EXECUTIVE SUMMARY

## 2.1 Study flow

The ESTEC Concurrent Design Facility (CDF) was requested by SCI-A to perform the design of innovative ice penetrating radar to be used for remote sensing of Europa. The instrument was designated as the Europa Low Resource Radar (ELRR) and the key task was to critically review and thereafter, provide a design for the radar instrument noting the limited system resources and system constraints. Therefore, the study was tasked to identify critical analysis, design and technology developments that would enable novel radar approaches that also can be applied in future science projects. The radar instrument is proposed as part of a scientific payload of the Jovian Minisat Explorer (JME) Technology Reference Study (TRS), RD[1], RD[2]. The JME comprises two spacecraft: a Jupiter Europa orbiter (JEO) and Jovian Relay Satellite (JRS). The mission and spacecraft are under assessment by industry and details were obtained from reference documents, RD[3], RD[4] .

The objectives of the CDF Instrument Design Activity (IDA) were to:

- Perform an instrument assessment study
- Demonstrate technical feasibility including:
  - o Science requirements compliance
  - o System and subsystem conceptual design
  - o Programme (testing), risk and cost assessment
  - o Orbit and platform design assessment where influencing the instrument design

The main emphasis of the activity was to show the accommodation of the radar instrument within the severe resource constraints imposed by such a mission and spacecraft system operating in the Jovian system and within Soyuz-Fregat launch vehicle constraints.

## 2.2 Requirements and design drivers

The JEO platform design RD[2] drives the system requirements for the antenna:

- Launch in the 2010-2020 timeframe with Soyuz-Fregat 2-1b (Soyuz-S fairing)
- A transfer duration of six years and a Jovian system tour of about 1.5 years
- An operational Europa circular polar orbit at 200 km altitude with a Sun angle tangential to orbit plane of 60°
- A lifetime of 66 days (science phase around Europa limited by orbit perturbation and radiation dose)
- 3-axis stabilised spacecraft
- A mass allocation for the payload of 30 kg of which 10 kg for the radar
- A power allocation of 25W
- A data rate of 40 kbps

The design drivers for the system are:

- The high radiation environment
- The platform constraints (low resources, configuration)
- The deployment mechanisms design
- Nadir-pointing payload

- AOCS pointing requirements and the distribution of the payload on two opposite sides of the JEO satellite

## 2.3 Design strategy

The design flow comprised:

- Establishment and analysis of an ice model for the Jovian moon Europa based on current knowledge.
- Assessment of different radar systems options to perform the key science requirement of sounding to, at least, 5 – 10 km depth with a goal of 20 km with a resolution of 100 m at the surface reducing by 10% as a function of depth.
- Selection of the appropriate radar frequency noting the high radio noise and radiation environment in the Europa orbit.
- Review of different antenna mechanical and radar electrical designs and deployment trades noting the low mass, power and data rate constraints and the configuration limits.
- Assessment of key mission and platform systems designs where their constraints impose difficulties for the radar design. Such cases comprised the AOCS, power and telecommunications bus systems and the relationship between the antenna stowed envelope and the deployed dimensions.

## 2.4 Instrument design

| | | | **Requirement** |
|---|---|---|---|
| **Centre Frequency** | 50 MHz | 20 – 80 MHz analysed, clutter too high at 80 MHz, noise limited at low frequency | - |
| **Altitude** | 200 km | 125 km reserved as option – better penetration and roll error tolerance | |
| **Bandwidth** | 850 kHz | 2.55 MHz reserved as option – increased penetration but also data rate | |
| **PRF** | 3300 Hz | | |
| **Duty cycle ratio** | 10% | | |
| **Pulse length** | 30 µs | At 10% duty cycle | |
| **Peak radiated output power** | 375W | | |
| **Antenna directivity** | 12 dBi | | |
| **Ice depth** | 14.5 km | 11 km at 100 m resolution, 150 m/dB with gain improvement | 5 – 10 km<br>20 km (goal) |
| **Mass** | 11.45 kg | Total with additional 20% margin | 10 kg |
| | 3.00 kg | Structure (including thermal coating) | |
| | 3.72 kg | Mechanisms (high number due to limited stowed volume) | |
| | 2.82 kg | RF electronics (HIPS approach adopted) | |
| | 9.54 kg | Total with subsystem design margins | |
| | 1.91 kg | 20% margin | |
| **Power consumption** | 33.6W | Average power with 20% margin (26.5W average without margin) | 25W |
| | 67.1W | Power required 50% of time. With 20% margin. | |
| | 63.5W | HPA average power with 20% margin | |
| | 3.6W | Electronics with 20% margin | |

| | | | Requirement |
|---|---|---|---|
| **Data rate** | 28 kbps | Full Resolution Mode (Depth resolution: 100 m, Along Track resolution: 1550 m) | 40 kbps |
| | 226 Mb | Storage per orbit at 50% duty cycle | |
| | 1.1 kbps | Reduced Resolution Mode (Depth resolution: 100 m, Along Track resolution: 10 km) | |
| | 8.9 Mb | Storage per orbit at 50% duty cycle | |
| **Antenna** | Yagi | Triple 3-element Yagi | - |
| **Gain** | 11.5 dBi | Frequency bandwidth feasible | 12 dBi |
| **Dimensions** | Deployed | 10 x 2 m (1.25 m from spacecraft) | - |
| | Stowed | 1340 x 470 x 300 mm | |
| **Stiffness** | >0.5 Hz | 1st eigenfrequency | |
| **Materials** | TBD | Dipoles: CFRP with Al coatings with GFRP isolating connections. Main frame: CFRP. Thermal coating: White plasmocer. | |
| **Options** | 1 | Baseline: joined elements: non-conductive connection material TBD, difficult electrical design safe and simple deployment | |
| | 2 | Separate elements: spacecraft collision possibility, simpler electrical design | |
| **Electronics** | HIPS | Highly Integrated Payload Suite approach | |

## 2.5 JEO mission, spacecraft design

The following data are obtained from input reference documents, RD[2], RD[3], and RD[4].

| | | |
|---|---|---|
| **Mission Objective** | • To perform Europa science measurements using low resource spacecraft<br>• To investigate the structure of the Europan ice, detect the presence of an ocean below the ice and the depth of the water-ice interface. | |
| **Payload** | The JEO payload instruments comprise:<br>• Radar Sounder (prime payload)<br>• Other payload<br>• Laser Altimeter (EuLat)<br>• Stereo Camera (EuS-Cam)<br>• Near Infra-red Mapping Spectrometer (EuVN-IMS)<br>• Radiometer (EuRad)<br>• Gamma ray Spectrometer (EuGS)<br>• Magnetometer (EuMAG)<br>• Radiation Environment Monitor (EuREM) | |
| **Launcher** | • Soyuz-Fregat | |
| **JEO Spacecraft** | **Design lifetime** | 7 years + |
| | **Attitude control** | 3-axis stabilised |
| | **Total mass** | 635.6 |
| | **Spacecraft main body dimensions** | 1340 mm x 470 mm x 300 mm |

| | | |
|---|---|---|
| | **Pointing accuracy** | 5° |
| | **Solar array** | Two wings GaAs cells with concentrators, 1.5 $m^2$ per wing |
| **Mission** | **Europa Orbit** | 200 km altitude, 90° inclination, 60° SAA |
| | **Nominal mission period** | 66 days |
| **Programmatics** | **Launch date** | 2016 |
| | **Model philosophy** | STM, EEM, PFM |
| **Risk** | **Mission success** | 65% |

## 2.6 Critical issues and conclusions

- A preliminary instrument design has been performed using the Astrium JEO design as the platform for the radar.
- A baseline ELRR design was derived considering the low resources requirements and the JEO configuration constraints in terms of location.
- The radar is feasible and once in low orbit around Europa it will be able to penetrate the ice to a depth of around 14 km assuming a dusty ice model. Other ice properties will have significant effects on radar performance. Penetration could be higher if some shielding from the background noise emanating from Jupiter is afforded when flying behind Europa. Sensitivity could be improved by flying lower with an added insensitivity to roll error.
- Depth penetration can be extended only by increasing bandwidth but at the expense of increased data rate and instrument complexity. Further improvement in gain through higher power, better efficiency or a larger antenna results in penetration depth improvement at a rate of 150 m/dB.
- Although optimisation of structural mass was performed, the final total mass of the antenna reached 11.45 kg, that is, 1.45 kg above the mass target of 10 kg. This was mainly due to the complexity required to deploy an antenna safely that has to be stowed in the surface available on the platform (by increasing the number of elements composing the antenna). The mechanisms became in that case a mass driver (33% of the radar mass). Note that the radar subsystem mass values in the above table include design margins leading to a mass of 9.54 kg. An additional 20% system margin leads to the 11.45 kg total.
- To achieve the above depth penetration an RF transmit power of 375W is required. As the instrument is operated only half the time, twice the power is available during the time of operation, that is, about 50W. The overall average power consumption of the instrument including margin in the Radar Mode is 67.1W including 20% margin (about 56W without margin). The average power consumption is 33.6W with a 20% margin or 26.5W without margin. However, without margin and accounting for the duty cycles the average DC power consumption is close to the 25W system constraint.
- To constrain the instrument power consumption to 25W including all margins for continuous operations, the peak RF transmit power requirement must be reduced by 4.5 dB to 133.75W; this will reduce the performance.
- The Highly Integrated Payload Suites (HIPS) approach requires the highest standard for Assembly, Integration and Verification (AIV) activities. Late payload availability and the

TBD method of deployment testing for the complex antenna require an emphasis on the early development of the AIV programme.

The critical issues associated to this baseline design are:

- The deployment of the antenna and the associated risk of collision.
- To define reliable materials for the antenna (stiffness, high-radiation resistive) and the part separating the dipoles (non-conductive, high-radiation resistive) and the radiation tolerance of the electronics.
- The AOCS technological issue to provide accurate and reliable Nadir and attitude pointing control in a high-radiation environment.
- Planetary protection guidelines and the requirement to crash-land the spacecraft on Europa at the end of mission is a critical issue and extensive activity for the AIV process.

# 3 SYSTEM REQUIREMENTS AND COMPLIANCE

This chapter summarises and reviews the study requirements and places them in the context of the analyses conducted and the critical areas identified for future assessment during Phase A. The system and radar sounder requirements are not, at this stage, enumerated, therefore, a provisional numbering sequence is allocated similar to that applied for the science requirements RD[1]. Note that the number of specific requirements were limited in that the task was to show what could be achieved for Europa ice radar sounding within the defined JME mission and system constraints.

## 3.1 Science requirements

The science requirements for the JMO science mission, that is those pertaining to the JEO ground penetrating radar, are reproduced from RD[1]. The overall requirements for the complete JME science payload are defined as level 0 (science objectives), level 1 (primary) and level 2 (secondary). The possibility of using the radar sounder as an altimeter was not investigated in this study, that is, requirement PR-1.

**Level 0 (Primary Objectives)**

0-1 Determine the presence or absence of a subsurface ocean (includes mapping of the ice thickness)

0-2 Measure the global topography and the tidal effects at Europa

**Level 0 (Secondary Objectives)**

None relevant to radar sounder instrument.

**Level 1 (Primary)**

PR-1 Obtaining measurements of the time variations of Europa's global topography and gravity field over a period of 30 to 60 Earth days (several tens of orbits of Europa around Jupiter), with a height accuracy of 2 metres to uniquely distinguish between tidal distortions of several metres (expected for a completely solid ice cover) and several tens of metres (expected if a global layer of liquid is present). The results of these efforts will allow a unique conclusion regarding the present-day existence of a global liquid-water layer. For the JME study the target accuracy shall be 1 m. (JEO)

PR-3 Performing radar sounding of Europa's subsurface structure to at least a depth of 5 to 10 km, to identify possible regions where liquid water might exist close to the surface. If the ice is less than 5 to 10 km thick, use of ice-penetrating radar may allow determination of the vertical extent of the surface ice layer (and possibly a direct detection of any underlying liquid water), as well as the local structure of the ice. For the JME, the actual penetration depth will be subject to trade-off with respect to the required resources. As mentioned, the penetration depth should at least be 5-10 km, but the goal for JEO is 20 km.

Taken from RD[6]: "Globally distributed radar sounding is recommended with a "depth resolution" of 100 m at the surface decreasing with depth, spatial resolution at, or better than the scale of major surface features, and designed to maximize the likelihood of detection of an ice/liquid interface. The thickness of ice that can be sounded on Europa is determined by the absorption of electromagnetic waves in the ice (which is dictated by its temperature and impurity content) and scattering characteristics of the ice body (including the surface and basal interfaces as well as any volume scatterers). Because of the variety of surface terrain types observed on Europa and geologic processes inferred to be at work, we expect Europa's absorption and scattering properties to be spatially inhomogeneous and its crystal ice thickness to be locally variable. The scattering properties of any assumed sounding model for Europa, as well as the Jovian radio noise environment, are frequency-dependent. Earth-based radar sounding of Europa at 3.5- and 13-cm wavelengths suggests that Europa's ice crust contains many high-order multiple scattering in-homogeneities in its uppermost few metres at decimetre scales, which prohibits probing of the ice to any great depth at these wavelengths. However, sounding at 70-cm indicates that scattering in-homogeneities at that wavelength are far fewer. Therefore, radar sounding appears viable at wavelengths of a few metres. (JEO).

**Level 2 (Secondary)**

None relevant to radar sounder instrument.

## 3.2 System requirements

- S-1 Europa orbit altitude shall be 200 km, 90° inclination, 60° Sun angle tangential to orbit plane. Lifetime maximum 66 Earth days. Launch 2010 – 2020.
- S-2 JME, JRS and JEO baseline, RD[3] and RD[4]
- S-3 Crash-landing on surface at end of mission baseline, planetary protection rules apply.
- S-4 Maximum mass: 10 kg (radar allocation).
- S-5 Maximum power: 25W (radar allocation).
- S-6 Maximum data rate: 40 kbps (radar allocation).

### 3.2.1 Planetary protection

S-3 above indicates that the subsequent planetary protection rules must be applied. The COSPAR planetary protection requirements for a mission to Europa are for the time being not very precise and lean mostly on a Space Studies Board study of the US National Academy of Sciences. The main requirement is to limit the biological contamination of a potential sub-surface ocean on Europa to less than 1E-4 per mission. The problem with this number is that in the case of a Europa mission, they recommend to include the bio-burden reduction due to the (radiation) environment in the Jovian system in the final estimate for contaminating Europa. For Mars missions it is different because the bio-burden estimate is based on the situation of the spacecraft at launch without considering any in-flight reduction due to environmental effects.

For the practical implementation – a Mission to Europa is classified as Planetary Protection Category IV. A Europa Orbiter is therefore Planetary Protection Category III. This means that the probability for the orbiter to crash onto Europa has to be lower than 1E-2 for the first 20 years after launch, and lower than 5E-2 for the subsequent 30 years. The probability for impact on Europa for any part of the launch vehicle and/or carrier/cruise stage has to be lower than 1E-4. The probability for impact on Europa for any fly-by has to be lower than 1E-2. Final disposal of a spacecraft or parts of a mission in general on Ganymede and Callisto shall be avoided.

If this lifetime requirement cannot be met (as S-3), the orbiter has to be cleaned to a total bio-burden (surface, mated, and encapsulated) of less than 5E5 bacterial spores over the entire spacecraft (which will most likely mean integration of pre-cleaned and sterilised subsystems).

## 3.3 Radar sounder requirements/goals

- RS-1 Frequency: 20 – 80 MHz, nominal: 50 MHz.
- RS-2 Antenna gain: 12 dB.
- RS-3 Pointing accuracy: ±5°.

## 3.4 Compliance matrix

The following table comprises a summary compliance matrix for the key requirements analysed during the CDF study. The results are applied to the Science Requirements Document for the Jupiter Minisat Explorer RD[1] and those defined in the System workbook of the CDF Model.

| Number | Requirement Comments | Compliance |
|---|---|---|
| 0-1 | Baseline radar instrument will penetrate down to 11 km and hence if subsurface liquid water. Not possible if ocean below 15 km. | Yes |
| 0-2 | Limited topography and tidal effects feasible within resolution limits. | Part |
| PR-1 | Direct altimetric measurement, for example time measurement, will not be accurate enough to satisfy the requirement. Higher accuracy to fit the measured echo shape with modelled echoes can identify precisely the peak of the return. However, this requires a good knowledge of the surface structure and orbital parameters. Radar altimetry performs poorly with rough terrain, a problem for Europa. Further analysis recommended (modelling reflected pulse shapes). | TBD |
| PR-3 | 5 – 10 km achieved (11 km at 100 m resolution). | Yes |
| | 14.5 km possible with 10% reduced resolution with depth (100 m resolution at surface). 20 km goal. 150 m/dB improvement possible | Part |
| S-1 | 200 km altitude gives ground coverage of 49% in 20 days (28.5% in 10 days). 60° orbit tangential Sun angle decreases coverage. | Part |
| | 125 km altitude improves penetration but reduces available power with increased eclipse time. | Part |
| | Need 0.1° pointing accuracy in roll axis. | Yes |
| S-2 | Communication operations feasible with system (4 – 6% science operations lost with fixed HGA) | Yes |
| | Antenna mechanical design feasible within JEO envelope constraints. | Yes |
| S-3 | Consequences for integration and test evaluated and included in risk assessment. | Yes |
| S-4 | 11.45 kg (with 20% system margin) achieved (high number of mechanisms required). (9.45 kg with subsystem design margins) | No |
| S-5 | Design feasible within power constraints | Yes |
| S-6 | 28 kbps data rate verified | Yes |
| RS-1 | 50 MHz selected | Yes |
| RS-2 | 11.5 dBi achieved, some further improvement TBC | Yes |
| RS-3 | Need 0.1° in roll at 200 km altitude. Need 0.5° in all axes at 125 km altitude. | Revise |

**Table 3-1: Compliance matrix summary**

# 4 WAVE INTERACTION ANALYSIS

The objective of this chapter is to propose and to implement an interaction model that can simulate the microwave signal observed by a VHF altimeter / sounder (ELRR instrument) over Europa's ice-crust. In the absence of any measurements, this model should help in assessing the requirements and the performance of such an instrument. Its main goal is to provide realistic signals to the instrument designers to support them in assessing the impact of various designs on the performance of the instrument. Here, performance is quantified by the ability of ELRR to detect various geophysical signals; and is quantified in terms of signal to noise and signal to clutter ratios. Because of the limited time available, other criteria for performance, for example pulse shape, will not be considered here.
This chapter comprises five parts: after setting the requirements, the medium interacting with the electromagnetic wave is described and the parameters that characterise it are expressed; in the third section, the microwave interaction model selected for these investigations is described; finally, the fourth section presents some of the simulation results and finally a fifth section proposes a preliminary investigation of the issue of Jovian radio noise.

## 4.1 Requirements

The objective of the instrument is to detect a potential interface between the ice crust and the subsurface ocean of Europa. Practically, the aim of the wave interaction task is to provide to the instrument design team, for an agreed test case:

- Radar cross sections of the ocean interface at nadir for various possible depths of this interface
- Radar cross-sections and off-nadir angles of the surface off-nadir echoes characterised by the same delay as the nadir returns RD[7]

The geophysical test chosen for this performance evaluation should be fairly realistic, considering current knowledge of Europa's outer and inner structure. The system parameters are provided by the instrument systems assessment (see Chapter 5, Instrument System Design).

## 4.2 Knowledge of the structure of Europa

### 4.2.1 Outer structure – surface topography and roughness

Voyager and Galileo imagery has provided images of the Europan surface (Figure 4-1). Looking at these images, planetary geologists have used surface shapes, textures, forms, layers, colour, and relative brightness to define geologic units. The five primary terrain types now recognised in Galileo images of Europa are plains, chaos, band, ridge, and crater materials, each of them characterised by different surface roughness. The best available data for extracting quantitative large-scale surface characteristics is obtained by using stereo-derived DEM (digital elevation models) obtained by using Galileo imagery RD[7]. As the best horizontal resolution obtained with Galileo is around 60 m, there are no quantitative measurements of roughness that exhibit a smaller scale.

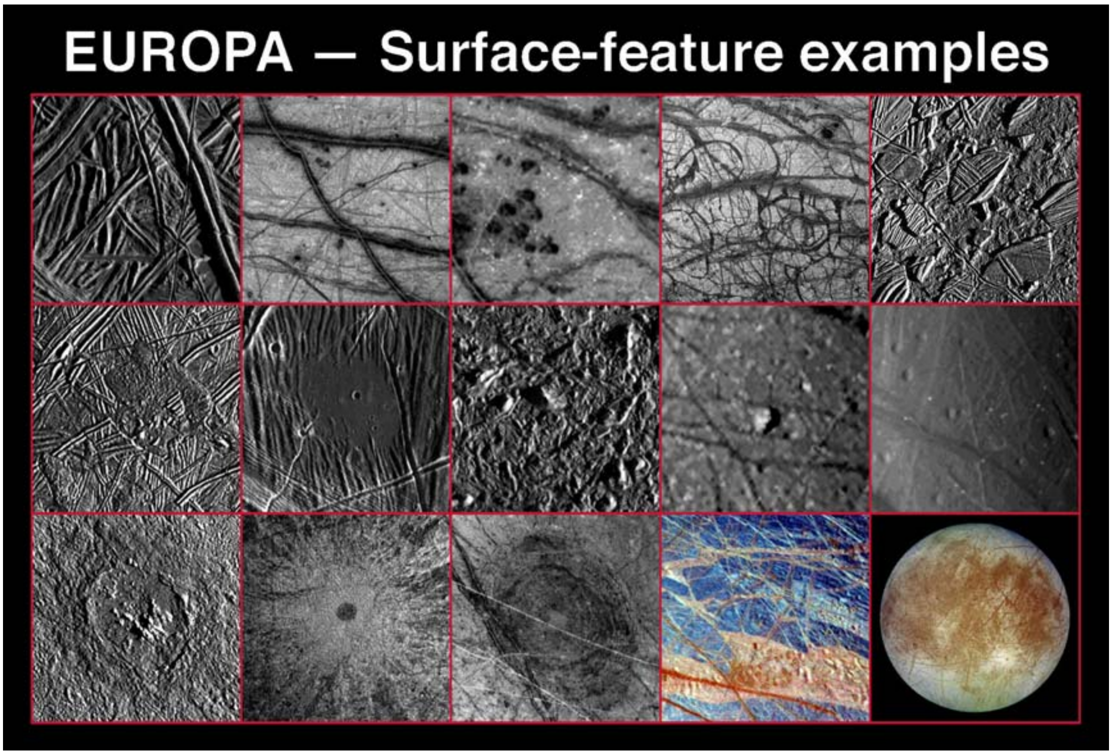


**Figure 4-1: Examples of images acquired by Galileo over Europa**

(http://photojournal.jpl.nasa.gov/newarchive/PIA00746.tiff)

### 4.2.2 Inner structure

Ice growth mechanisms present on Europa are subject to scientific debate. Three models are commonly considered (Figure 4-2) RD[8]: marine ice, “dusty” ice and convective ice. Each of these models results in different vertical profiles of temperature as well as in different dielectric properties of the ice; the propagation of microwaves will be diversely affected.

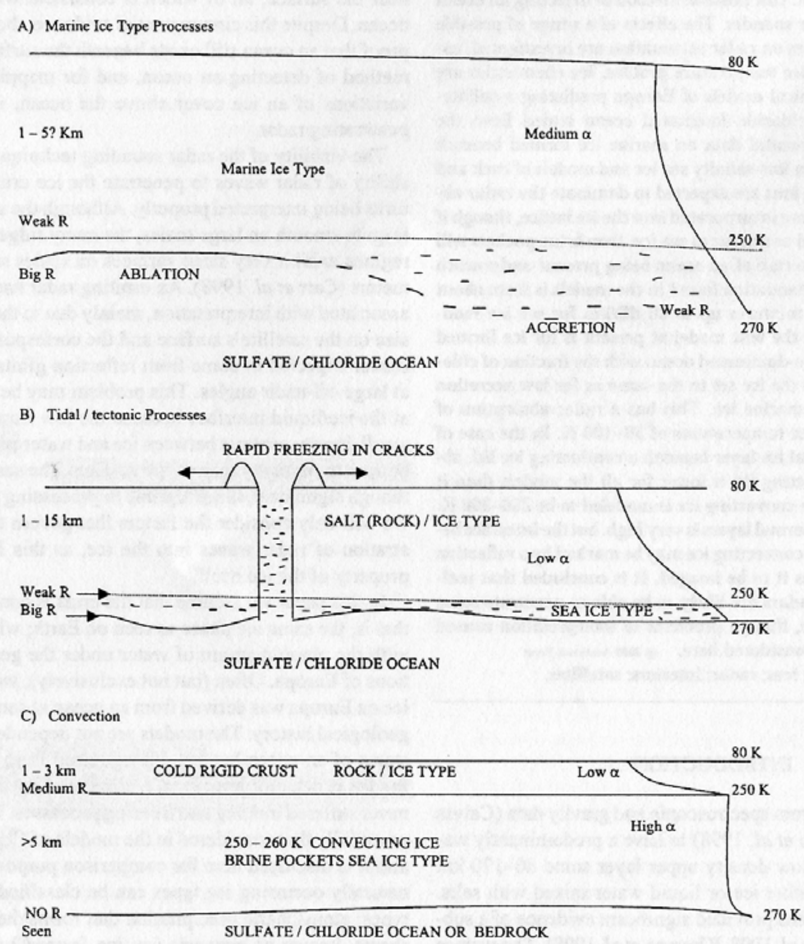


FIG. 2. Qualitative representations of ice types that may occur on Europa with radar absorption $\alpha$ and magnitude of radar reflection $R$ at interfaces in the ice, illustrative temperature profiles (each assuming a "mid-latitude" surface temperature of 80 K), and ice thicknesses. (A) Processes that could occur if the ice is similar to Earth marine ice (e.g., Europa's chaotic terrains) with parts of the base subject to melting and others to accretion from frazil ice crystals. (B) Ice formation via extrusion into cracks or fissures (e.g., Europa's ridged plains), where rapid freeze-boiling occurs if an ocean is exposed to the surface conditions. (C) One possible convection scenario with a cold rigid lid underlain by thicker isothermal convecting ice.

**Figure 4-2: Models for ice crust structure**

Note that some authors RD[9] mention the possible existence of a porous regolith layer at the interface with the atmosphere. As large gaps in the ice could scatter the microwaves and reduce the penetration potential of a microwave sounder, this hypothesis must also be considered.

## 4.3 Characterisation of the medium: assumptions and trades

Any structural characteristics hereafter are considered to exhibit azimuth symmetry around the main axis of radio propagation (that is nadir).

### 4.3.1 Parameters influencing the propagation within the ice

As an electromagnetic wave propagates through a medium, it may be attenuated and bent. The incident radiation loses energy along its path; this energy being absorbed by the material or scattered by inhomogeneities in the medium, or both. Additionally, when it impinges a dielectric interface that is not normal to its propagation vector, the ray path is bent (Snell's Law).
To investigate these effects, several characteristics of the medium must be known:

- Complex dielectric constant of the background ice (drives the absorption)

- Dielectric constant, shape, size and number density of in-homogeneities in the background medium (drives the scattering loss, if any).

#### 4.3.1.1 Temperature

The physical temperature of the ice has an impact on its loss factor. The temperature of a sub-surface layer is driven by two elements: the external forcing (surface temperature), and the basal forcing (temperature at the interface between the ice crust and the ocean). Authors RD[11] mention a variation of temperature with depth of the form:

$$T(z) = T_S \; e^{\frac{z}{b}\ln\left(\frac{T_b}{T_s}\right)}$$

Where $T_s$ is the surface temperature
$T_b$ is the basal temperature
$b$ is the thickness of the ice crust
$z$ is the depth.

For the simulations, a surface temperature of 100K and a basal temperature of 273K were chosen. Actually, the surface temperature may vary between 50K and 130K (day/night, equator/poles) and the basal temperature may vary by several Ks depending on the pressure level (melting temperature of ice). However, the temperature dependence on depth is exponential and as the absorption increases quickly with temperature (see below), its sensitivity to large fluctuations of surface (low) temperature is limited. At the same time, the temperature extension of the melting point is fairly restricted at these depths (273K to 250K below an ice crust of 0 to 80 km), thus limiting its impact on absorption.

#### 4.3.1.2 Complex dielectric constant

If the real part of the complex relative dielectric constant of ice is relatively constant ($\varepsilon_r = 3.12$), the imaginary part (linked to microwave absorption) depends on the type of ice that is related to the ice formation process (compare the models for ice crust structure in Figure 4-2).

- Type A, marine ice: the ice is assumed to be generated by a very specific process discovered recently on Earth. Input parameters were missing at the time of the study to propose a thorough modelling of the dielectric properties of such a medium. However, values tabulated in RD[8] show a total absorption that is ~3 times larger than for case B, with an ice crust that is 2-3 times thinner. It is considered that a system satisfying the detection requirements expressed for case B will also satisfy the requirements for case A.
- Type B, salty (dusty) ice: here the medium is a mixture of pure ice and of salty dust that increases its conductivity. The conductivities of both elements depend on temperature and on microwave frequency RD[11]. For the purpose of deriving the dielectric constant of the mixture, Maxwell-Garnett equation for mixtures is applied.
- Type C, convecting process: in this type of ice, the solid ice crust is thinner and the temperature increases quickly with depth. Beneath the rigid crust lies a layer of convecting ice that includes brine pockets. In this layer, microwaves are strongly attenuated and there is no way they could reach the ocean or the bedrock beneath it. However, with any system satisfying the requirements for case A and case B ice, the top ice crust could be easily penetrated and the interface between rigid ice and convective ice detected, thus providing information on the type of ice and its generation process. As a result, it was decided to drop this case from the analysis.

The focus of the investigations will be placed on the case B ice crust. Pure ice is contaminated with dust that increases its conductivity. In the literature, there are two suggested fraction volumes of dust in ice: 1% and 10% RD[8]. The dielectric parameters of dust as well as their dependence on temperature and electromagnetic frequency are derived from measurements conducted on moon samples RD[11] that are assumed to present similar characteristics. At these temperatures, the contribution of pure ice to the absorption is negligible when compared to the contribution of impurities.
Note that few dielectric measurements of ice/impurities are available at the frequencies of interest and that there is a noticeable uncertainty on the value of the loss factor. In view of the large distances over which the wave propagates into the medium, these uncertainties can generate large error bars on the attenuation budget.
Additionally, it is assumed that the dielectric constant varies slowly with depth, and that in the background medium there are no strong dielectric discontinuities (no strong layering). The medium can be decomposed into homogeneous horizontal layers, characterised by their physical temperature. Note that subsurface structures are not considered here, and would require a more thorough investigation.

#### 4.3.1.3 Inhomogeneities

Some dielectric inhomogeneities may be present locally and their scattering may limit the performance of the instrument in some areas of Europa, without jeopardizing the global scientific return of the mission.
However, RD[9] mentions the possible existence of a porous (and thus inhomogeneous) regolith layer of several 100s metres thickness at the top of the ice crust. This regolith would result from an accumulation of loose material (from meteoric or tectonic origin). In the absence of melting or weathering, its porosity could only be reduced by slow compaction.
In that regolith, the inhomogeneities are vacuum (thin atmosphere) bubbles embedded in the ice. The above reference mentions that such inhomogeneities could exhibit a radius of the order of tens of centimetres to metres and could constitute as much as 1% of the regolith volume.

#### 4.3.1.4 Speed of light – bending

Here, the real part of the dielectric constant of ice will be assumed constant, thus enabling the computation of the speed of light in the medium. In addition, an electromagnetic ray impinging on a dielectric interface in a non-normal configuration is bent, with a bending expressed by Snell’s Law. In the current implementation of the model, this effect is not taken into account and all the energy is assumed to be propagating perpendicularly to the interfaces.

### 4.3.2 Atmosphere-ice interface on surface of Europa

The atmosphere-ice interface is considered as a rough interface separating two dielectric media:

- Mean terrain slope within the footprint: topographic features that exhibit a horizontal spatial scale larger than the footprint of the instrument will tilt the plane of interaction. At this early stage of the study this effect – as well as the effect of the curvature of Europa – is not taken into account. The assumption of “flat Europa” is made.
- Large-scale roughness: the slow undulations of the surface within the footprint may be represented by a distribution of slopes characterising the orientation of smooth facets. This approach covers topographic fluctuations of the surface whose horizontal dimensions are larger than the electromagnetic wavelength but smaller than the size of the footprint. The average slope over the footprint is zero.

- Small-scale roughness: height fluctuations smaller than the electromagnetic wavelength will generate scattering. Various methods can be applied to compute it. For fluctuations much smaller than the wavelength, a small perturbation model can be applied RD[13].

As mentioned above, the existence of a non-null mean slope over the footprint is not considered. Some of the effects of a non-zero slope would be equivalent to a slight tilt of the instrument, which will be discussed in Chapter 5, Instrument System Design. Note that altimetric processing techniques can retrieve the average slope of the surface from the measurement itself, through considerations of the trailing edge of the reflected pulse RD[14]. The detailed impact of a non-null average slope on the return shall be considered in future studies. Classical roughness parameters, such as the root mean square height, the correlation length and the root mean square slope will be used as input parameters to the interaction model.

As mentioned in section 4.2.1, the only quantitative data available on the roughness and topographic structure of Europa comes from high-resolution Galileo imagery. Various techniques (for example, stereo imagery, photo-clinometry) have been used to derive DEMs from optical images. However, the quantitative data readily available is scarce. In the literature available at the time of the study, only a few sites are mentioned where the topographic slopes and the roughness spectrum have been derived (Pwyll, Wedges and Connamara Chaos, see RD[6]).However, more Galileo data are available that could help refine the investigation in the frame of a dedicated study.

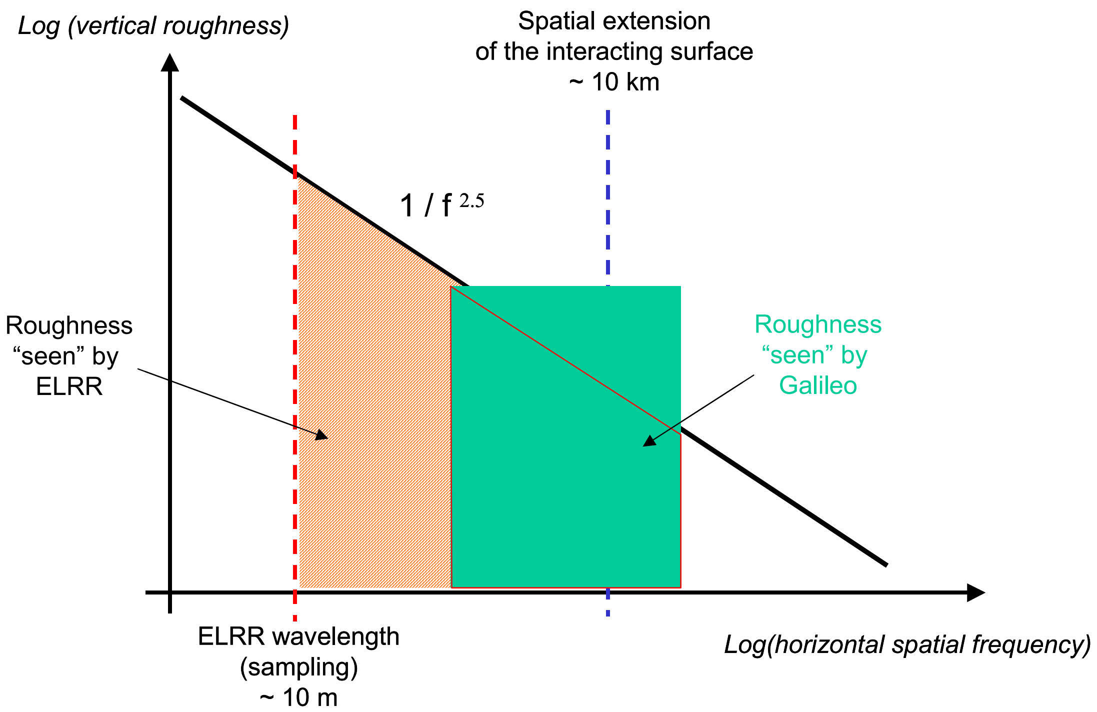


**Figure 4-3: Surface roughness spectrum and measurement windows**

Because the sampling and the spatial extension of the ELRR and Galileo measurements differ, the roughness characteristics derived from Galileo observations must be converted to the ELRR scale, based on the observed roughness spectrum RD[12]. This conversion relies on the strong hypothesis of a constant (scale independent) slope of the roughness spectrum (Figure 4-3). This hypothesis should be re-evaluated in further studies. Galileo images were acquired with various spatial resolutions and various horizontal samplings. The precise terrain scales to be considered for the ELRR depend on the system parameters. Roughly, the ELRR sensor can be considered "to see" a terrain with a spatial extent of tens of kilometres (pulse-limited footprint) and with a few metres sampling interval (electromagnetic wavelength).

### 4.3.3 Basal interface

The structure of the underlying ice/ocean interface depends on the type of ice crust. Here, it is considered as a rough interface between the last layer of ice and water. A more realistic description would include a slow percolation of water into the ice, and its corresponding volume scattering; but time constraints limit the degree of detail in the interface description.
Some authors also mention the possibility of bedrock below the ice crust. This could also be taken into account by replacing the dielectric constant of liquid water by the dielectric constant of rock in the interaction model (thus reducing the echo generated by the interface by ~5 dB) for a similar roughness state.

### 4.3.4 Summary

Table 4-4-1 summarises the descriptive parameters considered for the medium as well as the values used as input for the interaction model:

| **Geophysical parameters** | **A** | **B** | **C** | **D** | **E** | **F** | **G** |
|---|---|---|---|---|---|---|---|
| **"Dusty ice crust" model** | **Pwyll** | Wedges | Connamara | Smooth | Pwyll | Smooth | Interm |
| **Temperature** | | | | | | | |
| **Surface (K)** | **100** | 100 | 100 | 100 | 100 | 100 | 100 |
| **Basal (K)** | **273** | 273 | 273 | 273 | 273 | 273 | 273 |
| **Dust fraction ratio – fv** | **0.01** | 0.01 | 0.01 | 0.01 | **0.1** | 0.01 | 0.01 |
| **Roughness** | | | | | | | |
| **Power law** | **-2.5** | -2.5 | -2.5 | -2.5 | -2.5 | -2.5 | -2.5 |
| **Surface rmsh large scale (m)** | **143** | 143 | 143 | **0.02** | 143 | **0.02** | 143 |
| **Surface lcorr large scale (m)** | **824** | **718** | **390** | **100** | 824 | **100** | **3308** |
| ***Surface rms slopes large s. (°)*** | ***14.06*** | *16.14* | *29.71* | *0.02* | *14.06* | *0.02* | *3.50* |
| **Surface rmsh small scale (m)** | **0.2** | 0.2 | 0.2 | 0.2 | 0.2 | **0.02** | 0.2 |
| **Surface lcorr small scale (m)** | **1** | 1 | 1 | 1 | 1 | 1 | 1 |
| **Basal rmsh large scale (m)** | **1** | 1 | 1 | 1 | 1 | 1 | 1 |
| **Basal lcorr large scale (m)** | **200** | 200 | 200 | 200 | 200 | 200 | 200 |
| **Basal rmsh small scale (m)** | **0.2** | 0.2 | 0.2 | 0.2 | 0.2 | 0.2 | 0.2 |
| **Basal lcorr small scale (m)** | **1** | 1 | 1 | 1 | 1 | 1 | 1 |

**Table 4-1: Descriptive parameters of Europa used in the wave interaction model**

In this table, case A will be the standard case used for the derivation of the baseline of the instrument. The other cases will be presented in a sensitivity study.
Cases B and C correspond to the other sites where data from Galileo about large-scale topography are available. As all these sites present a quite rough terrain, artificial case D (no topography) and case G (intermediate topography, small slopes) are added to illustrate the sensitivity to topographic features.

As no data on small scale roughness was found in the literature, a decimetric roughness texture was applied, with an additional case (case F) where a very smooth surface is considered. Finally, a dust fraction volume of 1% was used. As this value is also mentioned in the literature, simulations were also conducted with a 10% value (case E) RD[8].
The time allocated to the study was too short to propose a full investigation of the data available on Europa and to conduct a full-scale sensitivity study. Note that the model representation of Europa external and internal structure is extremely simplified. More activities shall be undertaken by experts to gather the information that would enable to refine this characterisation.

## 4.4 Interaction model – assumptions and trades

The interaction model that is used here is derived from RD[15], RD[12] and was used to study the performance of the MARSIS radar sounder instrument on board Mars Express.
The assumption is that a nadir-oriented microwave pulse impinges the rough ground surface, propagates through the ice, is reflected by a dielectric interface deep under the surface and comes back to the instrument. For a given delay (range bin), several electromagnetic components add up at the receiver (Figure 4-4):

- The nadir echo coming from the reflection on the dielectric interface I
- The surface echo, resulting from coherent reflection as well as from incoherent interactions with the rough air-ice interface: close to nadir for low depths sounding and off-nadir for deeper layers (*c'*, *a* and *b*)

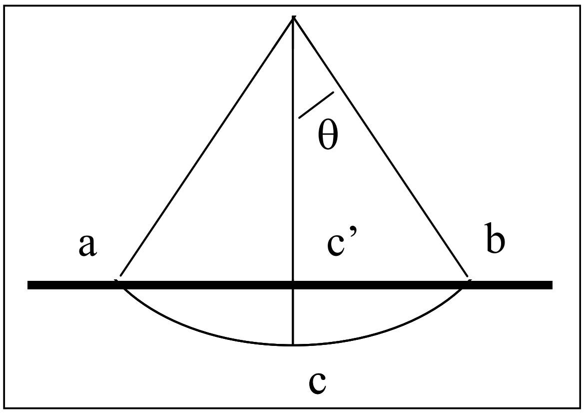


**Figure 4-4: Contributions to the power received by the instrument for a given range bin**

### 4.4.1 Scattering components

The scattering components to the measured echo are modelled as such:
The nadir responses *c*, (from the internal interfaces) and *c'* (from the surface) are modelled taking into account coherent and diffuse components, as done in RD[15]. The Kirchhoff approximation (smooth facets) is used here and the scattering field is given by:

$$E_S = \frac{-j}{2\lambda} \int_S G(P)\, R(P)\, \frac{\hat{n} \bullet 2\hat{R}_1}{R_1^2}\, e^{-jk(2R_1)} dS$$

Where *G* is the propagation/gain function, *R* the Fresnel reflection coefficient of the smooth facet, $R_1$ the distance to the reflecting source and $\lambda$ and $k$ the wavelength and wave number, respectively. This model is able to simulate the power reflected as a function of time, and is consequently capable of producing the shape of the reflected pulse. When a simple dielectric interface is considered (for example air/snow interface), the Fresnel coefficient *R* can be derived from knowledge of the dielectric constants on either side of the interface.

Off-nadir surface scatter (a) and (b) is a sum of coherent and incoherent contributions. The coherent contribution is derived through the previous equation whereas incoherent scattering can be evaluated through any surface backscattering model applicable to steep look angles (the model must be valid for the surface roughness under consideration). Here, the Small Perturbation Model (SPM) is used; it applies perturbation theory and as such is valid for small roughness values (when compared to the electromagnetic wavelength). It is acknowledged that in-depth studies would require the inclusion of a model also valid for other roughness states.

Geometric considerations (resolution, area contributing to off-nadir echoes, and so on) are also applied to derive the return power. The model generates the scattering cross-sections of the various contributions identified above, as a function of the characteristics of the layer of interest (for example type of geophysical discontinuity, depth, roughness), and of the surface clutter.

### 4.4.2 Attenuation

In addition to the scattering contribution, the effects of the two-way propagation have to be included down to the layer of interest. These effects are two-fold: attenuation and delay / bending. As discussed above, bending is not considered, and the delay caused by the propagation in the ice is taken into account through the computation of the corresponding speed of light in the medium. This section will focus on the attenuation. The attenuation of microwaves can have two causes: absorption by the homogeneous medium and scattering losses caused by inhomogeneities.

#### 4.4.2.1 Absorption loss

The rate of absorption of microwaves as they propagate within the slab of ice is mostly driven by the along-path distribution of the loss factor (imaginary part of the complex dielectric constant) of the material.
Hence:

$$\kappa = 2 \cdot 2 \frac{2\pi}{\lambda} \left| \mathrm{Im}\left(\sqrt{\varepsilon}\right) \right|$$

Where $\kappa$ is the power absorption coefficient (2-way), $\lambda$ is the electromagnetic wavelength and $\varepsilon$ is the dielectric constant of the medium (ice).
At the temperatures considered here, most of the absorption comes from the dust impurities embedded in the ice. For a concentration of impurities of 1%, the average absorption of the “dusty ice” crust is around 0.3 dB/100 m (one-way). It varies with temperature.

#### 4.4.2.2 Scattering loss

In the regolith hypothesis – as mentioned in RD[9] – inhomogeneities (for example vacuum cavities) in the dielectric structure of the medium may scatter some power from the forward wave. Simple models relate the scattering losses to the number density of homogeneities, their size, and the electromagnetic frequency used for the sounding. Such a model, based on the Mie formulation for the scattering of dielectric spheres, was implemented for this study RD[13].

This model uses as an input the fraction volume of inhomogeneities, the dielectric characterisations of the background medium and of the inhomogeneities (ice and vacuum, respectively), and the statistical distribution of the sizes of the inhomogeneities (here the radii as they are assumed to be spherical). The model outputs the scattering attenuation. Results show that the scattering attenuation varies a lot with the size of inhomogeneities. For the sizes and fraction volumes mentioned in RD[9], the scattering attenuation is very strong (~ 0.1 dB/m) compared to the absorption. In that case, the performance of the radar sounder would be considerably reduced for areas where the thickness of the regolith is larger than a few tens of metres.

However, this issue has to be investigated further as the presence of a regolith has not been demonstrated. Analysis of Earth-based low frequency data (such as the P-band data from Arecibo) could help assess the scattering mechanisms of the surface of Europa. As for now, the standard test case used here assumes that the ice is compact and that scattering attenuation is negligible.

#### 4.4.2.3 Atmospheric effects

The atmosphere of Europa is very thin and is not expected to have any consequences for the propagation of VHF waves. The ionosphere of Europa is also very thin. A few occultation profiles were acquired during Galileo mission (see RD[10]). It seems that the ionosphere is too weak to have any sensible effects on microwave propagation around 50 MHz.

### 4.5 Simulation results

In this section, some of the results of the simulations are presented. To assess the feasibility of the system, a standard test case has been selected (case A in Table 4-4-1). It is understood that this test case is far from being representative of all the conditions that can be encountered over Europa. “Case A” is an average/good case: the fraction volume of dust is on the low side (1%) – which makes the microwave penetration into the ice easier – and the roughness is one of the lowest of the roughness states measured in the available Galileo images (Figure 4-1) – which lowers the surface clutter. However, only limited quantitative data were available from Galileo during the study and it may be that the three images were focusing on the roughest environment (as it is more interesting to study it with high-resolution data than smooth plains, and the data rate on Galileo were expensive – Connamara Chaos for example is a very rough surface). According to the low-resolution images, many areas on Europa are much smoother, so, as regards all possible roughness states for Europa, the “case A” may be not such a favourable one. Based on the very limited datasets accessible within the small duration of this study, case A is a model that underestimates the absorption of the ice and that slightly overestimates the surface clutter (two effects that somehow compensate each other). The effect of moving to other (also realistic) cases is explained in the other plots and results presented in this section. Detailed sensitivity studies would be necessary in the next study phase.

The test conditions for the standard case (case A) are the following:

- The vertical temperature profile assumes a surface temperature of 100K and a basal temperature of 273K, with an exponential temperature dependence with depth RD[11].
- All interfaces (surface and base) are flat (in average) and exhibit two scales of roughness. Their characteristics are detailed in Table 4-4-1.
- The medium where propagation takes place is assumed to be a mix of pure ice and of 1% volumic fraction of dust. The dielectric characteristics of the dust are similar to those measured on lunar soil.

- The system parameters are imported from the instrument description: 50 MHz centre frequency, 850 kHz bandwidth and 200 km altitude.

### 4.5.1 Model output – sensitivity to descriptive parameters

The model outputs the power level (radar cross-section) of the signal to be detected (nadir echo) as well as the perturbing clutter echoes (surface off-nadir echoes). In a later stage, these outputs can be used in the radar equation to derive signal-to-noise and signal-to-clutter ratios. The variation of the strength of the nadir echo with depth is characterised by a quasi-linear behaviour, as the mean attenuation in the ice crust increases linearly with depth. Here, the fraction volume of dust in the ice drives the slope of the curve.

The strength of the clutter echo varies with the angle of incidence (which is related to the depth of the simultaneous nadir echo, as shown on Figure 4-5). The shape of this variation is related to the large scale and small-scale roughness. Small-scale roughness will drive the value of the incoherent surface backscatter at large angles of incidence (that is, large depth of the nadir echo) whereas the large scale roughness will impact the transition rate between the close to nadir coherent response and the backscatter at large incidence. A smooth surface will exhibit a fast decrease of the return with incidence angle (case D, Figure 4-12) whereas a rough surface will be characterised by a much slower decrease of the surface return (case C, Figure 4-10).

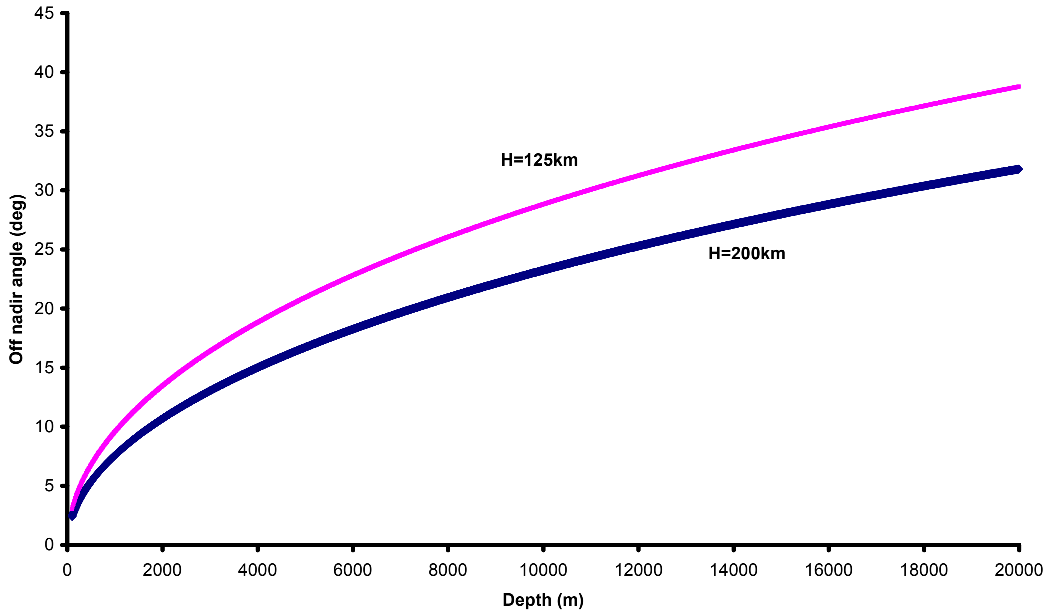


**Figure 4-5: Off-nadir angle of surface echo as a function of depth of simultaneous nadir echo**

The interaction model only outputs raw signals. Note that the cross-section of the surface off-nadir echoes that exhibit the same time delay as the nadir echo of interest can later be reduced by:

- Antenna pattern consideration: for a fine beam, the gain will drop quickly as a function of incidence angle.

- Doppler filtering: the area where the off-nadir backscatter takes place can be reduced through Doppler considerations without impacting the area of interaction of the nadir echo that is roughly limited to the 1st Fresnel zone.
- SAR-like advanced processing taking into account the effect of volume wave penetration into the medium.

A more detailed assessment of the filtering of the off-nadir echoes is discussed in Chapter 6, Instrument Electronics.

### 4.5.2 Standard case – Case A

In this case, the mean attenuation is moderate (~0.3 dB/100 m one way). If the nadir signals are lost in the raw clutter at ~5 km depth (Figure 4-6), the application of antenna pattern and of Doppler filtering can enhance the signal to clutter ratio considerably. In Figure 4-6, the off-nadir echoes are the surface echoes coming back to the sensor at the same time as the nadir echo of interest. The raw echoes have no filtering and no antenna. The standard case is Pwyll, Case A.

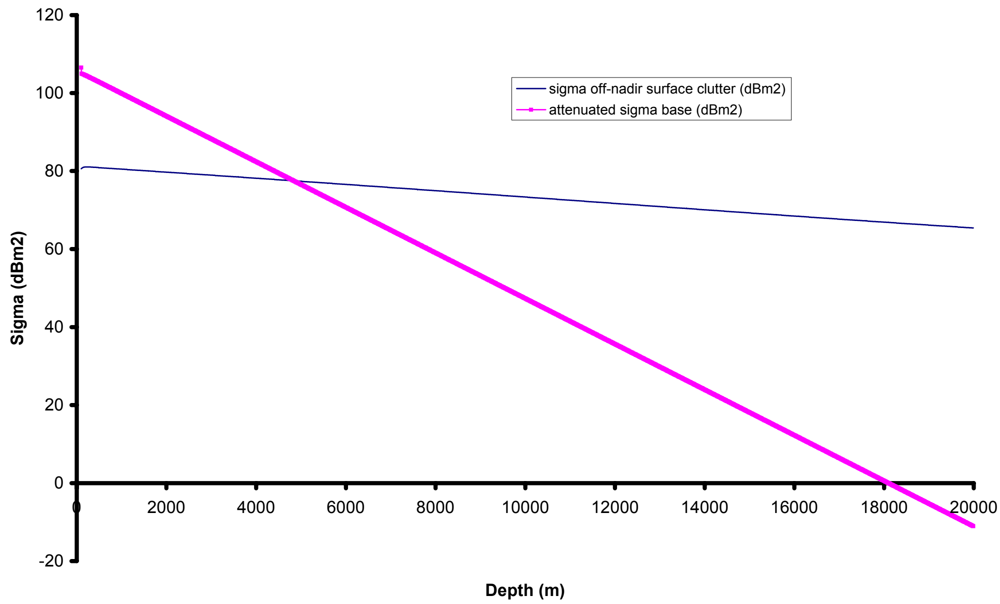


**Figure 4-6: Variation of the radar cross-sections with depth, standard case Pwyll, Case A**

### 4.5.3 High concentration of dust – Case E

In the case of a higher concentration of dust in the ice (10%, also quoted in literature RD[8]), the absorption is increased (0.6 dB/100 m one way). This considerably reduces the penetration performance of the system. Figure 4-7 shows that the attenuation rate of the ice-ocean interface is increased whereas the clutter level is the same as in the standard case. The off-nadir echoes are the surface echoes coming back to the sensor at the same time as the nadir echo of interest. The raw echoes have no filtering and no antenna. There is 10% dust, Case E.

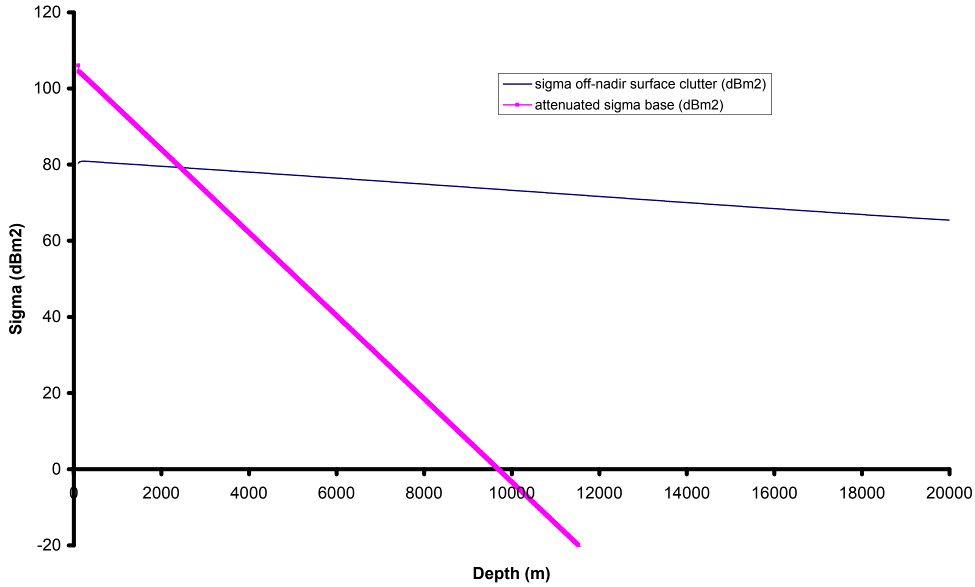


**Figure 4-7: Variation of the radar cross-sections with depth, 10% dust, Case E**

### 4.5.4 Smooth atmosphere-ice interface – Case F

In this case, the interface between the ice medium and the atmosphere is free of any topographic feature (rms slopes ~ $0^{o}$) and the small-scale roughness is also very small (2 cm rms height). This lowers considerably the level of the surface clutter both for small and large angles of incidence (see Figure 4-8). The off-nadir echoes are the surface echoes coming back to the sensor at the same time as the nadir echo of interest. The raw echoes have no filtering and no antenna. There are no topographic features. This is a smooth surface, Case F.

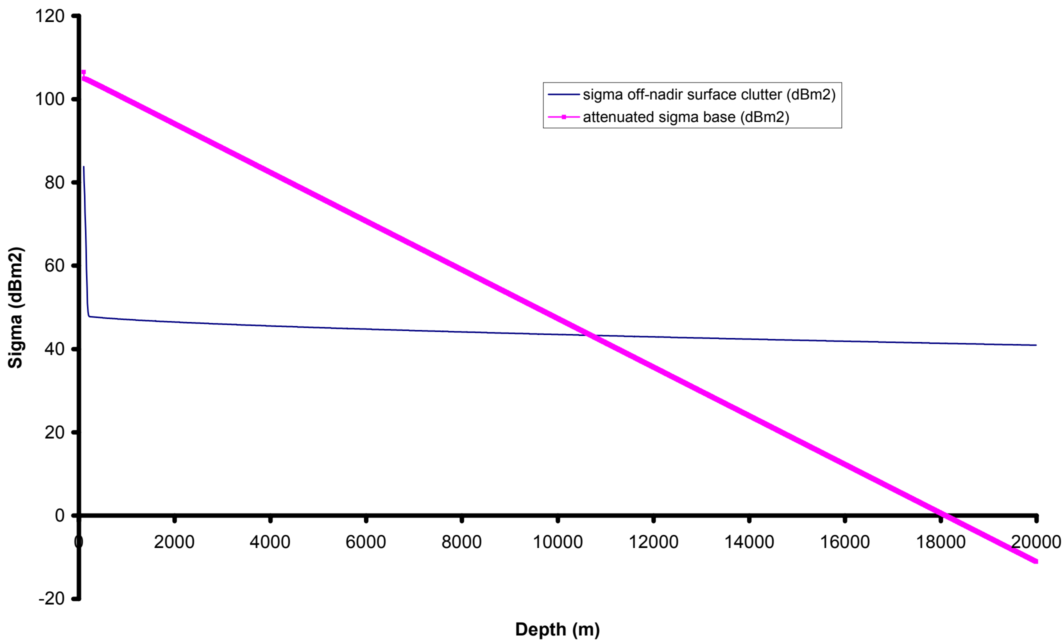


**Figure 4-8: Variation of the radar cross-sections with depth, smooth surface, Case F**

### 4.5.5 Other test sites

Figure 4-9 and Figure 4-10 show the simulation results for the other two test sites where data on the topography are available (Wedges and Connamara Chaos, respectively). There are few differences with Pwyll, where the surface was already quite rough. Here, a further increase of the roughness tends to slightly lower the strength of the nadir return from the surface. Note that all the test sites considered present quite strong topographic effects and that these large-scale effects drive the off-nadir backscatter, even for larger angles of incidence (large depths of the nadir return). The off-nadir echoes are the surface echoes coming back to the sensor at the same time as the nadir echo of interest. The raw echoes have no filtering and no antenna. This is Wedges, Case B.

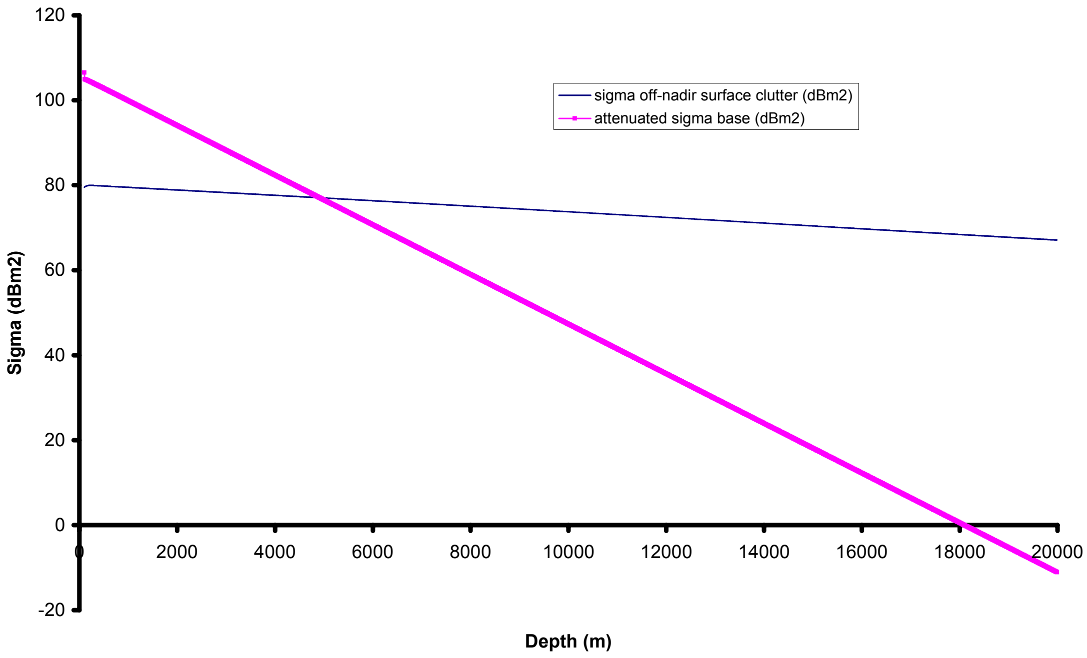


**Figure 4-9: Variation of the radar cross-sections with depth, Wedges, Case B**

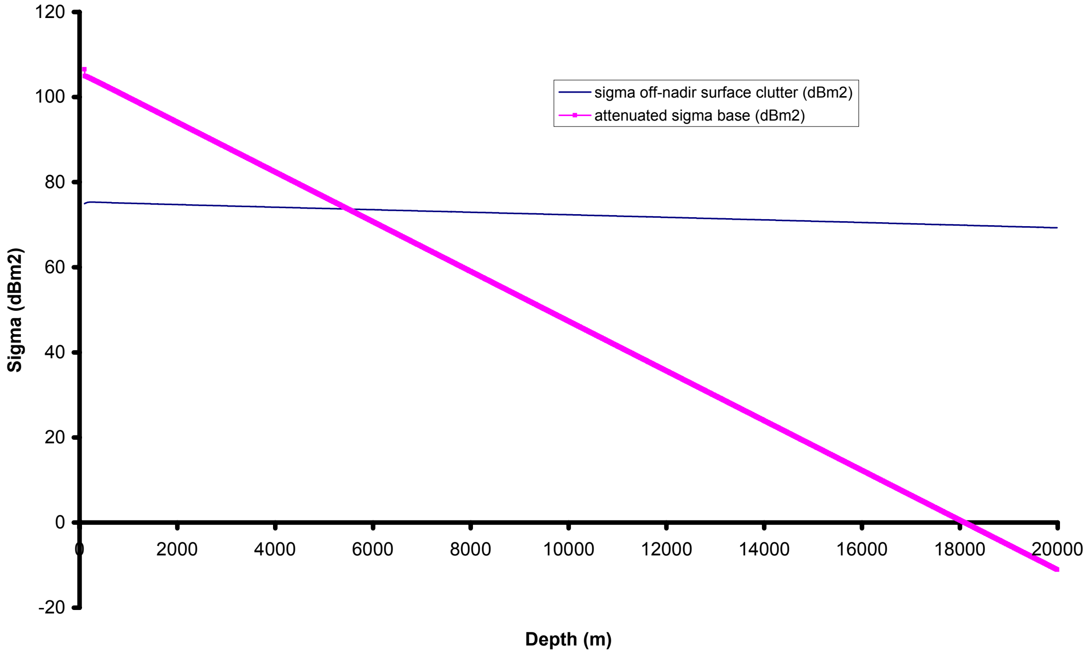


**Figure 4-10: Variation of the radar cross-sections with depth, Connamara Chaos, Case C.**

### 4.5.6 Other cases of surface roughness

The last two figures (Case G in Figure 4-11 and Case D in Figure 4-12) are based on the standard case but with a reduced topography (3.5° and ~0° rms slopes, respectively). Small-scale roughness and all other parameters are the same as in Case A (Figure 4-6). Note the effect of large-scale roughness on the surface clutter for small off-nadir angles. When topographic effects are less intense, small-scale roughness drives the backscatter for large off-nadir angles of incidence (compare Figure 4-12 with Figure 4-8).

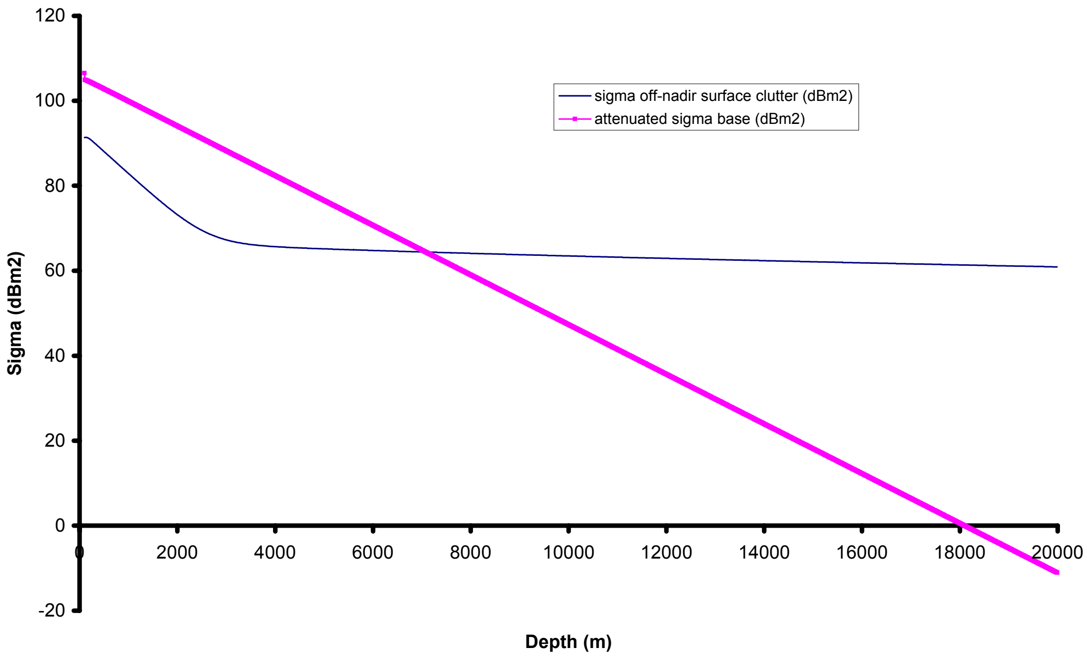


**Figure 4-11: Variation of the radar cross-sections with depth, Intermediate roughness, Case G**

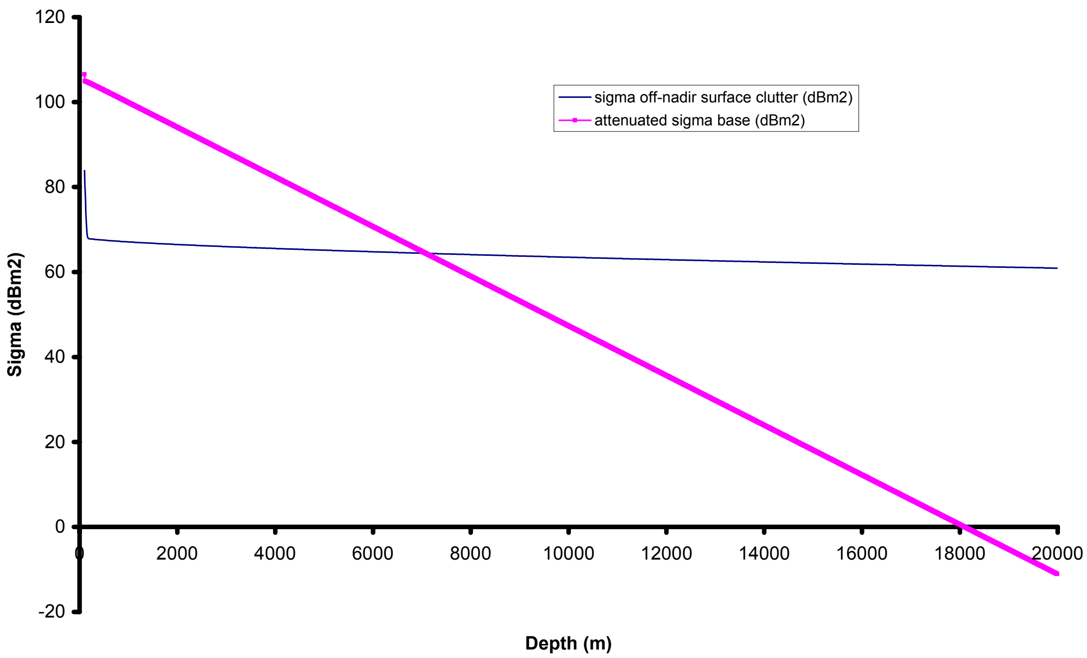


**Figure 4-12: Variation of the radar cross-sections with depth, Smooth surface, Case D**

### 4.5.7 Conclusions of the geophysical sensitivity study

The output of the simulations presented in this section is used to generate the signal-to-noise ratio (SNR) and signal-to-clutter ratio (SCR) needed to assess the performance of different system configurations. From the point of view of wave interaction alone, several conclusions can be drawn:

- The fraction volume of dust in ice has a large impact on the attenuation of the nadir echo. Its choice impacts both SNR and SCR to a great extent and will have to be consolidated.
- The presence of large-scale topographic features degrades the SCR. Light topography only increases the surface clutter for small off-nadir angles whereas strong topography has an impact throughout the range of off-nadir angles (that is, depths of the nadir echo).
- Small-scale roughness has a direct impact on the surface backscatter at large incidence angles (where the influence of topography disappears). As such, it may impact the SCR for large depths.

### 4.5.8 Alternative system configurations

The system configuration used for the geophysical sensitivity studies is (50 MHz, 850 kHz, 200 km) for the triplet (centre frequency, bandwidth, altitude). Other configurations were tested, changing the centre frequency to 20 and 80 MHz, the bandwidth to 2550 kHz and the altitude to 125 km.

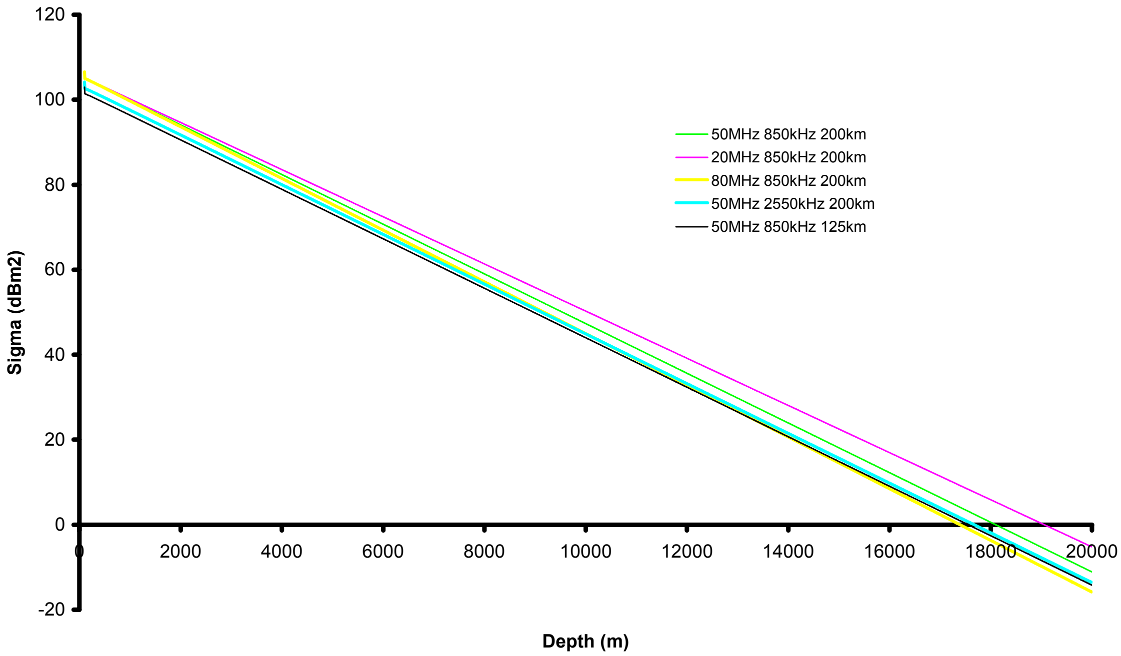


**Figure 4-13: Variations of the strength of the nadir echo with depth of the ice-water interface**

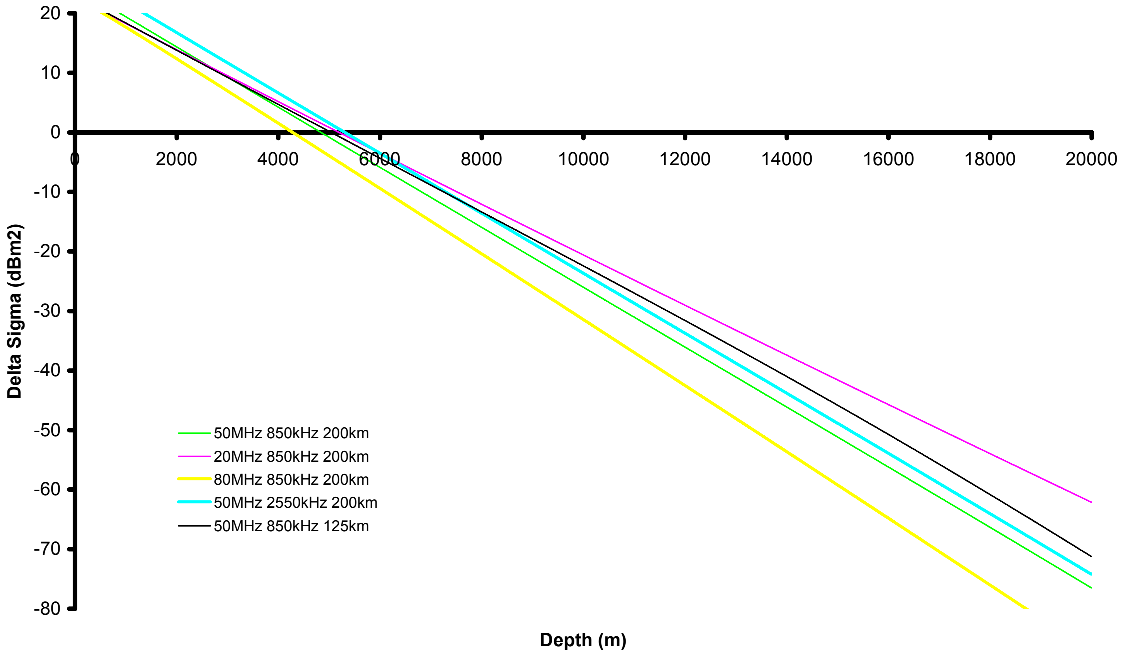


**Figure 4-14: Variations of the SCR ($\sigma_{\text{nadir echo}} - \sigma_{\text{clutter}}$) with the depth of the ice-water interface**

Figure 4-13 presents the variations of the radar cross-section of the subsurface ice/water interface to be detected as a function of depth, for the system parameters described above. This has to be considered together with the corresponding noise figures and will be an input to the S/N analysis. More specifically, lower frequencies (20 MHz) will be strongly affected by Jovian radio noise.

Figure 4-14 presents the variations of the SCR (raw signals, without any considerations of antenna pattern or filtering) as a function of the depth of the ice-water interface. The performance gain obtained by lowering the centre frequency of the measurement is already clear: at lower frequencies, the surface appears smoother and results in less backscatter. The impact of a larger bandwidth or of a lower altitude will be considered when the simulated signals are used in the radar equation in Chapter 6, Instrument Electronics.

### 4.5.9 Other simulations

The objective of the interaction model was to assess the performance of the proposed instrument in terms of SNR and SCR. Additionally, the model is able to simulate other parameters, such as the shape of the reflected pulses. This could be used for example to study the altimetric performance of the system. These capabilities were not used in the study.

## 4.6 Radio noise

Jupiter is a strong source of radio noise in the frequencies of interest for the ELRR. This emission occurs mostly for frequencies below the ionospheric cut-off, up to 40 MHz. The detailed emission mechanism is not precisely known. The radiation is highly circularly polarised which may suggest cyclotron radiation from energetic electrons orbiting Jupiter's magnetic field lines in the ionospheric regions of the planet. They appear to be dumped there through perturbations by the satellites passing through Jupiter's extensive magnetosphere.

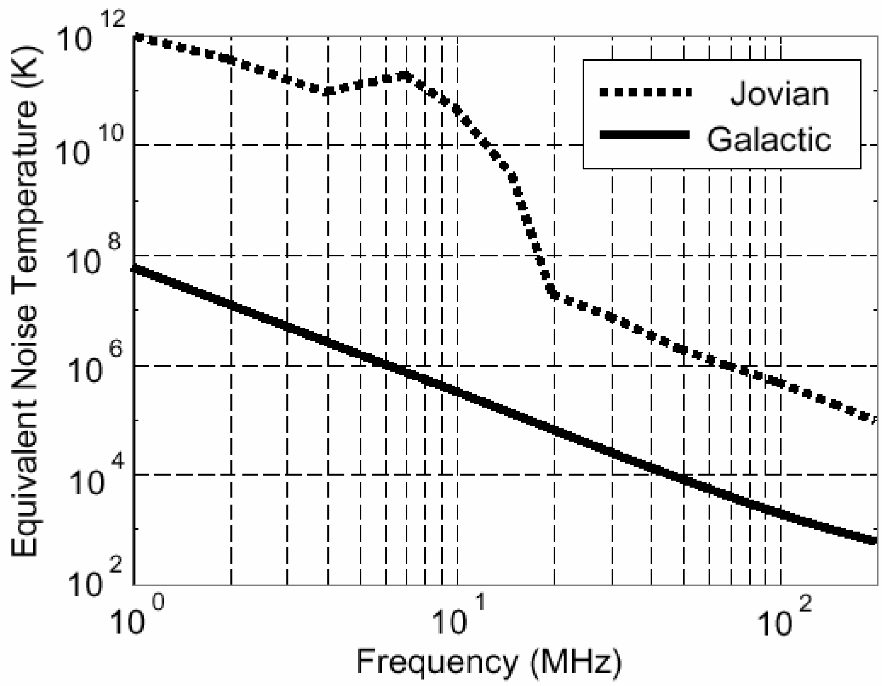


**Figure 4-15: Jovian and galactic noise temperatures as a function of frequency**

Figure 4-15, RD[6] shows the estimated variations of the radio noise as a function of microwave frequency. In the higher range of frequencies, the emission process is shifted from cyclotronic to synchrotronic (similar mechanism, but with higher energy electrons).
As this radio noise is very strong at frequencies of interest for the ELRR, the spatial location of the sources of this noise is interesting: if the spatial extension of the source is limited, the instrument could be protected from the noise using Europa as a shield. Similarly, the effect of a localised radio source could be reduced by the antenna pattern of the instrument.

At each point of the magnetic field lines, the frequency of the emission $f_c$ is close to the cyclotron frequency (or gyrofrequency). If gyrating electrons are the sources of the emission, $f_c \cong 2.8\,B$ where $f_c$ is expressed in MHz and $B$ is the magnetic flux density expressed in Gauss RD[16]. Some simplified models of Jupiter's magnetic field exist, see RD[17]. These harmonic decompositions of the magnetic field are based on Pioneer 9-10 and Voyager 1-2 measurements. Although limited in accuracy, they give an idea of the shape and strength of the magnetic field lines.

At 50 MHz, it appears that a magnetic flux density large enough for cyclotron emission can only be found below the ionosphere of Jupiter (for comparison, a 1 MHz cyclotron emission can exist two Jupiter radii away from its atmosphere). Cyclotron emission may not be the only process generating the radio noise (higher energy electrons moving at relativistic speeds could generate synchrotron emission) but this suggests that the main source of Jovian emission at 50 MHz would not extend very far away from the planet. Consequently, the source of the radio emission could be considered as localised and the ELRR could be shielded from it when orbiting on the dark side of Europa.

This is especially important as Jupiter is an active source of radio noise characterised by bursts that make the planet one of the strongest radio sources in the sky (and an unpredictable one). Clearly, knowledge of specifically where the source lies will greatly aid efforts to characterise the interrelated mechanisms responsible for this radio noise from Jupiter. This was done at higher frequencies, but at VHF a high-resolution radio observatory is still missing (see RD[18]). Assuming that the radio source is localised, and applying the antenna pattern to the noise environment, noise intensity could be reduced by ~20 dB compared to the worst case studied in the instrument systems (see Chapter 5, Instrument System Design). Similarly, acquisitions made on the Jupiter side of Europa would benefit from a 10 dB S/N gain as most Jovian emission in the antenna main lobe originates from Jupiter's reflection on Europa's surface. Jupiter's reflection is characterised by an albedo around 0.1 at these frequencies, as 50 MHz waves are absorbed by the icy medium. These conclusions are tentative and require further specialist review and analysis.

## 4.7 Critical issues and conclusion

The model described above was implemented and its output was provided to the instrument designers. However, some fundamental issues are still pending and must be emphasised for future work, as follows:

- *Some effort shall be dedicated to the collection of the data* available on the geophysical characteristics of Europa. This includes quantitative indicators of the surface roughness and of the topography (from Galileo data), consolidated models of its interior, and dielectric measurements at the frequencies of interest. VLA measurements shall also be investigated to analyse the issue of the regolith. It is expected that the various assumptions used in the modelling will have more impact on the simulated performance of the instrument than a fine-tuning of the system characteristics. Before strictly defining the system requirements, a future study should focus on the conversion from scientific to observation requirements, based on all the data on Europa available to the community. It is not easy to obtain something more accurate about the dust concentration, but a rough analysis of all Galileo images could definitely provide further insight on the statistics of the surface clutter.
- Because of time constraints, *the issues had to be oversimplified*. For example, one single signal was supposed to represent what can be observed over Europa and was used for the baseline definition of the system. Regional variability must be taken into account and both experimental observations (that is, high-resolution Galileo data) and advice from scientific experts in the field are fundamental to support any model output. A more detailed interaction model should be used, based on previous developments (MARSIS simulator) or on currently on-going work in the field of microwave/ice radio sounding models for Earth observation. This model shall, at least, be able to include subsurface structures and non-null mean slope within the footprint.
- The issue of *radio noise* is important because its proper handling could result in a sensible increase of the system performance. It is recommended to seek the analysis from experts in this field.
- The altimetric mode of the instrument (study of the pulse shapes) shall be investigated, because its performance could be sufficient for the scientific applications foreseen for altimetry.

# 5 INSTRUMENT SYSTEM DESIGN

## 5.1 Purpose and objectives

A future mission to explore the Jovian system and in particular Jupiter's moon Europa would probably have as its objective to provide a definite answer to the question of whether there is a liquid water ocean beneath Europa's icy crust. An exact figure for the likely depth of this ice can only be guessed at but current estimates put it anywhere between 5 and 50 km. A radar sounding instrument is therefore needed which can "look" through the ice and detect the presence of water beneath.

## 5.2 Scientific requirements and design drivers

The principle objective of the Europa Low Resources Radar (ELRR) instrument therefore is to be able to detect the presence of water beneath the ice and in designing the radar all other parameters derive from this. The maximum depth that the radar should be able to penetrate is, of course, as deep as possible but a practical goal is at least 5-10 km but closer to 20 km if possible. The vertical resolution does not need to be better than 100 m and this can be relaxed, if necessary, to 10% of the penetration depth, that is 2000 m at 20 km depth.

From the point of view of the radar, the altitude of the orbiter should as low as possible to improve the signal-to-noise ratio (SNR) or reduce the power requirements. The nominal altitude has been set to 200 km with an alternative of 300 km although there may be a possibility to reduce the orbit to 125 km if certain orbital and power generation issues can be resolved. The orbital velocity is dependent on the altitude and does not change too significantly over the three possibilities so for the purposes of this analysis a fixed value of 1375 m/s has been assumed.
The total DC power available to the satellite is given as 20-25W. Here the higher value has been assumed, should this not be feasible then it will in any case have a modest impact on either the instrument duty cycle (20% less) or reduce the achievable SNR by about 1 dB which would correspond to a reduction in depth penetration of around 15 m.
The main requirements and design drivers are summarised in Table 5-1:

| Parameter | Requirement/Limit | Comment |
|---|---|---|
| Depth Penetration | 5-10 km, 20 km if possible | Actual depth unknown but hopefully less than 20 km |
| Vertical Resolution | 100 m | Can be relaxed to 10% of depth with maximum resolution 100 m |
| Altitude | 200 km | Alternative of 300 km. 125 km might also be feasible |
| Satellite Velocity | 1375 m/s | At 200 km altitude |
| Max DC Power Available | 25W | For the entire satellite |
| Total mass | 10 kg | |

**Table 5-1: ELRR requirements and design drivers**

## 5.3 System analysis

### 5.3.1 Assumptions and trade-offs

#### 5.3.1.1 Radar frequency

To penetrate ice by any significant distance, a low-frequency radar is required. This is discussed further in Chapter 4, Wave Interaction Analysis but ultimately the indication is to go towards the tens of megahertz region to be able to penetrate ice down to about 20 km. However, for a very low frequency, the antenna dimensions are determined by the wavelength. In addition, as explained below, the background noise, which is already very high around Jupiter, gets significantly worse below 20 MHz making this the lower limit for radar frequencies considered. For the trade-off, three frequencies were therefore chosen: 20, 50 and 80 MHz.

#### 5.3.1.2 Noise

To achieve the kind of ice penetration that is required, a sounding radar should use low-frequency signals below 100 MHz. However, there are problems in this frequency range in terms of antenna gain and size and background noise. The galactic background is already high for these frequencies but in the Jovian system it is considerably worse. Figure 4-15 illustrates this, showing curves of noise temperature against frequency for both the galactic background and the Jovian system. Note that, at 20 MHz, the noise temperature for Europa is $10^7$K (70 dB) and drops to 700 000K (58 dB) at 100 MHz. For the purposes of this analysis, the worst-case noise temperature values shown in Table 5-2 were used.

| Frequency (MHz) | Noise Temperature (K) |
|---|---|
| 20 | $10^7$ |
| 50 | $2 \times 10^6$ |
| 80 | $10^6$ |

**Table 5-2: Worst-case noise temperatures**

#### 5.3.1.3 Power

From the maximum available DC power, a simple calculation can determine the peak transmit power to be used in the further calculations. Assuming:

- 25W maximum available DC power
- 50% instrument operational cycle
- 10% transmit duty cycle
- 75% efficiency of high power stage and taking into account DC power use of the radar electronics

give: *25/0.5/0.1*0.75 = 375W* of peak transmit power.

#### 5.3.1.4 Spatial resolution

##### *1.1.1.1.1 Depth resolution*

The maximum depth resolution required is determined by the pulse bandwidth of the radar. In free space, the range (depth in this case) resolution is calculated by:

$$\rho_z = \frac{c}{2B}$$

where c is the speed of light in a vacuum and $B$ is the bandwidth. However, the speed of light in ice is reduced by the square root of its relative permittivity and hence to determine the required bandwidth the following equation must be used:

$$B = \frac{c}{2\rho_z \sqrt{\varepsilon_r}}$$

where $\varepsilon_r$ is the relative permittivity of ice. Assuming a value of 3.12 for $\varepsilon_r$ gives a required bandwidth of 850 kHz. If a poorer resolution at depth is acceptable, this can be traded in for gain in SNR for coherent targets. At 20 km with a resolution of 2 km this is 6.5 dB

#### *1.1.1.1.2 Across-track resolution*

A nadir-looking sounding radar operates in a similar fashion as an altimeter over a smooth surface where "smooth" is defined as the surface roughness of the target area having an RMS value of less than *λ/4*. In this case specular reflection of the radar signal occurs which has a very favourable impact on the SNR. This advantage is a dependency in $1/h^2$ ($h$ is the height of the radar above the target) for the 1st Fresnel zone (the target area) as opposed to $1/h^3$ for returns coming from outside this zone – so-called clutter. The diameter of this 1st Fresnel zone, which can be assumed to be smaller than the radar's pulse limited footprint, therefore effectively determines the across-track resolution. This is given by the expression:

$$D_r = \sqrt{2\lambda h}$$

For a wavelength of 6 m and an orbital altitude of 200 km this gives an across-track resolution of 1549 m at the surface of Europa, reducing to 1224 m for an altitude of 125 km.

#### *1.1.1.1.3 Along-track resolution*

In the along-track direction, the antenna beamwidth is very broad which results in much ambiguous energy being returned to the sensor. Fortunately, these returns have a slightly different frequency to those coming back from the subsatellite point due to the motion of the satellite (Doppler). These frequencies can therefore be filtered out effectively making the antenna beam in the along-track direction much narrower. This technique is known as Doppler beam sharpening and apart from filtering out ambiguous clutter returns, it is also useful in improving the SNR since the total Doppler bandwidth is limited. All of this assumes that the target can be considered to focus like a "point target". Since the only desired returns from the along-track direction are also coming from the first Fresnel zone it makes sense to process the Doppler to obtain along-track resolution as across-track.

#### *1.1.1.1.4 Pulse Repetition Frequency*

To sample Doppler sufficiently there has to be a minimum value to the Pulse Repetition Frequency (PRF). This is given by:

$$PRF_{\min} = 2\frac{V_s}{\lambda}$$

where $V_s$ is the satellite velocity (1375 m/s), hence $PRF_{min}$ = 458 Hz.
The upper limit for the PRF is constrained according to the expression:

$$PRF_{\max} = \frac{1}{2\left[T_p + \dfrac{z_{\max}}{c/\sqrt{\varepsilon_r}} + \tau_g\right]}$$

where $T_p$ is the pulse length, $\tau_g$ the guard time and $z_{max}$ the maximum depth to be observed. Assuming that the intention is to capture the entire return from within the ice down to a depth of 20 km, the time for the pulse to travel through the ice and back becomes the dominant term. Ignoring the pulse length for 20 km depth this limits the PRF to around 4 kHz. To allow for a little margin a PRF of 3300 Hz is taken and since only 458 Hz are required this allows averaging to be performed providing an additional useful gain of 4.3 dB for coherent targets.

*1.1.1.1.5 Processed Doppler*

The processed Doppler bandwidth is given by:

$$B_{proc} = 2\frac{V_s}{\lambda}\cdot\sin\left[\tan^{-1}\left(\frac{D_r}{h}\right)\right]$$

which gives 3.55 Hz for the first Fresnel zone. Given that the noise is sampled by the reception of the radar pulses, its spectrum is not considered continuous but "folded" at the *PRF*, which for coherent targets, provides a Doppler processing gain approximated by: $PRF/B_{proc}$ or around 30 dB.

### 5.3.1.5 Ambiguous returns

The ambiguities in the along-track direction have effectively been eliminated thanks to the Doppler beam sharpening. In the across-track direction, however, off boresight returns (clutter) can arrive at the radar receiver simultaneously with target returns at depth, corrupting the wanted signal (see Figure 5-1).

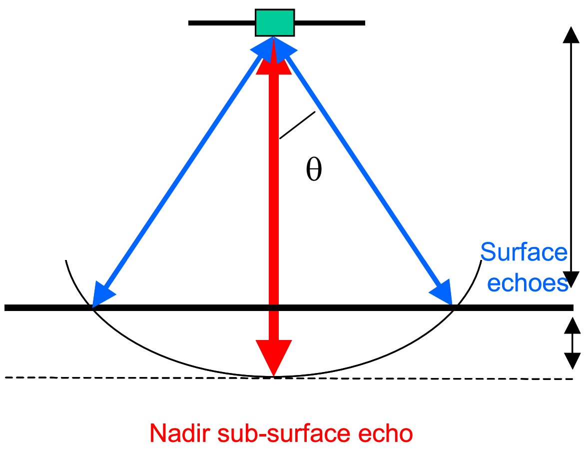


**Figure 5-1: Across-track ambiguities**

Compared to the target echo, these returns are suppressed for a number of reasons:

- The across-track antenna pattern (hence the desire to have this as narrow as possible)
- A factor of 1/h, since these returns are not specular

- The normalized radar cross-section (NRCS or sigma nought) drops quickly as the clutter returns depart from a zero-degree incidence angle (see Chapter 4, Wave Interaction Analysis)
- Clutter is incoherent and therefore is unaffected by processing gains which serve to enhance the target response

Nevertheless, due to the propagation loss through the ice, at depth the target echoes become so faint that ambiguous clutter can still dominate.

### 5.3.2 System trade-off and performance

To perform a systematic trade-off of the main instrument parameters which were not definitely fixed, namely altitude, centre frequency and pulse bandwidth, a matrix of seven different radars was drawn up, as shown in Table 5-3:

| Radar | Frequency (MHz) | Bandwidth (kHz) | Altitude (km) |
|---|---|---|---|
| A – standard | 50 | 850 | 200 |
| B – low frequency | 20 | 850 | 200 |
| C – high frequency | 80 | 850 | 200 |
| D – wide bandwidth | 50 | 2550 | 200 |
| E – high altitude | 50 | 850 | 300 |
| F – low altitude | 50 | 850 | 125 |
| G – high f, low alt. | 80 | 850 | 125 |

**Table 5-3: Radar trade-off matrix**

The performance measure used for each scenario was the target SNR as a function of depth through the ice. Clearly, when the SNR drops to zero or below, it is impossible to distinguish a target from the noise. Equally though, when the SNR is above zero but less than the clutter-to-noise ratio (CNR) it is impossible to distinguish a target from the clutter. Hence, in the following analyses, Figure 5-2 to Figure 5-8, both the SNR and CNR are given for each radar scenario.

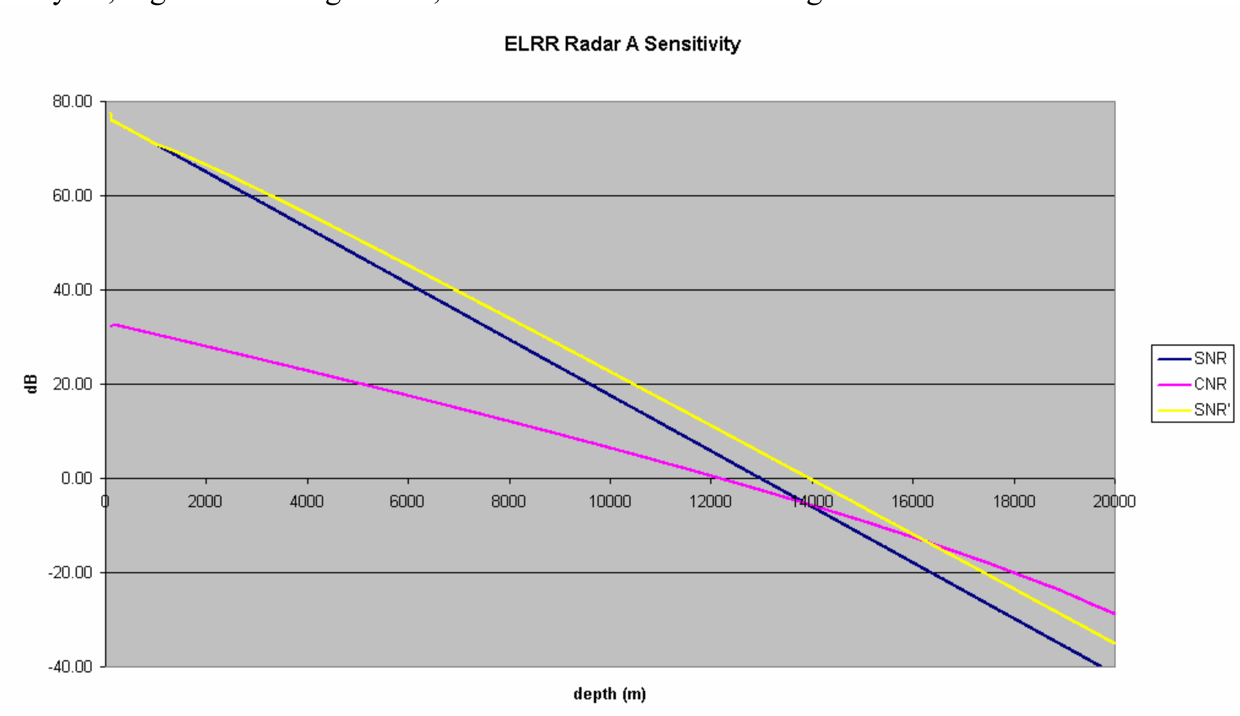


**Figure 5-2: Radar A – standard configuration**

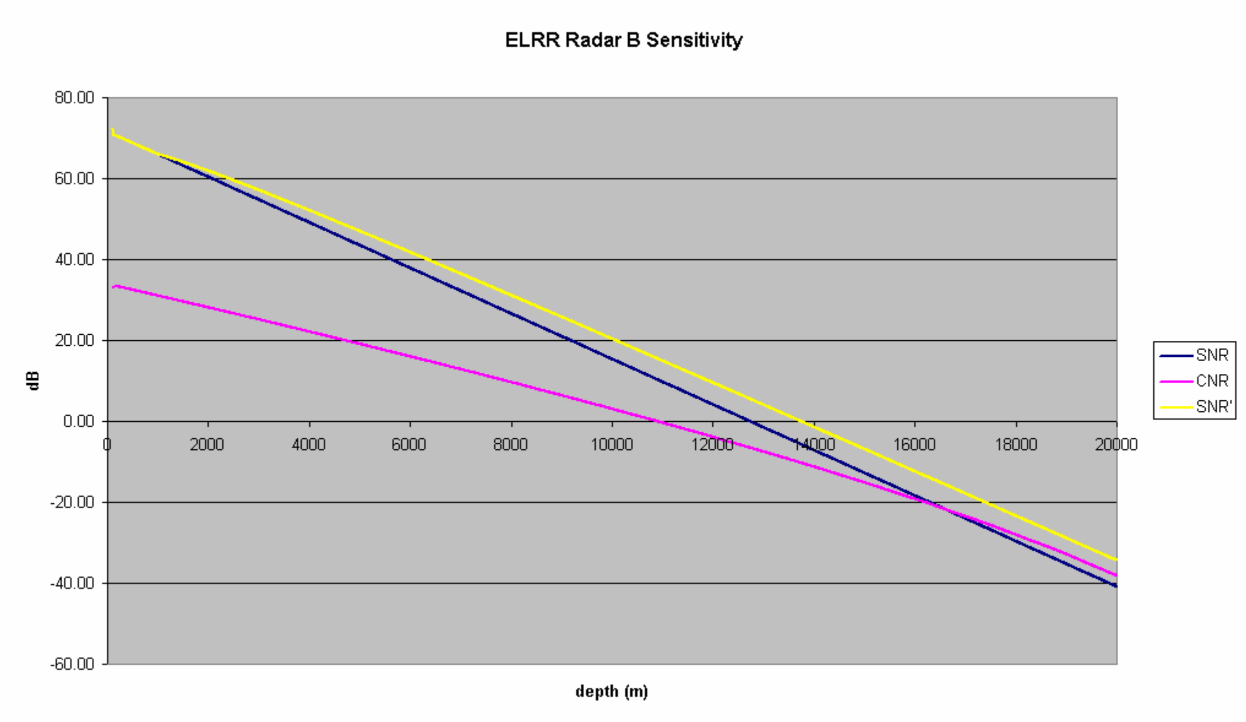


**Figure 5-3: Radar B – low-centre frequency**

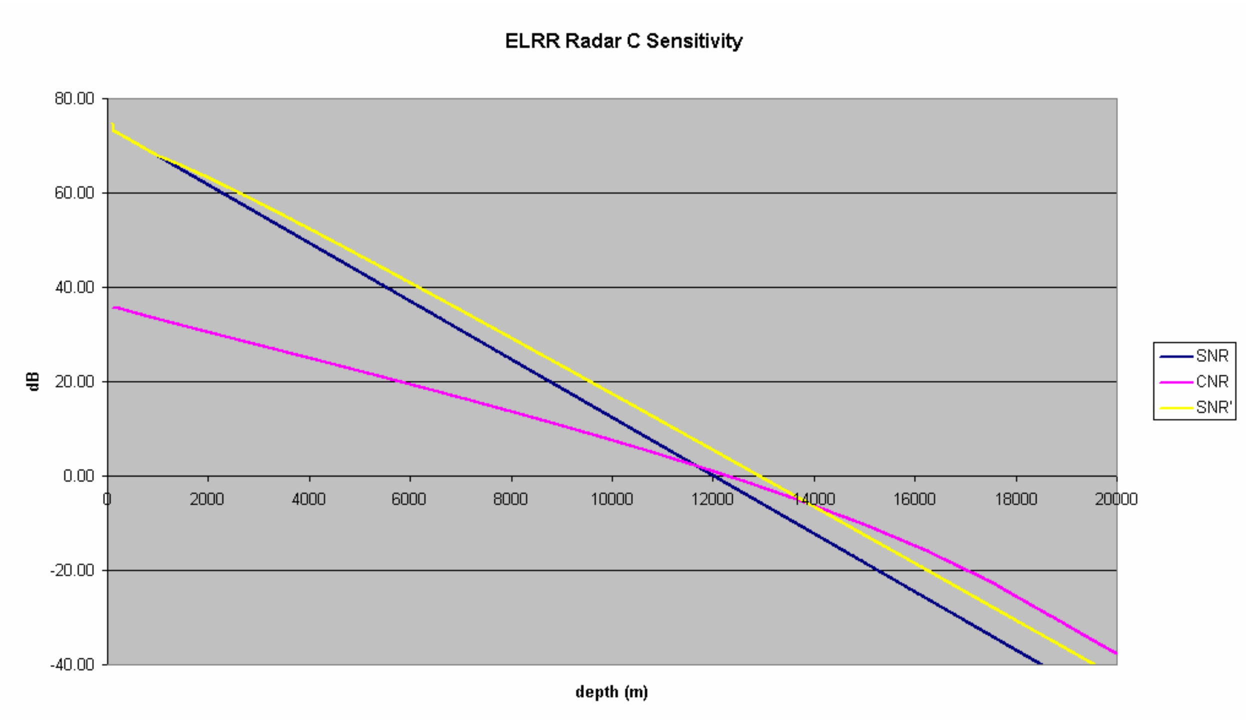


**Figure 5-4: Radar C – high-centre frequency**

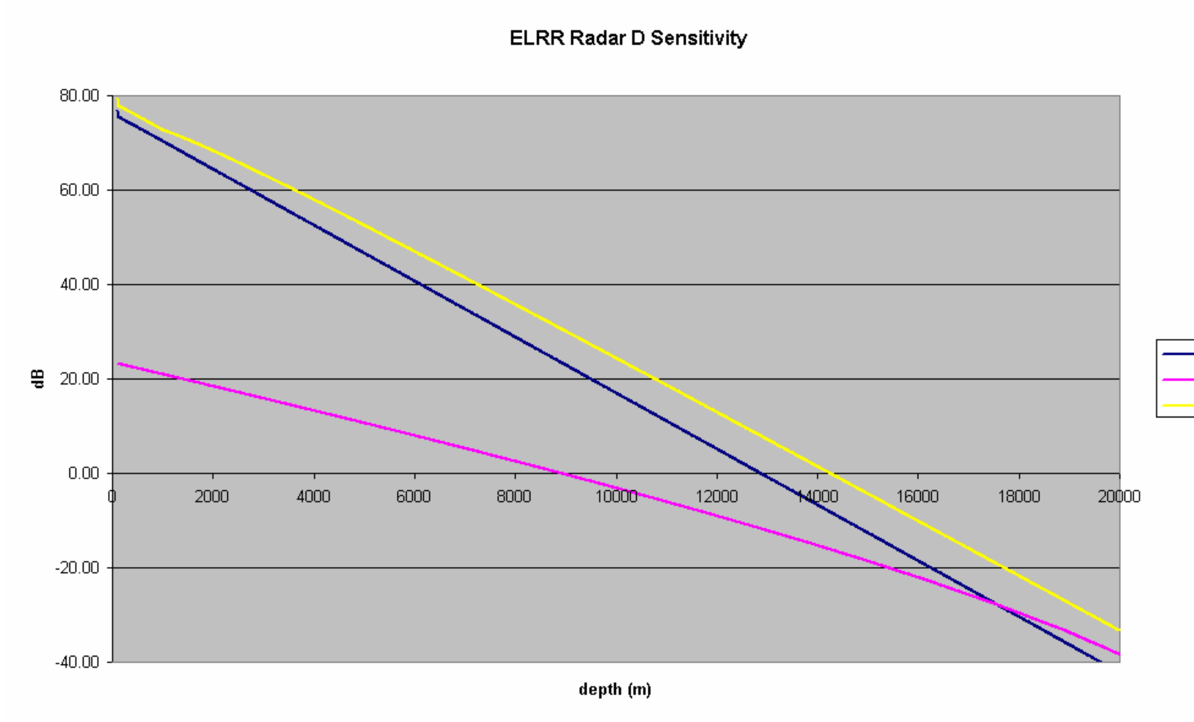


**Figure 5-5: Radar D – wide bandwidth**

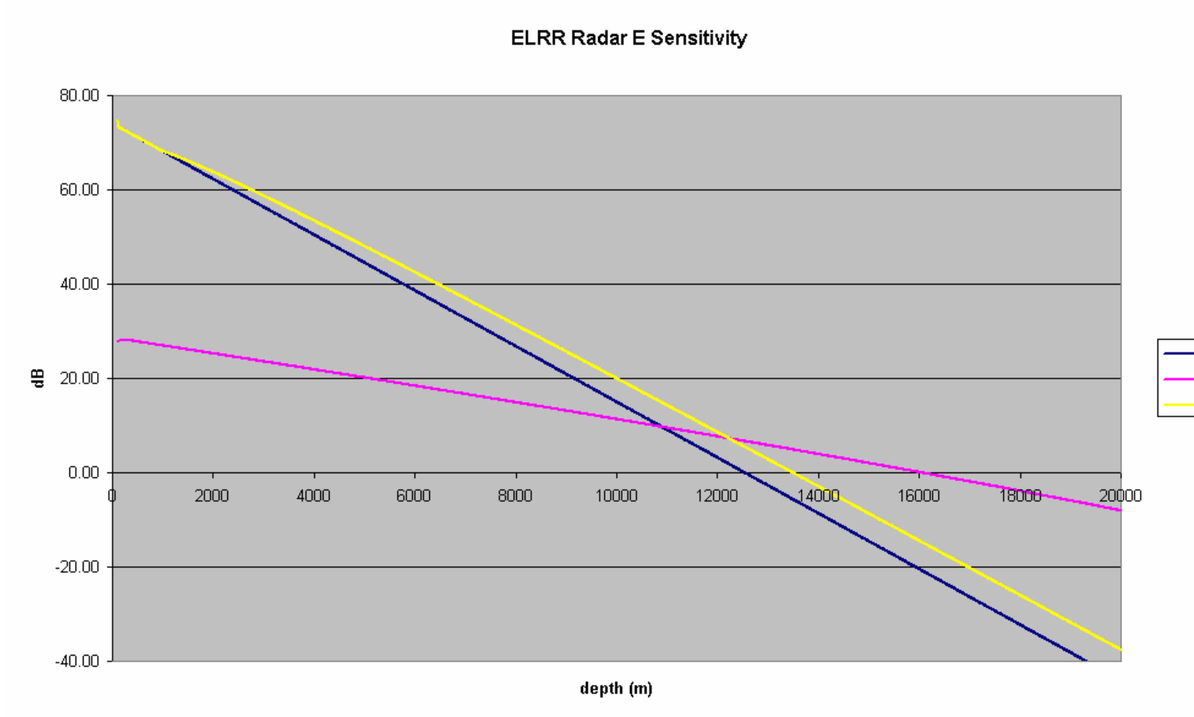


**Figure 5-6: Radar E – high altitude**

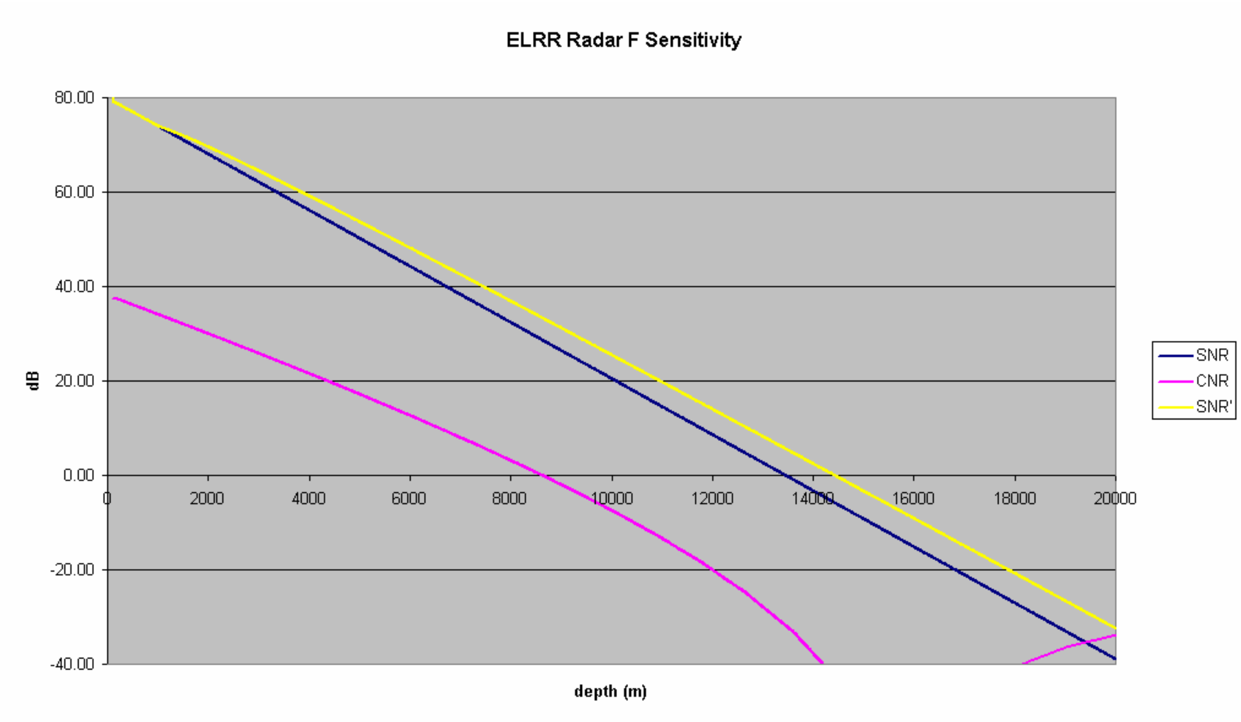


**Figure 5-7: Radar F – low altitude**

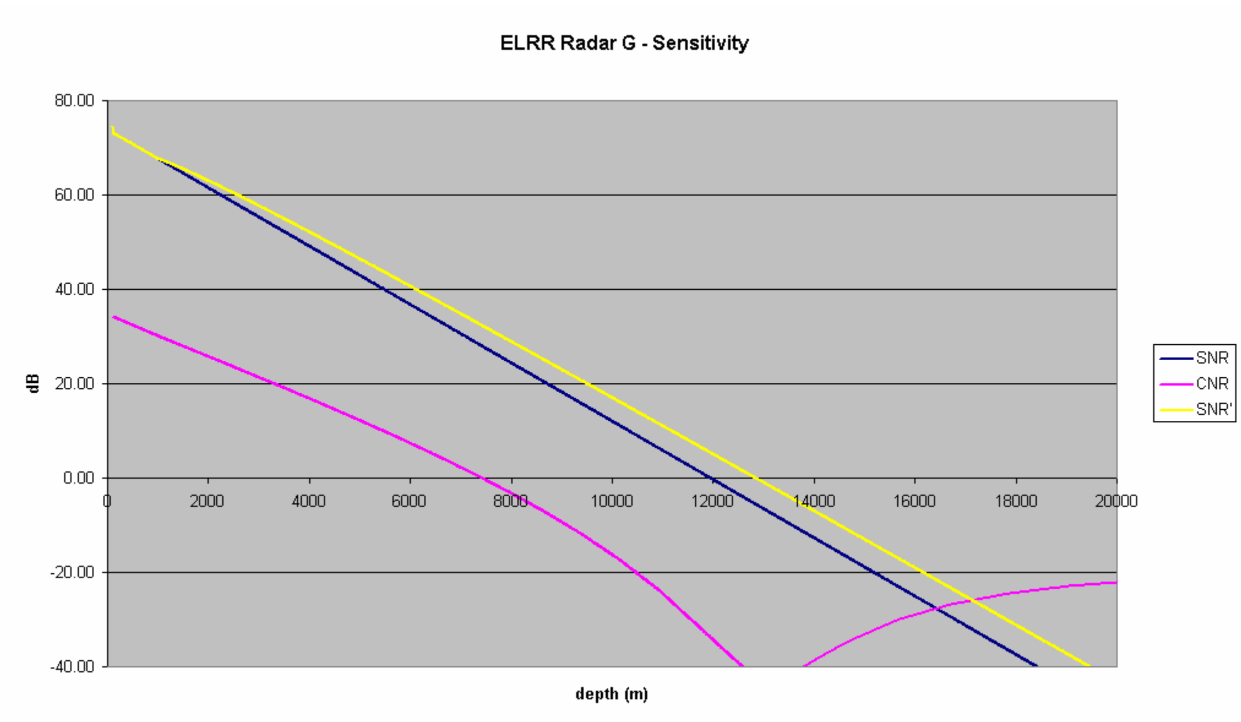


**Figure 5-8: Radar G – high-centre frequency, low altitude**

The general shape of the curves presented in Figure 5-2 to Figure 5-8 is very similar. The SNR typically cuts off (goes below 0 dB) beyond about 12 km depth. Also, the clutter very rarely affects the target return. An overview of the results obtained for these seven cases is shown in Table 5-4, where figures in bold represent the limiting factor:

| Radar | SNR Limit (m) | SNR' Limit (m) | Clutter Limit (m) |
|---|---|---|---|
| A – standard | **12980** | 13940 | 13880 |
| B – low frequency | **12730** | 13690 | 16610 |
| C – high frequency | 12010 | 12970 | **11670** |
| D – wide bandwidth | **12070** | 13430 | 15700 |
| E – high altitude | 12540 | 13500 | **10900** |
| F – low altitude | **13450** | 14420 | 19410 |
| G – high f, low alt. | **11950** | 12840 | 16430 |

**Table 5-4: Performance results for seven traded radars**

#### 5.3.2.1 Pointing considerations

Due to orbital constraints, the ability to keep the radar pointing precisely at nadir was considered quite challenging by the AOCS team. It therefore seemed reasonable to take a relatively worst-case scenario for pointing accuracy of around ±5°. Each of the three satellite axes was taken in turn to study its effect on performance for the two most promising radar designs as determined in the previous section.

The two baselines selected were:

Centre frequency = 50 MHz, bandwidth = 850 kHz
Radar A: 200 km altitude
Radar F: 125 km altitude

*1.1.1.1.6 Pitch*

Variations in pitch result in the radar gain being reduced since the peak gain of the mainlobe is no longer pointed to nadir. The changes that occur in the off-nadir along-track gain pattern can be discounted due to the Doppler filtering, hence the 5-degree pitch error can be simply modelled by reducing the across track antenna gain by the value of the drop in gain, with respect to the peak, of the along track pattern as found at 5 degrees.

Obviously this results in no change to the shape of the CNR curve. Moreover, both SNR and CNR curves drop by an almost negligible amount (~0.25 dB) and there is also no appreciable difference between the effects of mis-pointing in pitch on either radar A or F.

*1.1.1.1.7 Yaw*

The effect of an error in the yaw pointing is likely to be more serious than that of the pitch error since the across-track beam pattern will no longer be as narrow. Yaw error was modelled using the two-dimensional antenna gain pattern cut at an angle 5 degrees away from the normal across-track direction. In terms of performance, there is no effect on the SNR since the mainlobe gain remains unchanged, but there is a slight change to the CNR due to the broadening of the mainlobe and an increase in the sidelobes in the across-track direction. Figure 5-9 and Figure 5-10 show this minor impact on the performance of radars A and F:

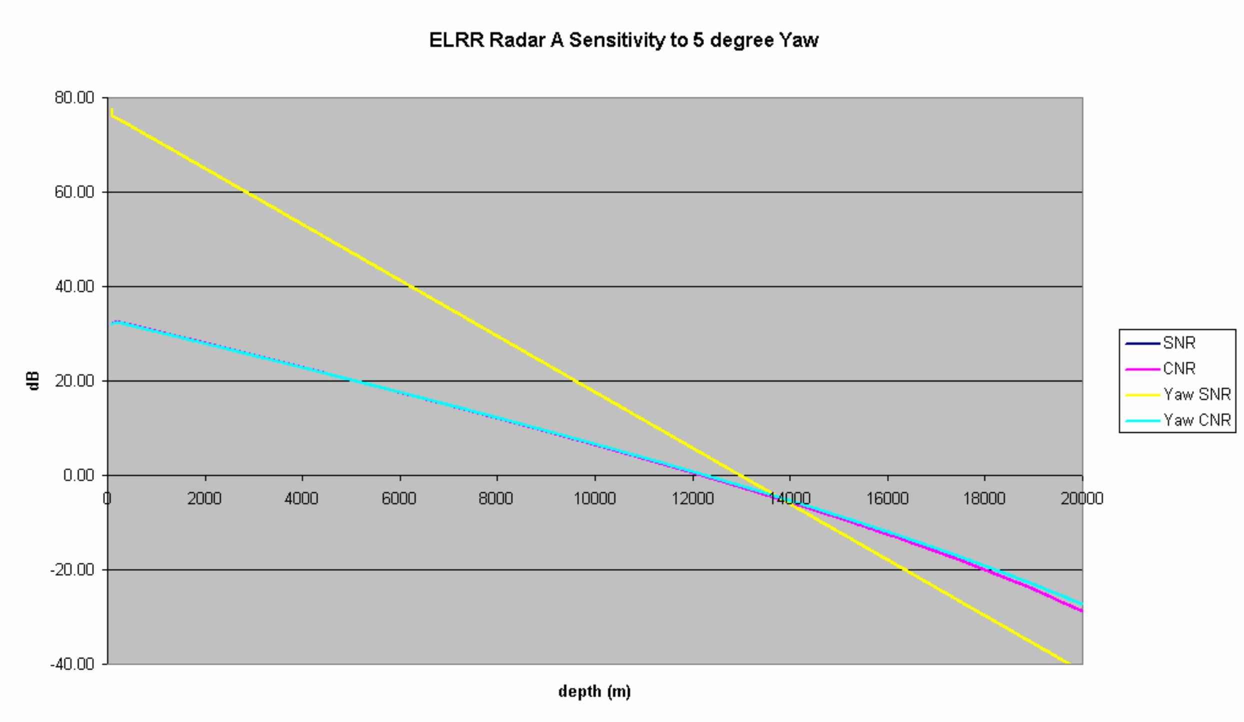


**Figure 5-9: Radar A sensitivity to 5-degree yaw**

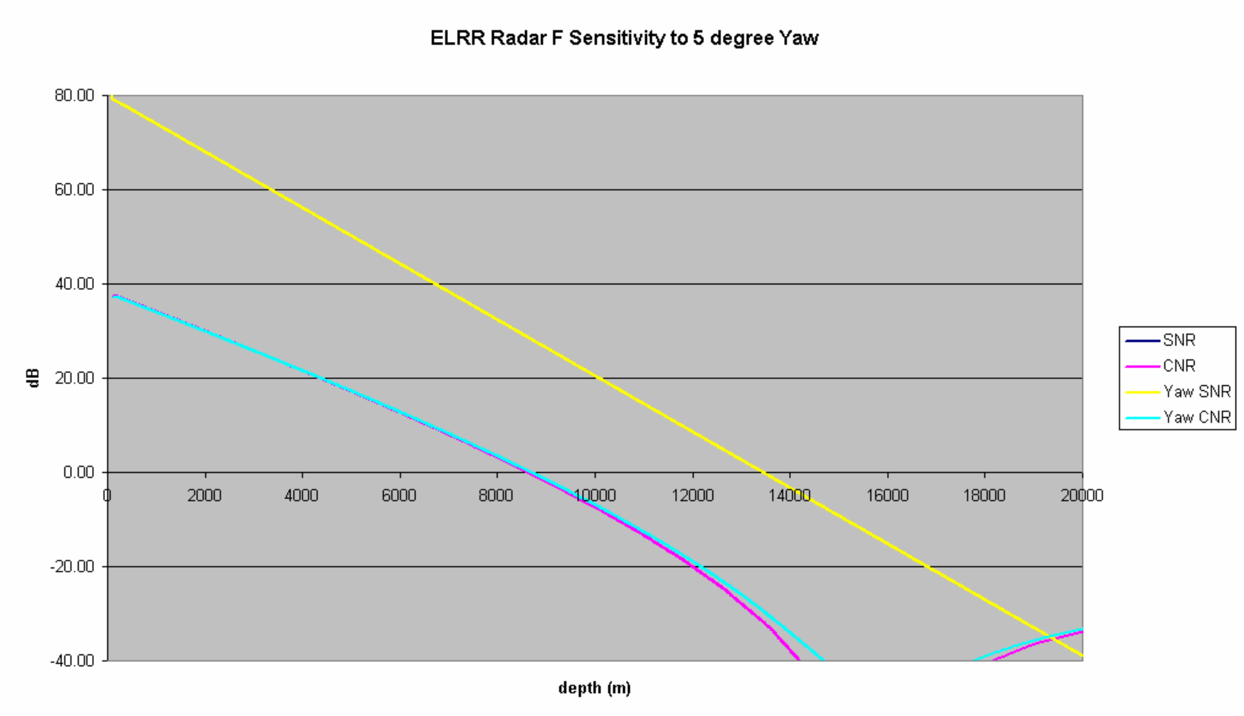


**Figure 5-10: Radar F sensitivity to 5-degree yaw**

*1.1.1.1.8 Roll*

An error in the roll pointing is very much the worst case in terms of performance; the gain obtained from the mainlobe is effectively reduced and more significantly so, as compared to the pitch case, since the mainlobe rolls off faster in the across-track direction. Also, the sidelobes away from the roll are effectively reduced while those towards the roll are equally increased. The roll error was modelled therefore by subtracting 5 degrees from the *x*-values of the antenna pattern before running the analysis. The result of this was a reduced mainlobe gain of 0.38 dB which barely influences the penetration depth. The impact on the CNR was, however, much more significant, particularly for radar A where the ambiguous clutter returns serve to mask the deep returns at around 10 km instead of 13 km without roll error (see Figure 5-11).

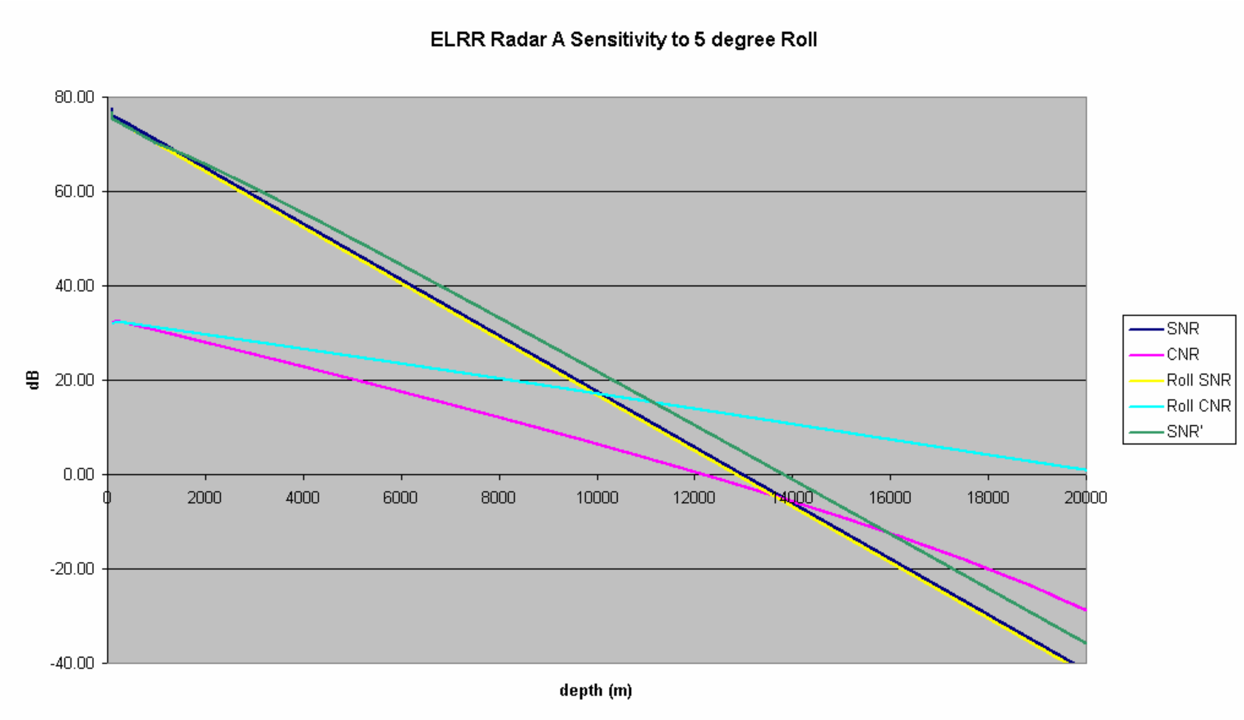


**Figure 5-11: Radar A sensitivity to 5-degree roll**

By contrast, the performance of radar F is unaffected by 5 degrees of roll error since, as a result of the lower altitude, the clutter appears at much higher incidence angles than for radar A. These returns are suppressed much more by the antenna pattern (see Figure 5-12).

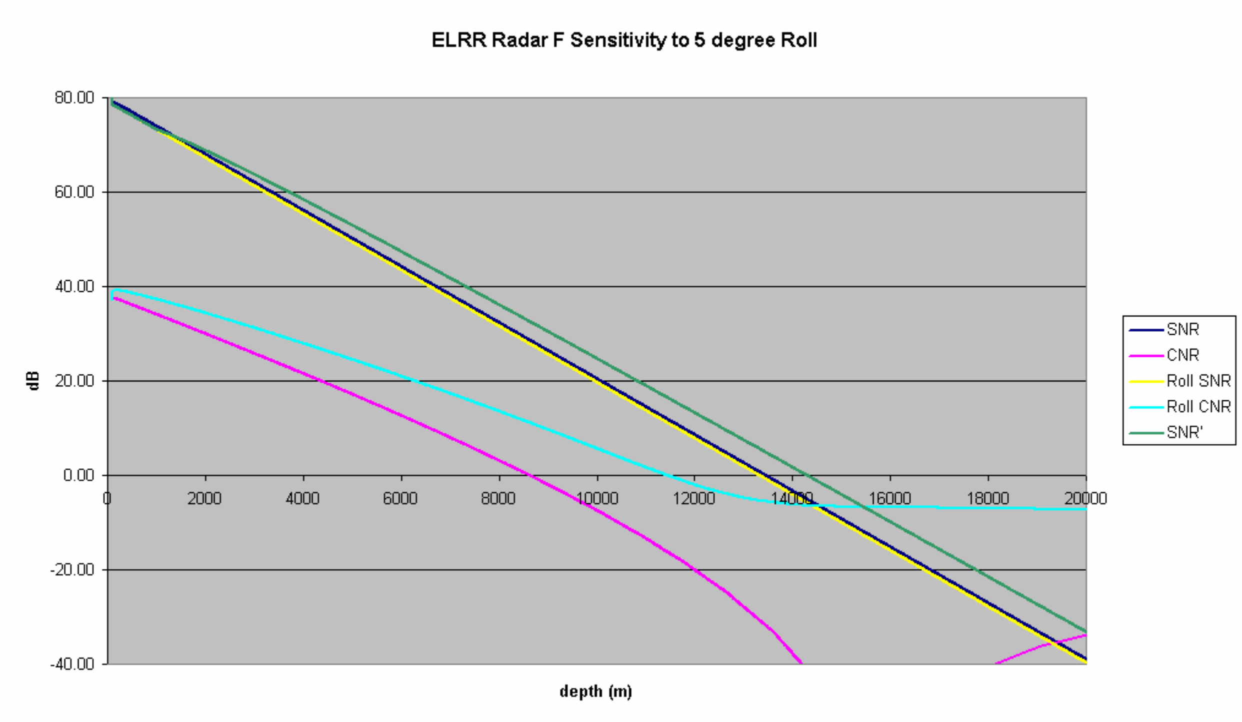


**Figure 5-12: Radar F sensitivity to 5-degree roll**

From the above analysis it is clear that although relatively high errors in pitch and yaw pointing are tolerable, any error in the roll attitude of the spacecraft should ideally be kept very low. However, if a lower orbit is acceptable, even 5 degrees of roll error need not seriously impair the ice penetration performance of the radar.

##### *1.1.1.1.9 Summary*

The 300 km orbit option was dismissed due to the additional $1/h^2$ loss and the mainlobe roll-off being too slow meaning that it was clutter limited rather than noise limited at depth. The 200 km orbit option is possible but depth penetration is not as good as for the 125 km orbit case, again due to the $1/h^2$ loss and it is more affected by roll than for the 125 km orbit. Overall therefore, the 125 km orbit is the preferred option from a radar performance viewpoint. However, this has a negative impact on the power supply (see section 12.3).

### 5.3.3 Baseline design

The parameters defining the baseline design of the Europa Low Resources Radar are listed in Table 5-5:

| Parameter | Value | Comment |
|---|---|---|
| Centre frequency | 50 MHz | |
| Altitude | 200 km | *125 km reserved as option – better penetration, better roll error tolerance* |
| Bandwidth | 850 kHz | *2.55 MHz reserved as option – increased penetration and data rate* |
| PRF | 3300 Hz | |
| Duty cycle ratio | 10% | *Could be increased to reduce peak power demand – would result in some reduction in averaging gain = penetration depth* |
| Pulse length | 30 µs | *At 10% duty cycle ratio* |
| Peak transmit power | 375W | |
| Antenna directivity | 12 dBi | |

**Table 5-5: ELRR baseline design parameters**

## 5.4 Conclusions

The main conclusion is that, from an instrument point of view, the radar is feasible and that once in low orbit around Europa it will be able to penetrate the ice to a depth of around 14 km, assuming the ice properties and 'dusty ice' model derived in Chapter 4, Wave Interaction Analysis. Theoretically, penetration might even be higher if some shielding from the background noise emanating from Jupiter is afforded when flying behind Europa.

The sensitivity of the radar is improved somewhat by flying lower, but also a significant benefit to the instrument of being in a lower orbit would be its much improved insensitivity to roll error. Other ways to extend the depth penetration of the radar are limited to increasing the bandwidth but at the expense of increased data rate and instrument complexity. Any further improvement in gain through, higher power, better efficiency, larger antenna and so on results in an improvement in penetration depth at a rate of only 150 m/dB.

# 6 INSTRUMENT ELECTRONICS

## 6.1 Requirements and design drivers

The central unit of the Europa Low Resource Radar is the Instrument Electronics. It shall comprise all the functionality of the radar and interface with the antenna for the transmission and reception of the radar signal. It provides a control and data interface towards the central Digital Processing Unit (DPU) that is implemented as one common unit for all payload instruments following the HIPS approach. The third electrical interface is towards the central power-conditioning unit.

The primary functions to be implemented in the instrument electronics are the following:

- Internal instrument control and house keeping
- Coherent timing generation
- Coherent frequency generation
- Transmit signal synthesis
- Frequency up-conversion to the RF band
- RF power amplification
- RF output power sensing
- Transmit-receive switching
- Low noise receive signal amplification
- Frequency down-conversion
- Analogue to digital conversion
- Radar data transmission to the DPU

Several radar data processing functions are foreseen for implementation in central DPU:

- Data compression processing
- Radar data packet formatting
- Receive radar data storage
- Master instrument control and interface to the OBC

| Parameter Name | Abbreviation | Value | Unit |
|---|---|---|---|
| Radar centre frequency | $f_c$ | 50 | MHz |
| Bandwidth | B | 0.84 | MHz |
| Sampling frequency | $f_{ADC}$ | 0.924 | MHz |
| Peak radiated output power | $P_{out}$ | 375 | W |
| Pulse repetition frequency | PRF | 3300 | Hz |
| Pulse length | $\tau_P$ | 30 | µs |
| Echo window length | $\tau_{echo}$ | 269 | µs |
| Maximum SNR of compressed echo | $SNR_{max}$ | 80 | dB |
| Orbit height | H | 200 000 | m |
| Europa radius | $R_{EUR}$ | 1 561 000 | m |
| Europa gravitational constant | $\mu_{EUR}$ | $3.2 \cdot 10^{12}$ | $m^3/s^2$ |

**Table 6-1: System parameter provided by instrument system for the Chirped Doppler Radar design**

Table 6-1 shows important parameters and their size as required by the instrument system. These nominal values are used for the trades performed and in the design of the radar instrument.
The main design driver for the Europa Low Resource Radar development is the stringent mass and power requirements defined by the mission. To fulfil these requirements, different radar instrument principles are investigated for their suitability.

## 6.2 Assumptions, design calculations and trades

The main function of a radar instrument is to measure time between the transmission of a pulse and the arrival of its echo that has been reflected by some object. If there are a number of objects at different distances, just like the subsurface features of Europa, a time series of the received echoes is recorded. The ability to distinguish two separate objects at different distances is referred to as range resolution. One way to achieve this range resolution is to use a short transmit pulse which is only half as long as the required range resolution. The disadvantage of such a short-pulse radar is that it requires a very high peak transmit power to fit the required signal energy in such a short period of time. However, there are several other radar instrument operating principles that overcome this problem and these are discussed below.

### 6.2.1 Stepped Frequency Radar

The Stepped Frequency Radar principle is simple with respect to the required hardware. For example, a vector network analyser can be easily used to produce an experimental radar for the laboratory environment. The principle is very popular for near-range and ground-penetrating radars. A typical functional diagram is shown in Figure 6-1 where the frequencies generated and transmitted between the units are indicated (RD[19]).

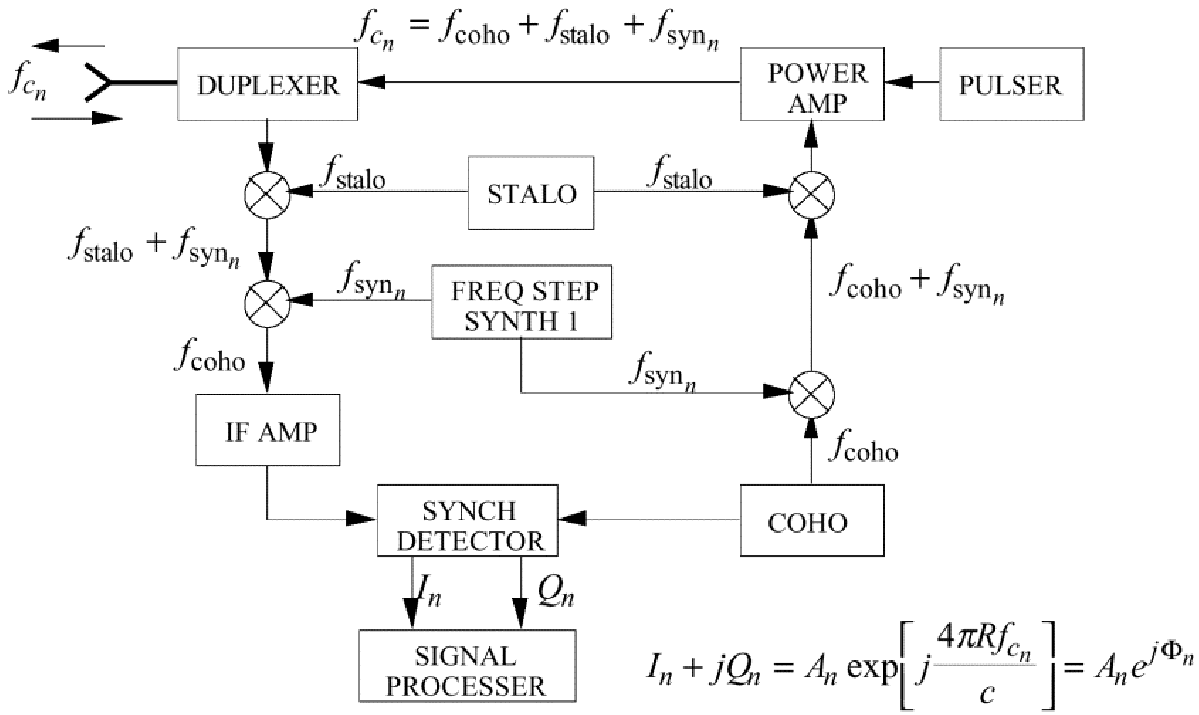


**Figure 6-1: Block diagram of a Stepped Frequency Radar (by David Jenn)**

The Stepped Frequency Radar sends out a series of long pulses containing only the sinusoidal signal of one specific frequency. The pulse length has to be long enough so that the echoes from all points in the target area overlap in at least one point in time at the location of the radar receiver. For every transmitted pulse only one echo signal sample is taken containing the amplitude and the phase. The bandwidth $B$ of the transmitted pulse is inversely proportional to its length $\tau_p$: $B=\tau_p^{-1}$. Therefore the instantaneous receiver noise bandwidth can be also made very small. This has a direct benefit for the radar equation. With a reduction of the noise bandwidth the transmit power can be also reduced by the same factor.

For the 20 km long target area in ice this means that the transmitted pulse must be at least 240 µs long, leading to a minimum instantaneous receiver bandwidth of $B_{instant}$=4.2 kHz. This must be compared to the $B$=840 kHz global bandwidth required for the 100 m depth resolution. The peak transmit power of the Stepped Frequency Radar compared to the Pulsed Doppler Radar could be reduced by 23 dB for the ELRR case. For the global energy balance, note also that the required transmit duty cycle is significantly longer in the stepped frequency case and the several pulses are required to measure the complete range line.

The range resolution of the Stepped Frequency Radar is obtained by transmitting and sampling a series of long pulses at different frequencies covering the $B$=840 kHz global bandwidth required. The minimum number of steps required is therefore $N=B/B_{instant}$=200. The result of a Fourier transform performed on the series of data samples provides the desired measurement, that is, the reflected signal strength as a function of distance that is called “range line”.

For the operation of the ELRR it is important to perform Doppler focusing in the along-track direction. This is to eliminate forward and backward returns from the echo signal. For the Doppler focusing it is essential that the full radar returns are sampled along the flight path with a distance less than half the wavelength <λ/2 = 3m. This means for the Stepped Frequency Radar that all 200 pulses have to be sent during this time. Taking the minimum pulse length required to cover the 20 km scene multiplied by 200 gives a minimum time of 48 ms required for one range-line measurement. This time translates into a maximum allowed platform speed of 62.5 m/s. This is 22 times slower than the satellite velocity of 1350 m/s of the required orbit around Europa. This therefore excludes the possibility of using the Stepped Frequency Radar for the ELRR.

### 6.2.2 Chirped Doppler Radar

The Chirped Doppler Radar overcomes the difficulty of the Short Pulse Radar, in terms of the very high required peak output power. Instead of transmitting a short pulse, a long but frequent modulated pulse is transmitted. The bandwidth contained in both pulse types must be the same and correspond to $B = \frac{c}{2\rho_z\sqrt{\varepsilon_r}} = \frac{1}{\tau_{short}} = 840\ kHz$ where $\rho_z$ is the required depth resolution of 100 m in the ice, c is the speed of light, $\varepsilon_r$ is the relative permittivity of ice and $\tau_{short}$ is the pulse length. This long pulse, which is called a linear chirp if the frequency is modulated linearly over time, is later compressed by means of signal processing. For the proposed system parameters given in Table 6-1 the long pulse is compressed in time by a factor of 25. The required peak signal power is reduced by the same factor compared to the short-pulse radar.

Due to the long pulse, the receive echo window has to be enlarged by one pulse length to collect all information. It can be reduced again after the pulse compression. The receive signal must be filtered and mixed down to base band for signal sampling by means of analogue-to-digital conversion. Two different designs are frequently used here. They are called real and complex sampling.

For real sampling, the receive signal is mixed down to a base band centred at a frequency above half the signal bandwidth. Then this signal is sampled at a rate at least twice as high as the signal bandwidth. Special care has to be taken during the mixing and the filtering to suppress the part of the spectrum that otherwise could pollute the lower side band of the signal. For this purpose, an additional intermediate frequency stage is often introduced in the frequency conversion scheme to simplify the filtering.

The other alternative is to use in-phase/quadrature (I/Q) down conversion. This is to mix down the signal to zero Hertz centre frequency using two channels and with the modulation frequency of the second channel being offset by 90 degrees in phase. Both channels are sampled synchronously at a rate corresponding to one times the signal bandwidth and their output represents the real and the imaginary part of the equivalent baseband signal. This complex signal can then be directly used in the following signal processing steps. Due to the simplified filtering, the I/Q down conversion is selected as the preferred solution.

#### 6.2.2.1 Pulse compression with analogue de-ramping

There are also two different approaches for the pulse compression. The first is called de-ramping and is frequently used in radar altimeters. The receive signal is mixed with a frequency ramp with the opposite rate of the chirp in the transmit signal. This leads to a signal where return from every range is mixed to one specific frequency. In the second step, a Fourier transform has to be performed to compress the de-ramped signal.

This type of analogue de-ramping is particular beneficial for radar systems where the target area to be covered is much shorter than the transmit pulse length (like for an altimeter). In this case, the bandwidth of the de-ramped signal is significantly reduced simplifying the signal sampling. The disadvantage of de-ramping is that it has to relay on a linear chirp. Advanced techniques for the reduction of the range side lobes in the compressed signal cannot be used.

#### 6.2.2.2 Digital pulse compression

The same operation as with the analogue de-ramping can be also performed on the sampled and digitised signal. For this the sampled signal is first multiplied with a frequency ramp and then a FFT (Fast Fourier Transform) is performed. To avoid ambiguities between returns from different distances, the processing of the complete range line has to be split up in several sections. The limitations of this approach are the same as described for the analogue de-ramping case.

Alternatively the pulse compression can be performed with a digital pulse compression filter. This consists of performing first a FFT on the echo data, then performing a multiplication with the pulse compression filter that could be the conjugate complex spectrum of the pulse in the simplest case. An IFFT (Inverse Fast Fourier Transform) is performed on the result to obtain the compressed pulse. This processing is not dependent on a linear chirp because the transmit signal and also the pulse compression filter can be designed to fulfil specific requirements or to compensate for imperfections of the instrument.

At first glance the computational complexity of the pulse compression filter appears to be higher because it requires the calculation of two FFTs. On the other hand, the digital de-ramping will require a split up of the data in overlapping sections, to perform overlapping short FFTs and to re-sort the data at the end. A detailed trade-off, taking also the processing hardware into account, should be performed to determine which approach is more efficient.

The purely digital pulse compression is preferred over the analogue de-ramping due to the simpler analogue hardware and the higher flexibility of the digital solution. A pulse compression on board is only required if the radar echoes are detected and averaged. This will be the case only in the proposed Low Resolution Mode described later.

### 6.2.3 HPA Assembly sizing, power consumption and dissipation

The High-Power Amplifier (HPA) Assembly comprises all equipment needed for high RF power amplification, the power conditioning for the pulsed power amplifier and the transmit/receive switching. The efficiency figures provided are based on a Solid State Power Amplifier (SSPA) operating in Class-E including the necessary pre-amplification. The Electronic Power Conditioner (EPC) included in the HPA Assembly has the task to stabilise and buffer the energy for the periodic load of the pulsed HPA.

A peak radiated output power of 375W is required by the instrument system. To size the HPA in the HPA Assembly, the expected losses in the path from the HPA to the antenna have to be taken into account. From the requirement and the assumed losses a minimum peak radiated output power is calculated. This figure is used to specify a design requirement for the peak output power of the HPA and to determine the resulting HPA peak radiated output power according to the design requirement (see Table 6-2):

| Parameter | Symbol | Value | Unit | Description |
|---|---|---|---|---|
| Minimum peak radiated output power | $P_{OUT\_min}$ | 375 | W | Minimum peak radiated output power required by the system |
| Transmit path loss | LTX | 0.3 | dB | Assumed transmit path loss – path from HPA to antenna incl. Tx-rx switch |
| Minimum HPA output power | $P_{HPA\_min}$ | 402 | W | Minimum required peak output power provided by the HPA, $P_{HPA\_min} = 10^{\frac{LTX}{10}} \cdot P_{OUT\_min}$ |

**Table 6-2: High-Power Amplifier output power sizing**

According to the design requirement for the HPA peak output power and the assumed transmit path losses, the DC power consumption and dissipation of the HPA Assembly is calculated. It is based on estimates of the HPA and EPC efficiencies and includes also a power margin of 20% because the HPA Assembly is a new development. The dissipation of the HPA Assembly is calculated by subtracting the radiated RF power from the HPA Assembly DC power consumption (see Table 6-3). The radar duty cycle describes the percentage of time within one orbit, for example, where the radar is making measurements. The rest of the time the radar instrument is assumed to be switched off. This is a top level parameter in general determined by the overall mission requirements according to the target location, extension and available time for imaging. The transmit duty cycle in contrast is a low-level instrument parameter describing what percentage of the pulse repetition interval (PRI) – that is the time between the start of two consecutive pulses) the radar is actually transmitting. The time within one PRI where the radar is not transmitting is used to receive the echo. Radio isolation constraints generally prohibit reception while a signal is transmitted.

| Parameter | Symbol | Value | Unit | Description |
|---|---|---|---|---|
| Transmit duty cycle | $dc_{TX}$ | 10 | % | $dc_{TX} = PRF \cdot \tau_P$ |
| HPA efficiency | $\rho_{HPA}$ | 80 | % | Class-E operation including pre-amplification |
| EPC efficiency | $\rho_{EPC}$ | 95 | % | Efficiency of power conditioning |
| Margin on power | $\delta_{power}$ | 20 | % | Item to be developed |
| HPA DC power consumption | $P_{HPA\_DC}$ | 63.43 | W | HPA Assembly power consumption including margin $P_{HPA\_DC} = \left(1 + \delta_{power}\right)\frac{P_{HPA} \cdot dc_{TX}}{\rho_{HPA} \cdot \rho_{EPC}}$ |
| HPA power dissipation | $P_{HPA\_diss}$ | 25.96 | W | Calculated dissipated power incl. Margin $P_{HPA\_diss} = P_{HPA\_DC} - \left(P_{OUT} \cdot dc_{TX}\right)$ |

**Table 6-3: High-Power Amplifier power dissipation sizing**

If it proves to be difficult to construct a High-Power Amplifier with 402W peak output power, the overall radar transmit duty cycle could be increased to up to 40% which will reduce the required peak power by a factor of four and reduce the PRF by a factor 4.5. This will have to be paid for with a reduction of gain of about 3 dB.

### 6.2.4 Number of bits required for analogue-to-digital conversion

The required number of bits for the analogue-to-digital conversion has to be determined according to the maximum SNR of the received echo signal. This ensures that the quantisation noise added by the Analogue to Digital Converter (ADC) is below the level of the noise present in the channel due to other contributions. The Signal to Quantisation Noise Ratio (SQNR) of a linear ADC is described by the following formula where $N_{bit}$ is the number of bits in the ADC:

$$SQNR = 6 \cdot N_{bit} - 1.25\,dB$$

The second effect that has to be taken into consideration is the use of a long-pulse radar. It employs pulse compression to achieve the final resolution. For specular reflections this means an increase of the SNR by a factor determined by the time bandwidth product of the pulse. As the maximum expected SNR is given for the "pulse compressed" signal, it has to be divided by this factor to obtain the maximum, raw data SNR, which is the basis to size the ADC.

| Parameter | Symbol | Value | Unit | Description |
|---|---|---|---|---|
| Pulse compression gain | $G_{pulse}$ | 14.06 | dB | $G_{pulse} = \tau_P \cdot B$ |
| Maximum SNR uncompressed raw surface echo | $SNR_{raw}$ | 65.94 | dB | $SNR_{raw} = SNR_{max} - G_{pulse}$ |
| Minimum number of bits for quantisation noise | $N_{ADC\_min}$ | 11.2 | bits | $N_{ADC\_min} = \dfrac{SNR_{raw} - 1.25}{6}$ |
| Number of ADC bits | $N_{ADC}$ | 14 | bits | Selected design requirement for the number of ADC bits |

**Table 6-4: Determination of the number of bits required for the ADC**

The result of the calculation shows that a minimum of 11.2 bits is required to cover the dynamic range. 14 bits were selected as design requirement for the number of bits of the ADC needed to still have some margin for variation of the reflectivity (see Table 6-4).

### 6.2.5 On-board data compression

With the system parameters given in Table 6-1 and Table 6-4 the burst raw data rate at the output of the ADCs will be 25.9 Mbit/s. This raw data rate is much too high for transmission to Earth and some extensive data reduction has to be performed to comply with the required maximum data rate.

#### 6.2.5.1 Full Resolution Mode

For the ELRR the signal of interest is the Europa subsurface echo return. This is the echo signal entering the antenna from the direction of the subsatellite point. Besides this echo signal the antenna also allows signals coming from forward and backward direction entering the receiver. This is due to the limited directivity of the antenna. Because of the relative motion between the satellite and the Europa surface the signal from forward and backward direction are shifted in Doppler frequency. This results in a spectral spread of the receive signal which, in turn, requires the relatively high PRF to avoid aliasing. The signal from the direction of the subsatellite point has no Doppler shift because the relative motion is only in the lateral direction.

This fact can be employed to extract only the echo signal coming from the subsatellite point by Doppler filtering. The Doppler filter shall be adapted to a target zone length of 1550 m corresponding to the 1st Fresnel zone. The simplest form of Doppler filtering is known as pre-summing where a synthetic aperture is formed by summing up a number of subsequent radar echoes. More elaborated filtering perform weighted summation echoes.

As a result of the Doppler filtering the dynamic range of the radar echo increases. This has to be taken into account by either increasing the number of bits in the integer representation or by changing to a floating-point format. It is recommended to use a complex hybrid short floating point format for the complex output data of the Doppler filter. A complex hybrid short number has 32 bits, where together 12 bits represent the real and imaginary mantissa and the other 8 bits represent one common exponent.
The net compression factor resulting from this operation is 828 (see Table 6-5), thus reducing the continuous data rate to 28 kbit/s including a radar header of 80 bit per range line. The data processed in this way are said to be in the Full Resolution Mode. They still contain all phase information and represent a measurement of 340 m on the ground.

| Parameter | Symbol | Value | Unit | Description |
|---|---|---|---|---|
| Diameter of target zone | $L_{target}$ | 1550 | m | Defined by the expected size of the Fresnel zone |
| Synthetic aperture length corresponding to a resolution of the target zone diameter | $A_{syn}$ | 385 | m | $A_{syn} = \frac{c_0 \cdot H}{2 f_c \cdot L_{target}}$ |
| Sampling distance | $\delta x$ | 0.4 | m | $\delta x = \frac{v_{sat}}{PRF}$ |
| Number of pulses in synthetic aperture | $n_{syn}$ | 947 | | $n_{syn} = \frac{A_{syn}}{\delta x}$ - Selected number of pulses in synthetic aperture. By this factor the number of pulses can be reduced. |
| Number of bits per complex sample | $N_{cplx}$ | 32 | bit | Number of bits in the complex hybrid short format used at the output of Doppler filtering |
| Net compression factor | $F_{comp}$ | 828 | | Resulting compression factor of the Doppler filter processing |

**Table 6-5: Doppler filter processing to achieve raw data compression**

#### 6.2.5.2 Reduced Resolution Mode

In the Reduced Resolution Mode, the along-track round resolution is reduced to 10 km with an along track sampling every 5 km. It is based on incoherent averaging of Full Resolution Mode data. The depth resolution remains unchanged 100 m for all depth.
First the radar echoes are range compressed and detected therefore all phase information is lost. Then 14 pulses are averaged to form one range compressed, multi-look range line. The resulting data are stored in a short floating point format of 20 bits length, containing 12 bits for the mantissa and 8 bits for the exponent.
The continuous data rate after this processing step will be 1.1 kbit/s corresponding to an additional compression factor of 25 (see Table 6-6).

The instrument operation can be selected to image different areas of Europa in either Full or Reduced Resolution Mode to be overall compliant with the available signal bandwidth for the data transmission to Earth.

| Parameter | Symbol | Value | Unit | Description |
|---|---|---|---|---|
| Radar header | $H_{RADAR}$ | 80 | bit | Per range line |
| Bits per range line | $N_{range}$ | 7052 | bit | $N_{range} = f_{ADC} \cdot \tau_{echo} \cdot 2 \cdot N_{ADC} + H_{RADAR}$ |
| Data rate at ADC output | $DR_{ADC}$ | 25.872 | Mbits/s | $DR_{ADC} = 2 \cdot N_{ADC} \cdot f_{ADC}$ |
| Bits per pre-summed range line | $N_{range\_pre-summed}$ | 8048 | bit | $N_{range\_pre-summed} = f_{ADC} \cdot \tau_{echo} \cdot N_{cplx} + H_{RADAR}$ |
| Data rate after pre-summing | $DR_{pre-summed}$ | 27.994 | kbits/s | $DR_{pre-summed} = \frac{N_{range\_pre-summed} \cdot PRF}{n_{syn}}$ |
| Number of bits per detected sample | $N_{real}$ | 20 | bit | Number of bits in the real short format used at output of the detection and multi-looking |
| Number of along track looks | $n_{looks}$ | 14 | | Number of detected range lines summed up to obtain one resulting pulse every 5 km ground distance corresponding to an along-track resolution of 10 km |
| Bits per range compressed range line | $N_{range\_compressed}$ | 4500 | bit | $N_{range\_compressed} = f_{ADC} \cdot \tau_{echo} \cdot N_{real} + H_{RADAR}$ |
| Data rate after multi-looking | $DR_{multi-look}$ | 1.118 | kbit/s | $DR_{multi-look} = \frac{N_{range\_compressed} \cdot PRF}{n_{syn} \cdot n_{looks}}$ |

**Table 6-6: Instrument data rates**

## 6.3 Baseline design

The baseline design described in this section provides the basic radar functions to fulfil the requirements on the instrument electronics. It further takes into account the trades and evaluations made in section 6.2.

The ELRR instrument electronics is split into two units: the Radar Electronics and the High Power Amplifier Assembly. The instrument electronics use the regulated power supply of the centralised Payload Power Conditioner and the data processing power in the centralised DPU for the data compression processing and data storage. This is in line with the Highly Integrated Payload Suite (HIPS) concept that is to be applied. The instrument electronic will include a prime and a redundant unit of both electronic units, all integrated in one common flight box. The primary units and their interconnections are shown in Figure 6-2:

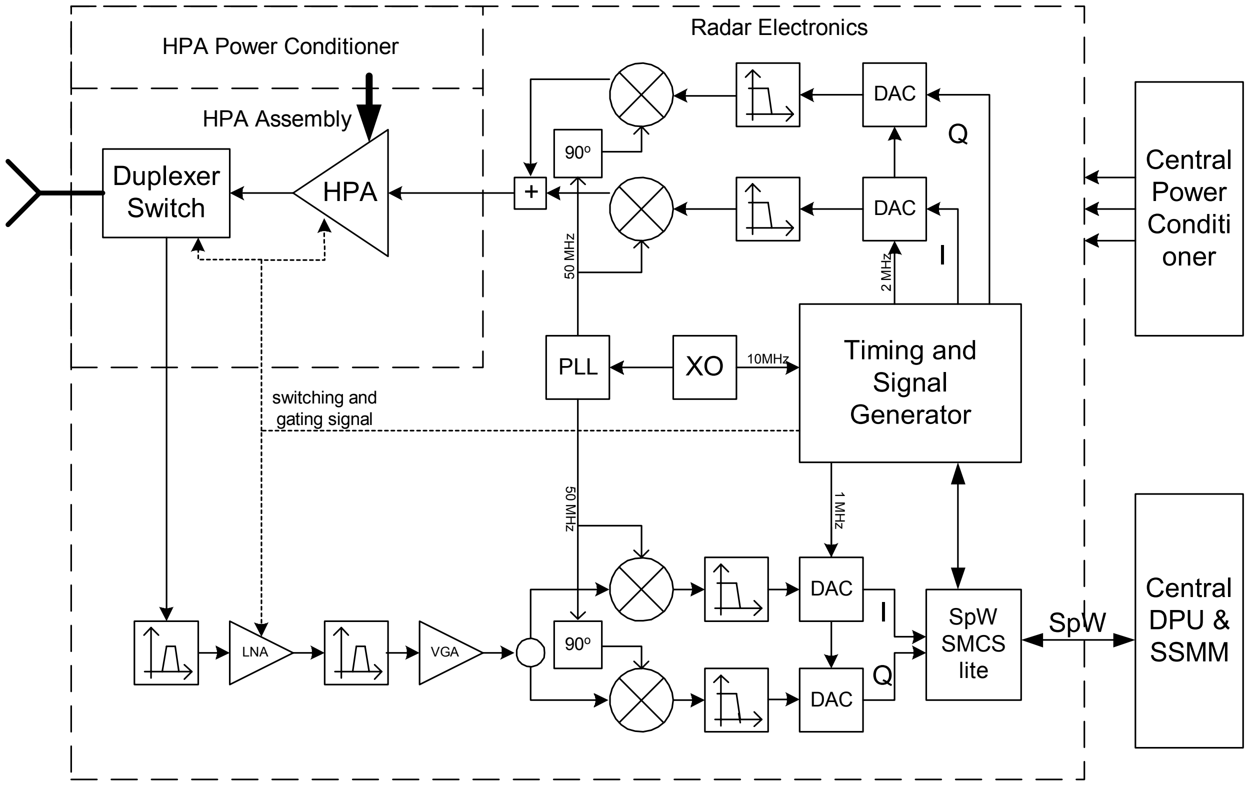


**Figure 6-2: Radar instrument design comprising Radar Electronics and HPA Assembly**

## 6.3.1 Radar electronics

### 6.3.1.1 Radar electronics functional requirements

The radar electronics have to perform the following functions:

- Internal instrument control and house keeping
- Coherent timing generation
- Coherent frequency generation
- Transmit signal synthesis
- Frequency up-conversion
- Low noise receive signal amplification
- Frequency down-conversion
- Analogue-to-digital conversion
- Radar data transmission to the DPU

### 6.3.1.2 Radar electronics design

The radar electronics combines all digital as well as all RF functions in one highly integrated circuit board. The Timing and Signal Generator is the core unit for all radar functions. It is implemented in one Filed Programmable Gate Array (FPGA) (or one Application Specific Integrated Circuit (ASIC) if required due to radiation) and includes the chirp signal generation using the Direct Digital Synthesis (DDS) principle. Further it includes the generation of all timing and switching signals required by the radar. Its operation and the mode switching in the Radar Electronics are controlled via the SMCS-lite SpaceWire link interface by the central DPU. The clock is derived from the same Stable Oscillator that is used for the modulation frequency synthesis performed by a PLL (Phase Locked Loop). The chirp signal, which is synthesised in the baseband, is directly up converted to the radio frequency using I/Q modulation and subsequent filtering to generate the RF transmit signal.

On the receive side, the received echo is filtered and low noise amplified before being I/Q demodulated. A LNA noise figure of 1.5 dB, in addition to a 1 dB receive path loss due to the switch and the filter, appears realistic at 50 MHz. The subsequent analogue-to-digital conversion operates only with 10% oversampling to keep the data rate low and therefore requires a good anti-aliasing filter. The data are transmitted per range line in bursts via the SMCS-lite and the SpaceWire link to the central DPU. The data compression to Full Resolution as well to Reduced Resolution mode is performed in the DPU. The power consumption during the radar operation is estimated to be 3W.

If the size of the FPGA or ASIC to be qualified for the radiation environment around Europa is sufficiently large, the SpaceWire interface as well as the Doppler filtering could be integrated into the Timing and Signal Generator. Then only Full Resolution Mode radar data are transmitted to the DPU allowing a much slower data rate.

### 6.3.2 High-Power Amplifier Assembly

#### 6.3.2.1 High-Power Amplifier Assembly functional requirements

The High-Power Amplifier Assembly has to perform the following functions:

- RF power amplification
- RF output power sensing
- Amplifier electrical power conditioning
- Transmit-receive switching

#### 6.3.2.2 High Power Amplifier Assembly design

The High-Power Amplifier (HPA) shall use an amplifier operating in Class-E in its output stage. The transistor in a Class-E amplifier acts as an on/off switch with a resonant output network. Power efficiencies of up to 90% can practically be achieved with this amplifier circuit design. In addition a minimum of two driving amplifier stages will be needed to provide the required overall power gain of about 50 dB.

Using commercial MOS-FET transistors as a reference it appears feasible to obtain the required output power of 402W using two power transistors in parallel in the output stage. Taking a transmit path loss of 0.3 dB into account, the RF output power results to 375W. The Diplexer performs the switching between transmit and receive. It is based on PIN diodes to allow fast switching in combination with low loss at the same time. For the switching between the primary and the redundant RF chain, a mechanical switch can be used.

Each of the redundant HPAs is equipped with an Electrical Power Conditioner (EPC) of its own. This is required as the central Power Conditioning Unit is not prepared to serve the specific needs of a pulsed load with a high power consumption like the HPA. The EPC will provide all voltages required by the HPA and on the other side act as a stable load according to the requirements of the Power Conditioning Unit. It is expected that the overall power added efficiency of the High Power Amplifier Assembly including the EPC will be above 75%. During the detailed design of the High Power Amplifier Assembly special care should be taken to avoid the possibility of multipaction. This shall also include the cable connectors.

## 6.4 Budgets

Table 6-7 gives an overview on the mass and size estimated for each unit and the resulting budget of the complete Radar Instrument Unit.
The primary and the redundant units are integrated in one flight equipment box with walls of 4 mm aluminium. While the prime and the redundant HPA assembly occupy a slice of their own the two radar electronics can fit together in one slice. This results in an extremely small and light-weight radar instrument.

| Element 2: ELRR (Payload 1) | | | MASS [kg] | | | | DIMENSIONS [m] | | |
|---|---|---|---|---|---|---|---|---|---|
| Unit | Element 2 Unit Name<br>Click on button below to insert new unit | Quantity | Mass per quantity excl. margin | Maturity Level | Margin | Total Mass incl. margin | Dim1 Length | Dim2 Width or D | Dim3 Height |
| 1 | Radar Electronics (prime) | 1 | 0.150 | To be developed | 20 | 0.180 | 0.150 | 0.075 | 0.015 |
| 2 | HPA assembly (prime) | 1 | 0.550 | To be developed | 20 | 0.660 | 0.200 | 0.150 | 0.040 |
| 3 | Radar Electronics (redundant) | 1 | 0.150 | To be developed | 20 | 0.180 | 0.150 | 0.075 | 0.015 |
| 4 | HPA assembly (redundant) | 1 | 0.550 | To be developed | 20 | 0.660 | 0.200 | 0.150 | 0.040 |
| 5 | Box structure | 1 | 0.800 | To be developed | 20 | 0.960 | 0.210 | 0.160 | 0.110 |
| 6 | Cable Assembly 1m incl conn. | 1 | 0.150 | To be developed | 20 | 0.180 | | | |
| - | Click on button below to insert new unit | | | To be developed | 20 | 0.000 | - | | |
| ELEMENT 2 SUBSYSTEM TOTAL | | 6 | 2.35 | | 20.0 | 2.820 | | | |

**Table 6-7: Overview of the mass and size budget**

### 6.4.1 Power

The radar electronics have an estimated power consumption of 3.6W including a 20% margin during radar operation. The High-Power Amplifier Assembly generates the RF power with an overall power added efficiency of 75%. With the 402W HPA peak output power and a transmit duty cycle of 10% this results in 63.5W average power consumption during radar operation including a 20% margin. Of this power, 26W is dissipated as heat in the unit.

### 6.4.2 Data rates

In the Full Resolution Mode with a depth resolution of 100 m and an along-track resolution of 1550 m, the average data rate is 28 kbit/s. In the Reduced Resolution Mode with a depth resolution of 100 m but with an along-track resolution of 10 km the average data rate results in 1.1 kbit/s.

## 6.5 Critical issues and conclusions

The main critical area for the radar instrument electronics is the availability of electronic components able to withstand the total radiation dose of 1 Mrad. This is specifically the case for the Power MOS-FET in the HPA and the EPC as well as for the VLSI digital components in the radar electronics.
As these components do not exist today the performance figures taken for the study can only be estimates based on commercial components.

Very stringent requirements on the mass and power allowed for the ELRR lead to an intensive use of data processing and power conditioning resources provided by the platform through HIPS. When reviewed from the overall system level, this might not always be the preferred solution for example, in case the HIPS has to provide additional resources only used by the radar. In this case, the functionality might as well be integrated in the radar itself, to simplify the interfaces and save overall mass and power.

# 7 ANTENNAS

## 7.1 Requirements and design drivers

The antenna to be designed is part of the low-frequency ground penetrating radar and this puts requirements on beam-widths, size and mass. In the next list the most important requirements are summarised:

- Gain around 12 dBi
- Beamwidth (-10 dB) around 50 degrees in across-track plane
- Frequency between 50-80 MHz
- Frequency bandwidth around 1 MHz
- Sidelobe and backlobe below –15 dB
- Dimensions not exceeding approx. 10-11x2-3m.

It should be noted that not all of the requirements are hard requirements, but should be used more as design drivers. For example, the dimensions of the final antenna will be limited by the maximum allowed stowed volume and by the way the deployment is achieved. The design strategy was to first provide an electrically viable design configuration and then to assess the constraints imposed by the mechanical deployment leading to mechanically coupled elements.

## 7.2 Assumptions, design calculations and trades

### 7.2.1 Basic antenna trade-off

To find an antenna solution that meets all of the above requirements and also has a low mass, only a few designs are feasible at these low frequencies. Possible principle antenna designs are the dipole and the Yagi Uda[1]. To make a selection between these two antenna types, the directivities and gain are computed for a dipole array and for a Yagi array and the results are listed in Table 7-1.

Table 7-1 shows that an array of dipoles is not sufficient if a gain of around 12 dBi is considered. The array of three Yagi Uda elements, however, is able to generate a beam with more or less the required gain. The explanation for this is that a single dipole antenna does not have a good forward gain because half of its power is radiated to the backside. By using a Yagi type of antenna instead of a dipole, most of the back radiation is eliminated (redirected) and more forward gain is achieved.

Initially, titanium was assumed as a conductor material and the low conductivity of this metal explains the relatively high conductor losses of 0.4-0.5 dB. A design of the three-element Yagi array is depicted in Figure 7-1:

[1] Invented by H. Yagi and S. Uda at Tokyo Imperial University (now Tokuha University), Japan in 1926.

| Antenna option | Directivity (dBi) | Gain (dBi) Ti |
|---|---|---|
| 1 x λ/2 dipole | 2.15 | 1.63 |
| 2 x λ/2 dipole | 5.16 | 4.64 |
| 3 x λ/2 dipole | 6.9 | 6.38 |
| 1 x 3 element Yagi | 7.85 | 7.46 |
| 2 x 3 element Yagi | 10.11 | 9.74 |
| 3 x 3 element Yagi | 11.64 | 11.27 |

**Table 7-1: Directivities and gain for antenna arrays of dipoles and Yagi Udas**

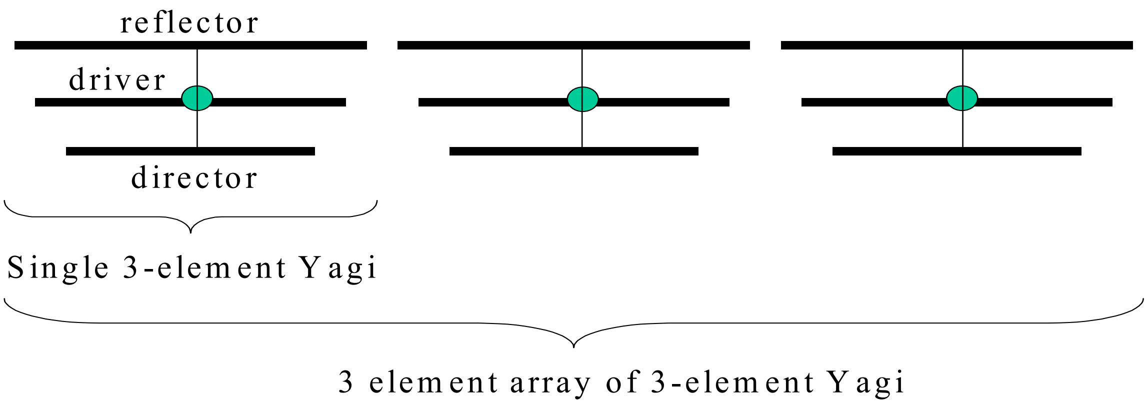


**Figure 7-1: Radar antenna design**

### 7.2.2 Optimisation of selected antenna

The selected Yagi array radar antenna configuration is made up of three separate (later mechanically coupled for optimum deployment design) Yagis each of which has three dipole elements. Only one of these dipoles is driven (central one) and the other two are needed for low backward radiation (reflector dipole) and improved forward directivity (director dipole). Normally, if the number of directors is increased the directivity also increases. However, the deployment of this array is a complex issue and a higher number of directors are not an option. Therefore, the only parameters to adjust in the further optimisation are the lengths of and the distances between the separate dipole elements. The excitation of the separate Yagi antennas is kept constant to achieve the highest possible gain. However, if for some reason the Yagi antennas become very different, it will be important to take the feeding law into account for the optimisation.

After the necessary optimisation runs, assuming straight dipoles and no interconnections in between the dipoles (for example isolators), the antenna design parameters become as follows:

- Reflector dipole length is 3 m
- Driver dipole length is 2.8 m
- Director dipole length is 2.76 m
- Distance from reflector to driver is 1.2 m
- Distance from driver to director is 0.76 m
- Distance between Yagi elements is 3.5 m (centre to centre)
- Thickness of dipole elements is 10 mm (diameter)
- Aluminium metal with electrical conductivity of 3.6 $10^7$ S/m

As an outcome of the radar system performance analysis (see Chapter 5, Instrument System Design), the frequency of operation has been set at 50 MHz, because of the favourable achievable penetration depth. A view of the resulting three-element Yagi array is shown in Figure 7-2 shown without mechanical coupling for deployment optimisation.

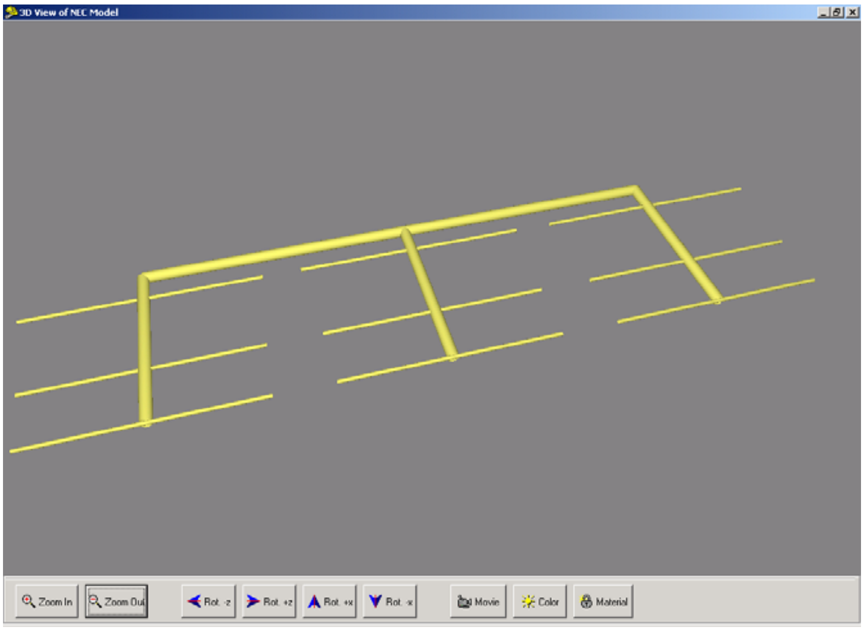


**Figure 7-2: 3D-view of the Yagi array**

The corresponding radiation pattern of the above antenna is given in Figure 7-3:

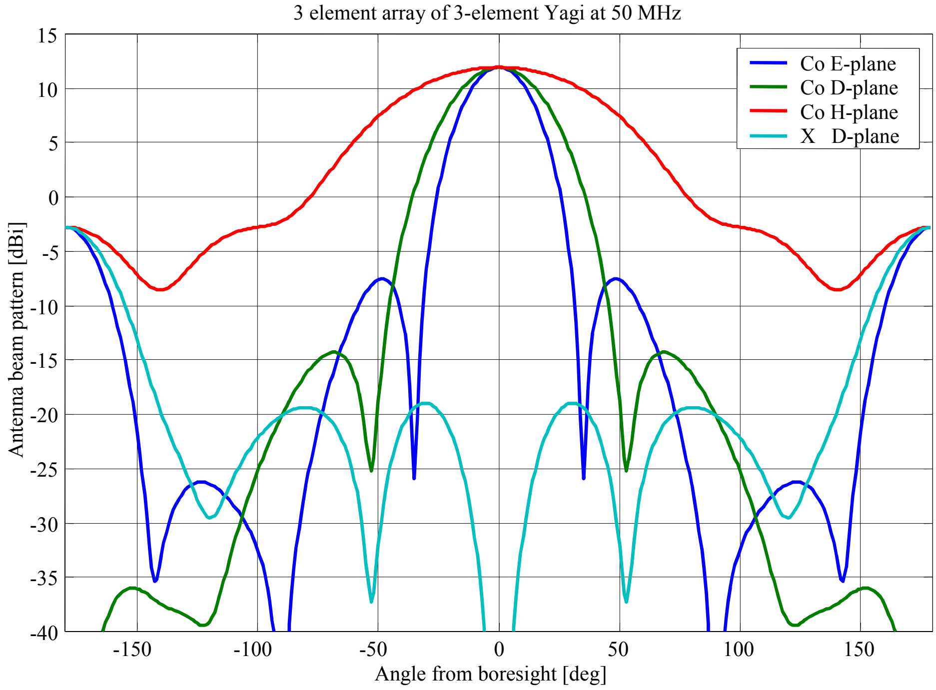


**Figure 7-3: Far-field radiation pattern**

The gain and 10-dB beamwidth of this Yagi array antenna are 11.9 dBi and 48.7 degrees, respectively. Both values meet or are close to the requirements. If the sidelobe (-20 dB) and backlobe levels (-15 dB) are considered, they also meet the requirements (as shown in Figure 7-3).

### 7.2.3 Frequency bandwidth

An important requirement for any radar antenna is its bandwidth. In this case, the ground penetrating radar needs a frequency bandwidth of around 1 MHz that corresponds at 50 MHz to 2%. Although the Yagi antenna consists of resonating dipole elements, this bandwidth should not pose any problem to the design of the antenna. Over the 2% bandwidth the following variations can be observed:

- Gain variation +/-0.2 dB
- Sidelobe variation +/-2 dB
- Backlobe variation +/-2 dB

These results are very dependant on the actual configurations, but similar results can be expected for other Yagi designs. Note however that the impedance matching has not been considered here, but for future work this should be taken into account.

### 7.2.4 Influence of satellite body and solar panels

Another important issue that needs to be checked is the influence of the satellite body and solar panels on the radiation properties of the Yagi antenna array. As the antenna could generate electric currents onto the spacecraft and solar panels, which could affect the antenna performance, the distance between the antenna and the spacecraft is a critical parameter. Typical distances of 0.5 m to 1.0 m were analysed, as these are the distances needed for deployment and stowage reasons.

To estimate the effect of the spacecraft and solar panels on the radiation properties of the Yagi antenna array, several simplified geometrical models were derived using the electromagnetic analysis software, Numerical Electromagnetics Code (NEC) RD[20]. The spacecraft body is modelled as a rectangular box and the solar panels as simple flat plates (see Figure 7-4). For this analysis, the dipole elements are not tapered and have a diameter of 10 mm and are shown without mechanical coupling as required for the deployment. Furthermore, all the structural parts (not the dipoles) are made of metal as well. Due to the orthogonal direction of most of these parts, as compared to the dipoles, their influence is negligible.

The conclusions of the analyses are that the spacecraft does not affect the radiation properties of the Yagi. Even if a larger satellite body is assumed there is no problem for the performance of the radar antenna. The minimum distance that should be respected is about 20-30 cm. A slightly larger distance is preferable for the performance of the antenna. Another conclusion is that the solar panels have very little effect due to the low backward radiation of the Yagi antenna array.

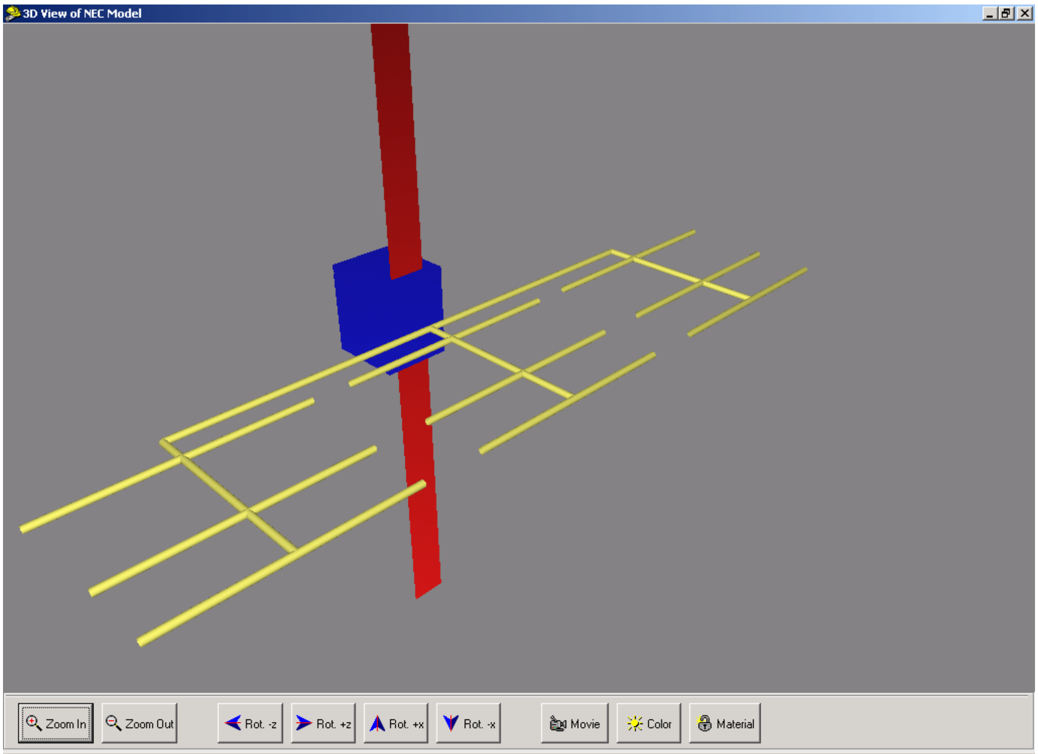


**Figure 7-4: Simplified model of Yagi antenna, spacecraft and solar panels**

### 7.2.5 Mechanical stability requirement

The mechanical stability is one of the important issues for the deployed radar antenna. Possible error sources are the deployment mechanism (hinges) and mechanical resonances due to AOCS operations. From an RF point of view both static and dynamical displacements can be treated as similar. Therefore, in the analysis it is assumed that some kind of worst-case bending of the dipoles exists (in any direction) and its influence on the radiation pattern is assessed. For the worst-case scenarios, symmetric as well as non-symmetric errors are analysed.

The results and conclusions of the extensive simulations are as follows:

- A λ/20 (30 cm) tip-tip displacement (in an arbitrary axis) of the dipoles is tolerable without significant degradation of the antenna performance.
- Gain variation is less than 0.1-0.2 dB, de-pointing of the antenna beam is negligible and lobes (side-lobe and back-lobe) change less than 1 dB.
- No radar performance degradation is expected with above variations.

### 7.2.6 Tapering of the dipole elements

To reduce the mass of the complete Yagi array antenna, without reducing the stiffness, a tapering of the dipoles was suggested. A visualisation of the tapering is shown in Figure 7-5 without the mechanical coupling for deployment, where it is clear that the single Yagi radiators are not identical anymore. A diameter tapering from 40 to 10 mm is assumed measured from the centre of the complete radar antenna to the tip. The thickness of the wires has been exaggerated for visualisation purposes only.

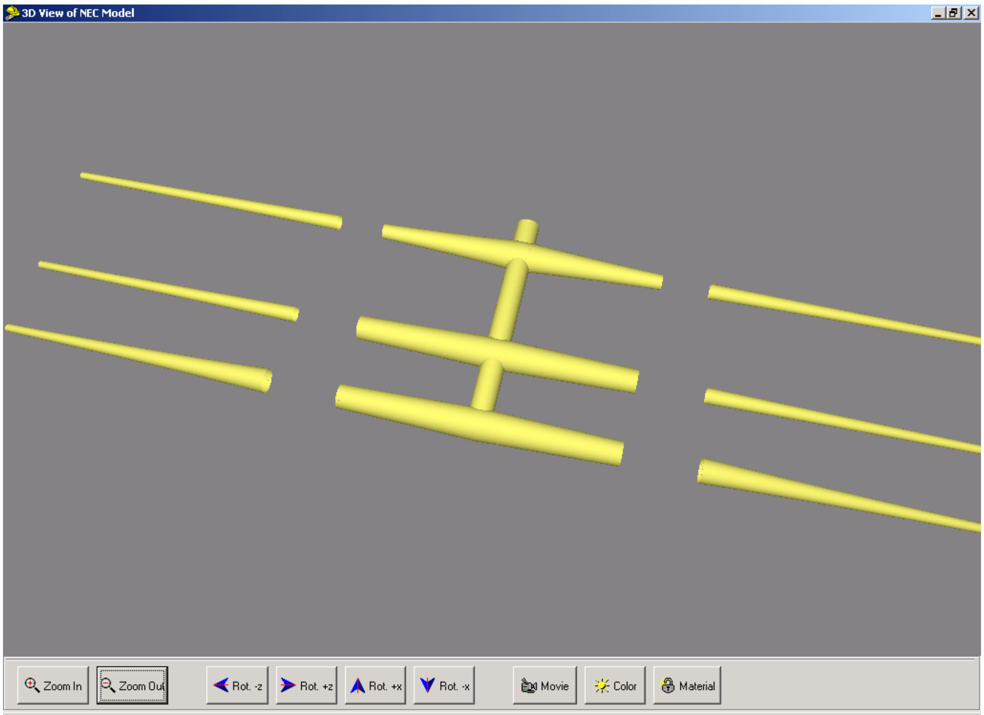


**Figure 7-5: Tapered radar antenna**

The conclusions of the simulations of the tapered radar antenna array are:

- Similar antenna performance (slightly lower) can be obtained as for the non-tapered design, but this requires a further optimisation.
- Due to the tapering, this optimisation has become more difficult (also antenna input impedance needs to be taken into account).
- Because the Yagi radiators are not identical in the case of a tapered design, a different feeding law (of the sources) has to be applied for optimum performance.

### 7.2.7 Conductivity of interconnecting tubes

To enable an easier deployment strategy, the adjacent dipole elements should be put on the same metallised CFRP tube. From an RF point of view, however, a proper operation of the array of Yagi antennas can only be assured if the dipole elements are separated by electrically isolating connections (represented by the thicker cylinders in Figure 7-6). This is due to the resonant behaviour of the dipoles that require a zero electric current at the ends of the elements. However, because it is not easy to find a material that provides excellent RF isolation, can withstand the harsh Jovian radiation environment and has also sufficient stiffness, it is important to determine the maximum electrical conductivity that is tolerable for the interconnecting tubes.

To see the effect of the electrical conductivity (σ) on the performance of the radar antenna, the radiation patterns and the electrical current distribution on the surface of the structure have been computed using NEC. Figure 7-6 shows the results for four different values of electrical conductivity (σ), ranging from $10^{-6}$ to $10^{0}$, where the bright colours (white and yellow) represent high currents and the dark colours (red and black) low currents. Note that for small electrical conductivities the dipoles behave as resonant antennas with zero currents at the edges. Figure 7-6 also shows the three separate resonating dipoles with close to zero currents on the interconnecting tubes. However, for the higher conductivities ($\sigma=10^{-2}$ and $\sigma=10^{0}$) the dipoles do not have a clear resonance anymore and this is because the currents can flow now on the interconnecting tubes. This is best visible in the last plot ($\sigma=10^{0}$).

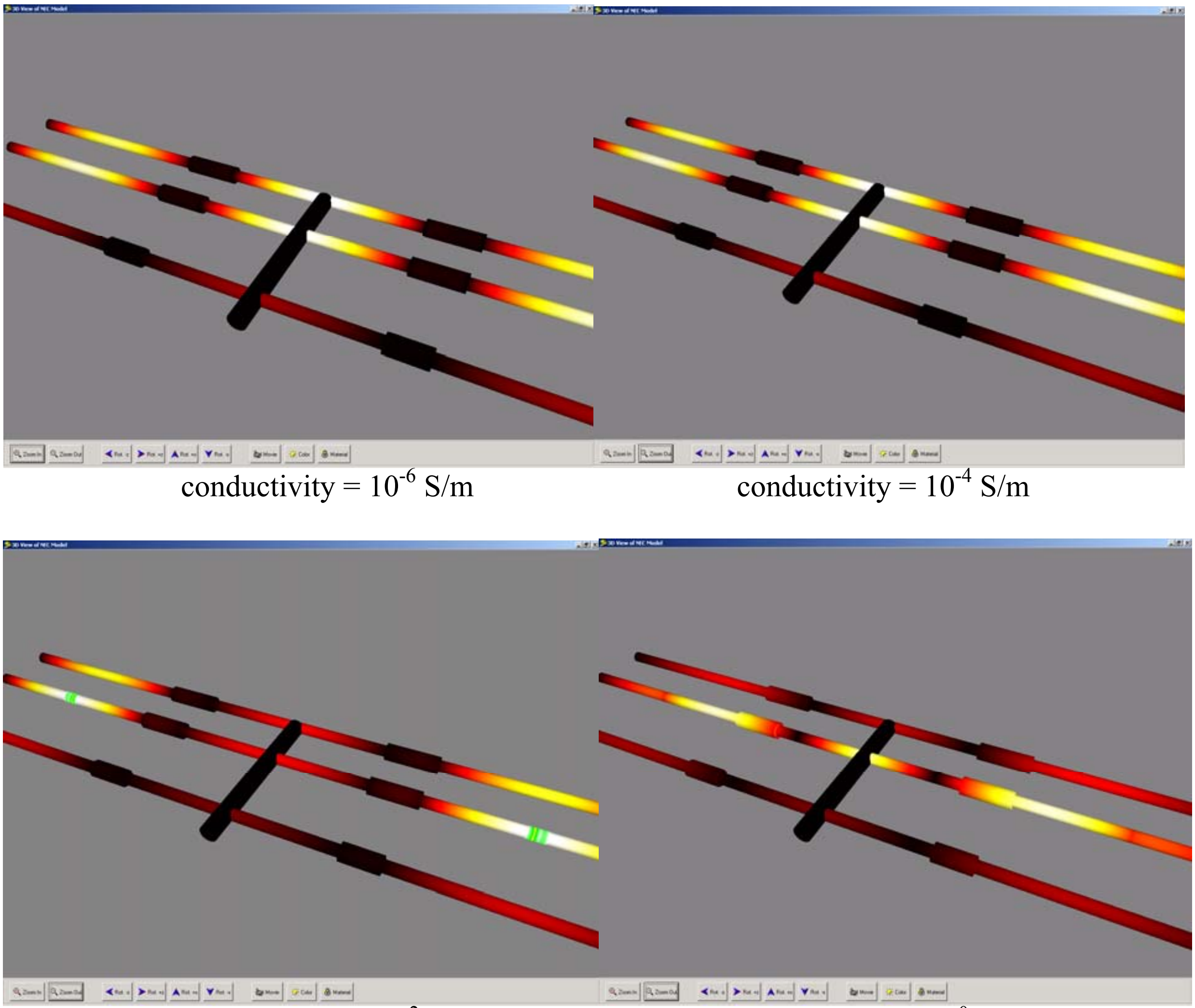

conductivity = $10^{-6}$ S/m

conductivity = $10^{-4}$ S/m

conductivity = $10^{-2}$ S/m

conductivity = $10^{0}$ S/m

**Figure 7-6: Current distributions on the Yagi antenna array**

The general conclusions from the analyses performed are:

- A minimum of 3-5 cm length of isolating material is needed at each end of the dipole elements
- The thickness of the interconnecting tubes is not so critical
- Electrical conductivity of the isolating tubes should not exceed $10^{-3}$ S/m. The lower the conductivity, the better the performance.
- A similar effect of the coaxial cables running through the central tube is expected.

## 7.3 Baseline design

### 7.3.1 Geometry

From the performed calculations and trade-offs done in section 7.2 it is easy to derive a baseline design for the 50 MHz Europa ground-penetrating radar antenna. To achieve a gain of around 12 dBi a linear array consisting of three Yagi antennas is needed. The deployment strategy and the necessary mass saving lead to the following baseline design.

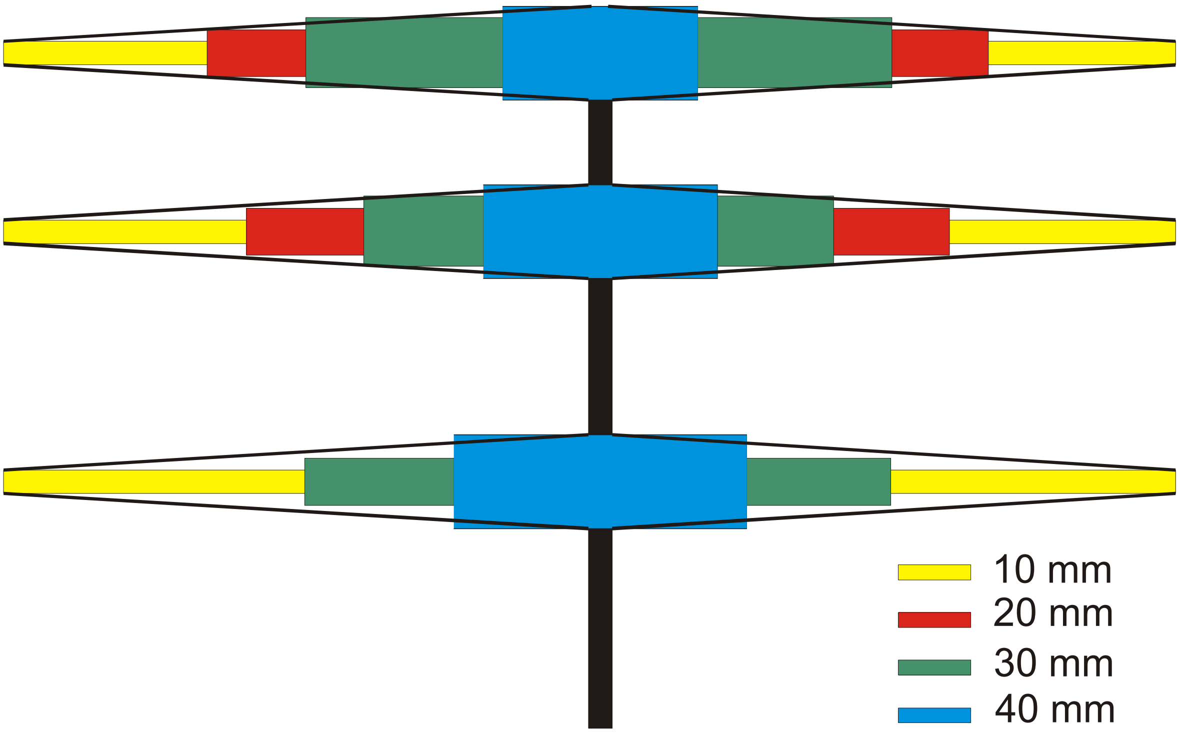


**Figure 7-7: Radar antenna baseline design**

The individual tubes (cylinders) are all tapered from centre (40 mm) to tip (10 mm), as shown in Figure 7-7. Although in the proposed antenna baseline design the diameter of the tubes changes in a series of steps, for the RF performance analysis it is assumed that the tubes are tapered. This simplification should not introduce too much error because of the good geometrical approximation. The configuration of the Yagi array is unchanged, that is, the length and distances between the dipole radiators are as in section 7.2.2, and so the only difference is in the tapered diameter. For the tubes a CFRP material is used, which has a metallic coating for good electrical conductivity ($\sigma$=3.7x$10^{6}$). Then non-conductive GFRP cylindrical sections are used in between the dipole elements for good electrical isolation ($\sigma$<1x$10^{-3}$).

### 7.3.2 Antenna performance

The most important antenna performance values at 50 MHz are summarised as follows:

- Gain is around 11.7 dBi
- 10-dB beamwidth is 48.7 degrees
- Side-lobe level is –16.5 dB
- Back-lobe level is –12 dB

The corresponding radiation pattern is depicted in Figure 7-8, where the E-plane is the across-track plane and the H-plane is the along-track plane. Although the back-lobe level does not meet the requirement, it is expected that by proper optimisation this level can be reduced by a few dB.

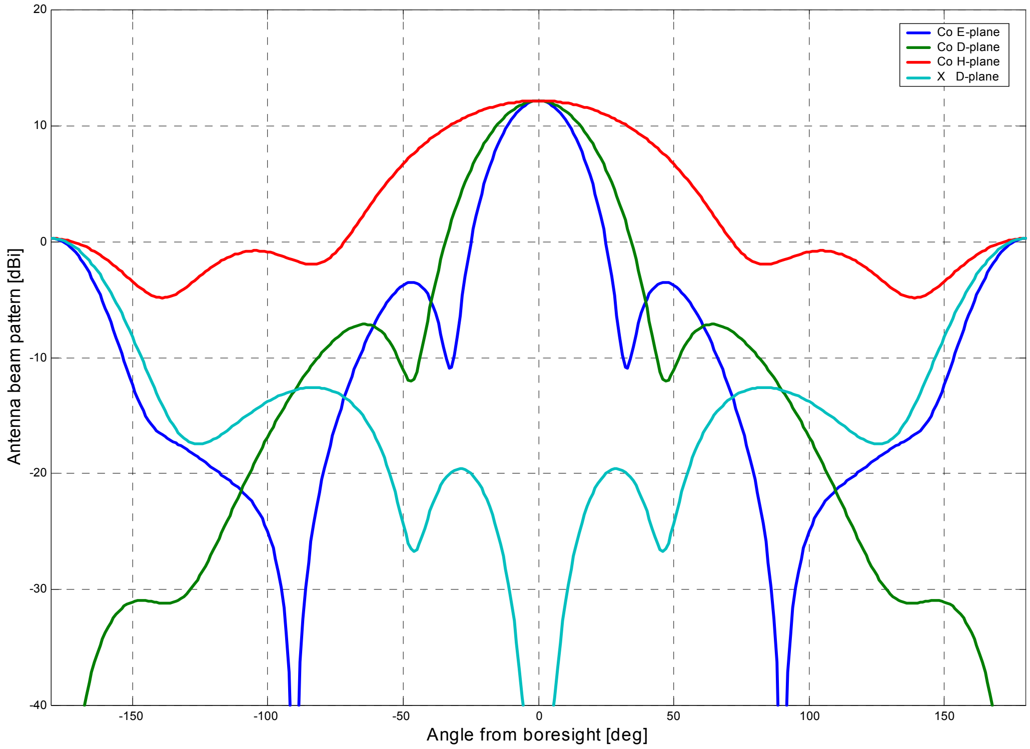


**Figure 7-8: Far-field radiation pattern baseline design**

## 7.4 Critical issues and conclusions

### 7.4.1 Critical issues

- Non-conductive material that can be used in between the dipole elements and that can withstand the radiation environment and has sufficient stiffness
- Low-loss coax cable that will be bent for the a very long period
- RF losses of the hinges

### 7.4.2 Conclusions

- Gain requirement has almost been met (11.7 dBi).
- Beamwidth and side-lobe levels requirements are met.

- Back-lobe requirement has not been met for the baseline design, but it is expected that with proper optimisation of the present design the back-lobe level can be further reduced.
- Frequency bandwidth of 1 MHz (2%) is in general not a problem for the Yagi antenna array, but this should be analysed in more detail for the baseline design. Especially, the input impedance matching of the driving dipole elements with the coaxial cables needs to be evaluated.
- Performance of the radar antenna is not affected by spacecraft body and solar panels
- A $\lambda/20$ (30 cm) tip-tip displacement (in an arbitrary axis) of the dipoles is tolerable without significant degradation of the antenna performance. The gain variation is less than 0.1-0.2 dB, de-pointing of the antenna beam is negligible and lobes (side-lobe and back-lobe) change less than 1 dB. No radar performance degradation is expected with such variations.

### 7.4.3 Future activities

The following antenna activities should be undertaken to finalise the baseline design:

- New optimisation of tapered dipoles with the proper materials (conducting and non-conducting)
- Impedance matching at input of active dipoles, for example slight changes are needed to adapt the active dipoles to the (50-Ohm) coax cables
- Take the frequency bandwidth into account in the optimisation procedure (including extra bandwidth due to temperature variation)

Besides the necessary actions that need to be performed, there are also possible options that might be interesting for the radar antenna. These options are:

- Replace coaxial cables by a coaxial “wave-guide like” structure using the structural tubes
- Set frequency of operation at around 80 MHz, which enables the antenna designer to improve the antenna performance by a few dB (one way), keeping the same mass, size and structural complexity. However, this is not optimal for the instrument performance as shown in Chapter 5, Instrument System Design.

# 8 CONFIGURATION

Configuration of the baseline design of the radar antenna will be described in this chapter.

## 8.1 Requirements and design drivers

The main configuration requirement is the accommodation of the radar antenna on the JEO spacecraft. The risk of collision with any other instruments needs to be investigated. The design drivers of the radar antenna are:

- Available stowed envelope on the JEO spacecraft
- Antenna requirement and sizing: number of dipole, wave length and so on
- Mechanisms deployment sequence

## 8.2 Assumptions and trades

It is assumed that there is no other instrument on the same panel where the antenna will be attached. Trades have been performed for the antenna frame architecture and bar materials; details are provided in Chapter 7, Antennas.

## 8.3 Baseline design

Using bars and hinges for the antenna, an architecture has been selected as the baseline design and is shown in Figure 8-1. Mass optimisation can be achieved when using a different type of cross-section for the bars.

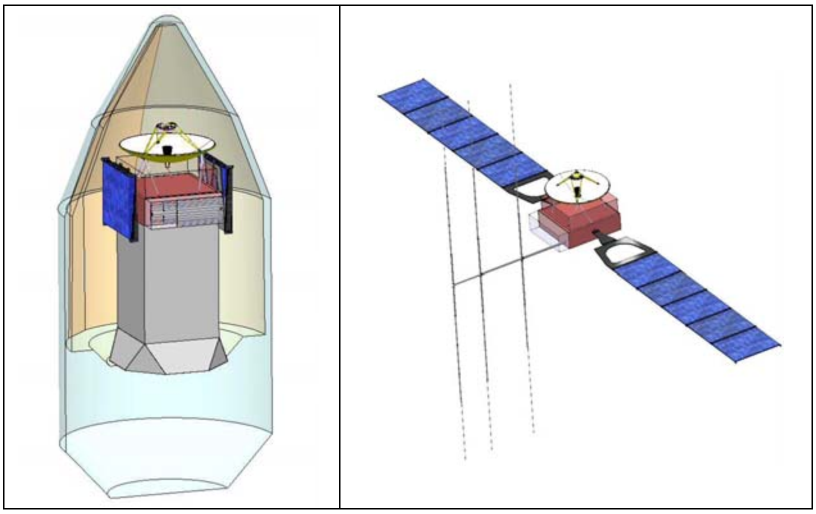

**Figure 8-1: Antenna stowed and deployed configuration**

Figure 8-2 shows the deployment sequence of the antenna. No clash or collision occurs during the kinematics simulation of the deployment sequence of the antenna. The simulation was performed using CATIA – DMU Kinematics.

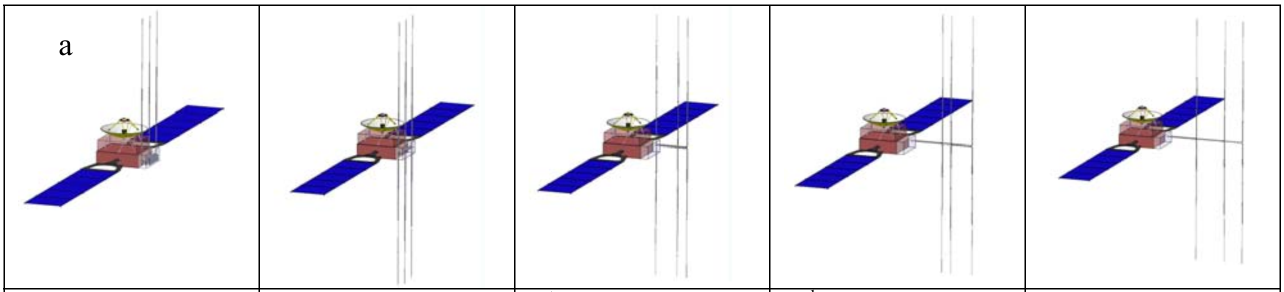


| Upper part | Lower part | 1st main beam | 2nd main beam | Fully deployed |
|---|---|---|---|---|

Figure 8-2: Antenna deployment sequence

Clash analysis was performed using a CATIA function to detect any collision between the antenna envelope and Soyuz fairing. Figure 8-3 shows that no clash occurs:

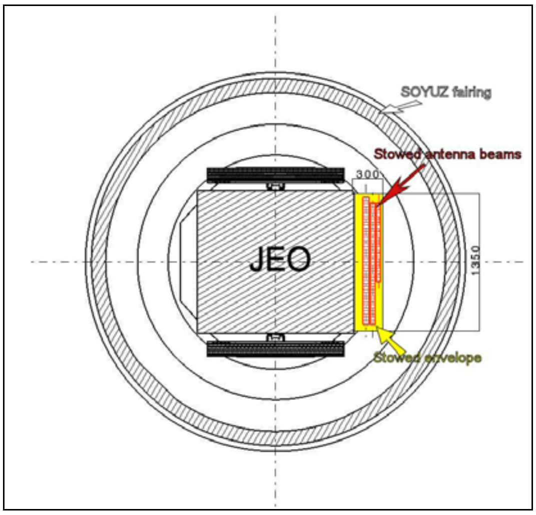


**Figure 8-3: No clash between the antenna and the fairing**

## 8.4 Overall dimensions

Finally, Figure 8-4 and Figure 8-5 show the overall dimensions of the radar in the stowed and deployed configuration. The 1350 mm spacecraft panel dimension is shown as available, the antenna stowed envelope analysis baseline used 1340 mm to allow for design margins.

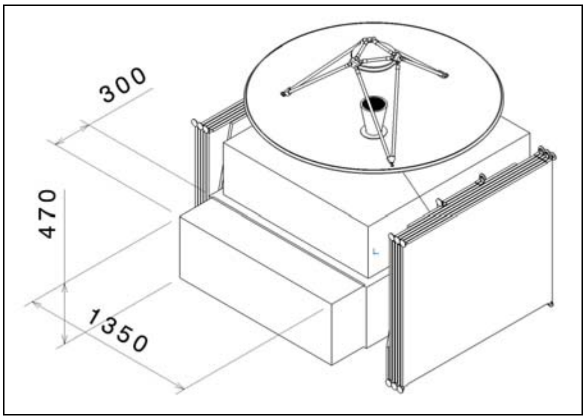


**Figure 8-4: Dimensions of the stowed envelope**

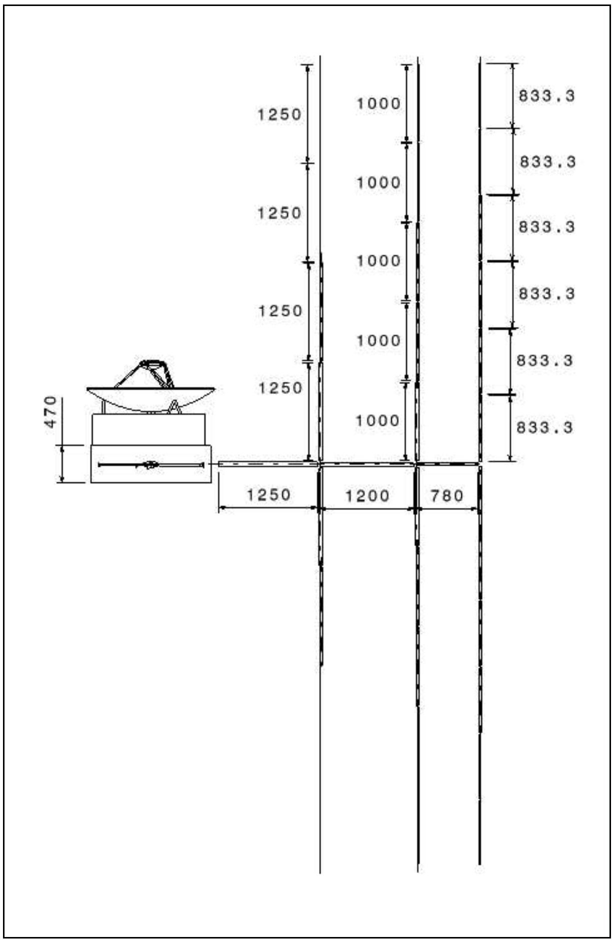


**Figure 8-5: Overall dimensions of the antenna in deployed configuration**

# 9 MECHANISMS

This chapter presents the mechanical and structural design activities performed in the frame of the ELRR CDF.

## 9.1 Requirements specification

Table 9-1 summarises the main requirements to be taken into account for the mechanical and structural design activities of the ELRR. They are extracted from the specification established at system level and from technical constraints resulting from required antenna operational Radio Frequency (RF) performances:

| | Value | Remarks / Impacts |
|---|---|---|
| **Antenna type** | *3 x 3 elements Yagi* | 50 MHz – Overall dimensions: 10 x 2 m |
| **Mass – Deployed** | *< 4 kg* | Depends on material selection and structural frame architecture<br>According to first natural mode, strength and structure stability with regard to deployment and in orbit loads |
| **Mass – Fixed on spacecraft** | *< 2 kg* | According to antenna complexity and resulting HDRM's arrangement |
| **Stowed envelope** | *1.34 x 0.47 x F* | Tailor antenna design and deployment complexity<br>Tailor antenna number of elements<br>The last dimension( F) is according to the fairing envelope |
| **Deployment envelope** | *TBD* | TBD by CAD according to satellite equipment arrangement<br>Tailor antenna deployment kinetics and deployment time sequence |
| **Distance from spacecraft** | *> 0.3 m* | Impact on mass, deployment kinetics and complexity |
| **First deployed frequency** | *> 0.1 Hz* | According to hinges stiffness, antenna structural architecture and material selection |
| **Maximal in-orbit loads** | *0.2 g*<br>*0.4 rad./s$^2$*<br>*22 N (Thrusters) x 8* | Deployed structure strength and stability |
| **Radiations** | *1 MeV*<br>*6.1010 e/cm$^2$* | Selection of tolerant materials and mechanisms<br>Material and performances degradation |
| **Maximal stowed duration** | *2 years storage*<br>*7 years cruising* | Material ageing and end of life deployment reliability<br>End of life properties of materials to be considered |
| **Pointing accuracy/stability** | *+/- 0.2 m wrt mean antenna plane* | Includes deployment inaccuracies, structure stability with regard to thermal environment and structure flexibility and damping properties with regard to in orbit loads |

**Table 9-1: ELRR Mechanical/Structural requirements specification**

The main requirement that appears to be the most challenging is the mass considering both deployed structure stiffness and stability. In addition, the low available storage envelope results in a high deployment complexity.

## 9.2 Design drivers / objectives

According to the main requirements, the following design drivers for the mechanical and structural design of the antenna are anticipated:

- Mass reduction
- Optimisation of the deployed mass with regard to the first eigen-frequency
- Optimisation of the deployed mass with regard to the structure stability according to in-orbit and deployment inertial loads
- Selection of high-performance materials
- Division into storable bar length according to the available storage envelope

- Reduction of design and deployment complexity
- Deployment architecture and kinetics according to deployment envelope and antenna shape
- Reduction of the number of elements and actuators
- High deployment reliability
- Decreased risk of collision with the spacecraft and antenna components during deployment
- Harmonisation with antenna RF performances

## 9.3 Trade-offs

Based on the selected antenna pattern and size (see Chapter 7, Antennas), the following trades have been performed:

- Structural frame architecture
- Material selection

### 9.3.1 Structural frame architecture

Six main technologies have been identified and traded off. Table 9-2 shows the main criteria, deduced from previously mentioned design drivers and objectives, for the selection of the most suitable technology / configuration for the ELRR's structural frame. The exclusion criteria are shown in red.

| | Bars | Bars/ Membrane | Bars/ Ropes | Inflatable | Telescopic bars | Collapsible mast |
|---|---|---|---|---|---|---|
| **Mass – Deployed** | < 4 kg | **> 4 kg** | **> 4 kg** | **> 12 kg** | **> 5 kg** | **> 4 kg** |
| **Mass – Fixed on spacecraft** | < 2 kg | < 3 kg | < 3 kg | **> 4 kg** | **> 3 kg** | **> 4 kg** |
| **First deployed frequency** | > 0.5 Hz | > 0.5 Hz | > 0.5 Hz | < 0.5 Hz | < 0.5 Hz | < 0.5 Hz |
| **Deployment complexity** | ++ | + | + | -- | **++** | **++** |
| **Number of elements** | ++ | + | + | -- | +++ | + |
| **Number of hinges** | ++ | + | + | / | + | / |
| **Technology readiness** | Yes | **No** | **No** | > 2010 | Yes | In progress |
| **Critical issues** | Deployment kinetics | **Shielding of Solar Arrays TBD**<br>Tightening of the ropes | **Shielding of Solar Arrays TBD**<br>Tightening of the ropes | Mass | Overall complexity and mass | Overall complexity and mass |

**Table 9-2: Structural frame architecture trade-off**

As regards the *bars/membrane* or *bars/ropes* technology, the external frame is composed of bar elements tightening in between respectively a membrane (Figure 9-1) made out of a Kevlar or Kapton foil and deployed over the size of the antenna, or a defined number of ropes made out of a Kevlar or Dynema™ (Figure 9-2) according to the number of RF elements. The RF elements of the antenna are respectively patterned by deposition of an electrical conductive material on the membrane or, in addition to the rope material by twisting dedicated fibres or by deposition of an electrical conductive material at the location of the RF elements. The main advantage of this architecture is in the reduced number of elements. However, it results in a larger structure and requires hinges providing high deployment torque capabilities to enable the proper tension of the membrane or of the ropes. The possible shielding of the solar panels by the membrane is considered critical, as well as the impact of the plume of the thrusters located nearby the antenna once deployed.

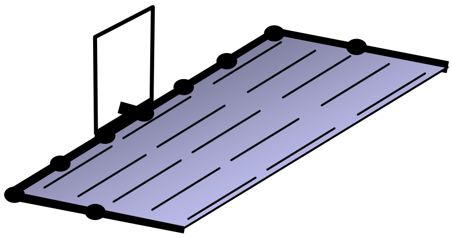

**Figure 9-1: Bar/membrane configuration**

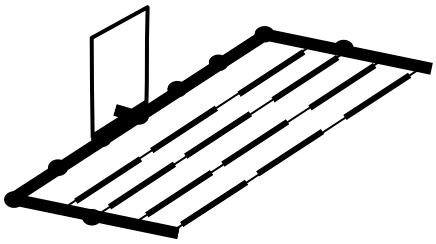

**Figure 9-2: Bar/ropes configuration**

As regards the *inflatable* technology, the external rectangular frame is composed of inflatable tubes tightening in between a membrane made out of Kevlar or Kapton foil deployed over the size of the antenna. The RF elements of the antenna are patterned by deposition of an electrical conductive material on the membrane. This is conceptually the simplest solution. The main drawback lies in the high deployed (flexible tubes material implies the need of high diameters) and fixed (inflation system) masses. In addition, the deployment reliability of the folded elements after 7 years storage is a major issue. The technology is under development and flight demonstrators should not be ready before 2010 in Europe. The possible shielding of the solar panels by the membrane is critical.

As regards *telescopic bars* technology, the frame is composed only of telescopic bar elements, which have to be folded and linked to each other by specific hinges due to the very small available storage envelope on the spacecraft. Several arrangements of bars can be investigated but the resulting solution would require complex mechanisms associated to the telescopic and synchronisation elements. In addition the resulting total mass would not comply with the requirements.

As regards *collapsible masts* technology, collapsible masts are currently the baseline for the deployment of solar sails where the length required is generally superior to 20 metres. For deployable lengths of this order of magnitude, the mass of the mechanism required to unroll, guide, and assemble the boom is not considered as critical as the mass over length ratio as the achieved deployed mass can be very low. However, deployment in two dimensions according to the design of the antenna makes this technology not feasible for the ELRR. Then, several booms would have to be considered combined with a membrane to achieve the required antenna pattern.

As regards *bars* technology, a structure based on an arrangement of bars has been selected as the most promising solution for the ELRR according to specified antenna pattern. The frame is composed only of bar elements linked to each other by specific hinges. Several arrangements of bars have been investigated and the selection of the most promising configuration is mainly dependent on the number of elements (conceptually high) and on the resulting deployment complexity and associated risk of collision with the spacecraft and the antenna elements themselves. The number of bars is tailored by the maximal available storable length on the spacecraft. To reduce the number of elements, the dipoles elements, reflectors, drivers and directors will be part of the structure of the antenna. The selection of bar elements makes possible the use of elastic/collapsible hinges, which can be fully integrated within the frame of the structure. This results in a homogenate and lightweight design.

A structural frame based on bars elements only will therefore be considered as the design baseline for the rest of this study.

### 9.3.2 Materials

To meet the specified requirements, the structural members of the antenna have to be made out of high-performance materials that shall combine high stiffness and very low mass density. Table 9-3 shows the relevant criteria for the selection of potential materials commonly used for primary and secondary structures:

| | Aluminium | Titanium | CFRP UHM fibres + Cyanate ester resin | Beryllium | AlBeMet 162 | SiC/SiC |
|---|---|---|---|---|---|---|
| **Young modulus (Mpa)** | 71000 | 110000 | 190000 | **304000** | 193000 | 230000 |
| **Mass density (kg/m$^3$)** | 2700 | 4400 | 1900 | **1850** | 2100 | 2400 |
| **Max. strength (Mpa)** | 340 | **900** | 300 | 226 | 226 | 200 |
| **Specific stiffness** | 26 | 25 | 100 | **164** | 92 | 96 |
| **Specific strength** | 0.13 | **0.20** | 0.16 | 0.12 | 0.11 | 0.08 |
| **Criticality** | **Flexibility** | **Mass** | **Radiation Low strength at cryogenic temperatures** | **Low toughness Toxicity** | **Toxicity** | **Low toughness** |

**Table 9-3: Materials selection**

As the main criterion for the ELRR is the specific stiffness, beryllium appears to be the most suitable material. Nevertheless being twice as brittle as aluminium and having relatively low fracture toughness at cryogenic temperature, it appears as being too risky to use it even for a secondary structure like the ELRR. Beryllium-aluminium alloys like AlBeMet 162 do not have as many drawbacks.

The preferred material would be Ultra High Modulus (UHM) Carbon Fibre Reinforced Plastics (CFRP) combined with Cyanate ester resin. However, their low-strength properties at cryogenic temperature (50% less than at room temperature) combined with the lack of information concerning the sensitivity/degradation of material performances with regard to the radiation environment such as specified for the ELRR makes the confirmation of the selection uncertain. Further experimental testing activities of this material is needed. For example, no significant change of properties for Carbon/acrylic-bismaleimide composites under 2 MeV / $6.10^{10}$ e/cm$^2$/s during 2h40 has been noticed (see RD[21]). This is not representative enough of ELRR environment and materials but contains relevant information for further investigations. In addition, using FRP material would enable having fully integrated isolation elements in the structure using glass or Aramid fibres (Radio frequency transparency material) where needed instead of carbon fibres.

Further investigations, analyses and tests would be required to assess the suitability of the proposed material, so the rest of this study will be based on mean properties of material which are most likely to be used: E=190Gpa; υ=0.3; ρ=2000 kg/m³ In any case, the material selection at different location of the antenna shall be tailored according to antenna design drivers like stiffness, strength, stability or electrical isolation. FRPs can be tuned according to electrical, thermal, strength and stiffness requirements.

## 9.4 Mechanical and structural design baseline description

### 9.4.1 Parts list and materials

Table 9-4 shows the selected mechanical and structural configuration:

| | Type | Material | Quantity | Unitary mass (g) | Total mass (g) | Remarks |
|---|---|---|---|---|---|---|
| **Structural frame Main arm** | Hollow tube | E: 190 Gpa<br>ν: 0.30<br>ρ: 200 kg/m3 | 3 | / | 2700 | The main arm carries most of the loads |
| **Structural frame Dipole arms** | Hollow tube | | 26 | / | | Material selection according to environmental constraints |
| **Structural frame Dipole arms Isolating elements** | Hollow tube<br>or<br>Washer | Glass / Aramid FRPs<br>or<br>Ceramic | (6) | / | | Two possible solutions according to the structural frame material<br>Integrated in the structural frame of the dipoles arms |
| **Electrical conductive layer** | TBD | TBD | TBD | TBD | TBD | To be tailored according to antenna operating performances |
| **Hinges (Dipoles)** | Tape springs | Same as associated structural tubes | 26 | / | / | Fully integrated in structural elements – Under development |
| **Hinges (Main arm)** | | | 3 | 80 | 240 | High-stiffness hinges |
| **Synchronisation and stiffening mechanisms** | 'Manchet' | Same as structural tubes | 2 | 100 | 200 | Reduce kinetic energy<br>Decrease main arm instabilities<br>Increase stiffness |
| **Drivers feeding** | Coaxial wires | TBD | 15m | TBD | 200 | Guess<br>Resistive bending torque TBD |
| **Structural inserts** | / | TBD | 55 | 20 | 1100 | Material pair according to tribology issues related to risk of adhesion between surfaces in regard |
| **Ejection mechanisms** | Leaf springs | TBD | | | | |
| **HDRM's / Actuator** | Thermal knife | / | 3 | 150 | 450 | Company: Dutch Space<br>Power consumption: 15 W during 120 s<br>-70°C < T operational < +90°C |
| **HDRM's / Brackets + release mechanisms** | / | Aluminium | 4 | 250 | 1000 | Depending on detailed FEM analysis |
| **Deployment sensing** | NA | NA | NA | NA | NA | By operation of the antenna once deployed |
| **Casing** | NA | NA | NA | NA | NA | Deemed not necessary<br>TBD with regard to thermal issues |
| | | | | **Total mass** | **5890** | **No margins considered** |

**Table 9-4: Parts list and material**

Figure 9-3 shows the selected structural design baseline and location of the main mechanical components:

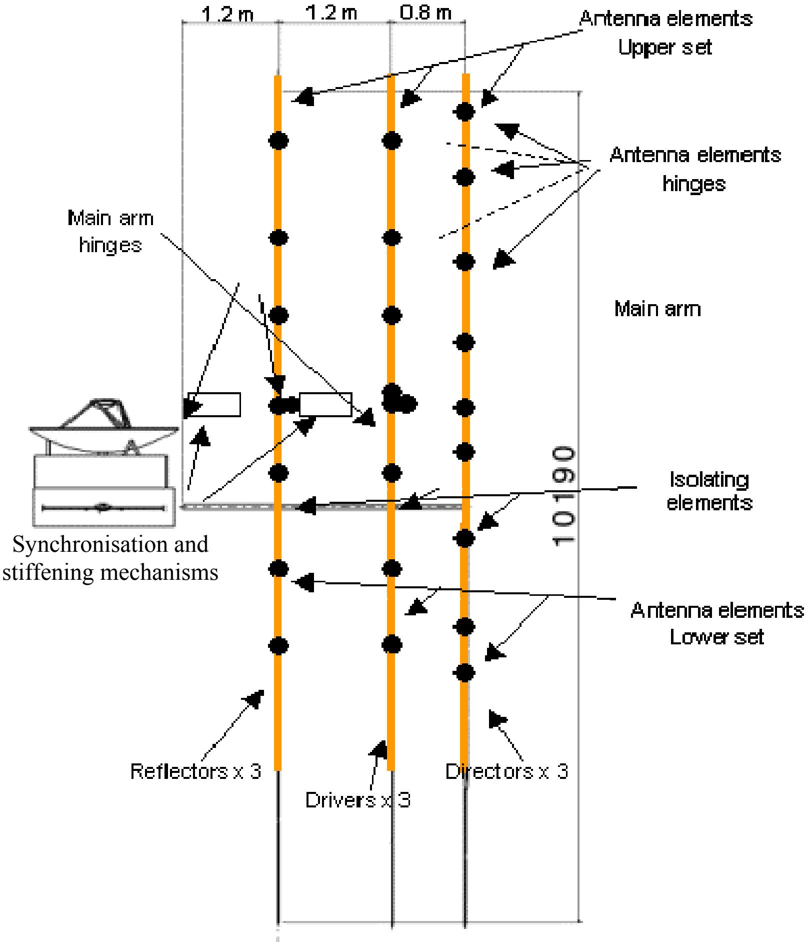


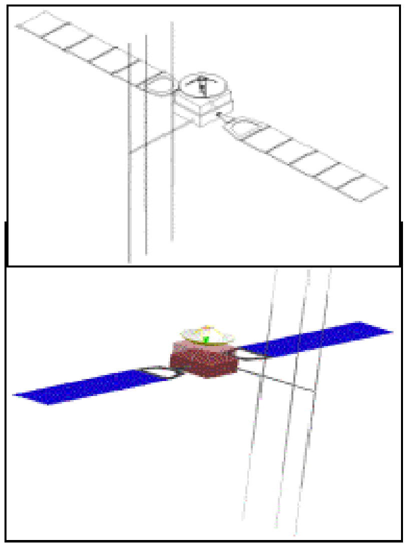

**Figure 9-3: Structural and mechanical design baseline**

### 9.4.2 Hinges

Each bar will be hinged to the neighbouring bar using elastic/collapsible hinges. The principle of elastic/collapsible hinges is to allow pure structural elements, typically curved tape/leaf springs, to elastically buckle and then to bend over wide ranges of angular positions up to more than 180°. Mounted in place of conventional deployment mechanisms, they enable the positioning of deployable appendages in stowed configuration. Once the appendage is released, the strain energy stored within the buckled tape springs provides the necessary deployment motorisation torque and then, once the original stable straight shape is recovered, high-deployed stiffness.

The basic concept of elastic/collapsible hinges offers attractive highly integrated/coupled functionalities like self-actuation and self-lathing. This reduces drastically the complexity, mass, number of parts, volume and cost. In addition, typical drawbacks inherent to traditional deployment mechanisms such as friction, backlash, slippage and sensitivity to contamination are no longer a matter of concern.

The main required hinge performances are:

- Available torque > 0.4 N.m
- Deployed stiffness > $10^4$ N.m/rad. (goal)

- Pointing accuracy > $0.1^{o}$ (goal)
- Reliability: 0.999 (deployment + latching)
- Low-performance degradation related to material sensitivity to the environment
- Design according maximal allowable loads to avoid structural instabilities

These hinges can be fully integrated in the structural frame as they might be made of the same material as that of the structural members.

Figure 9-4 shows a typical elastic/collapsible hinge made of CFRP material in different angular positions:

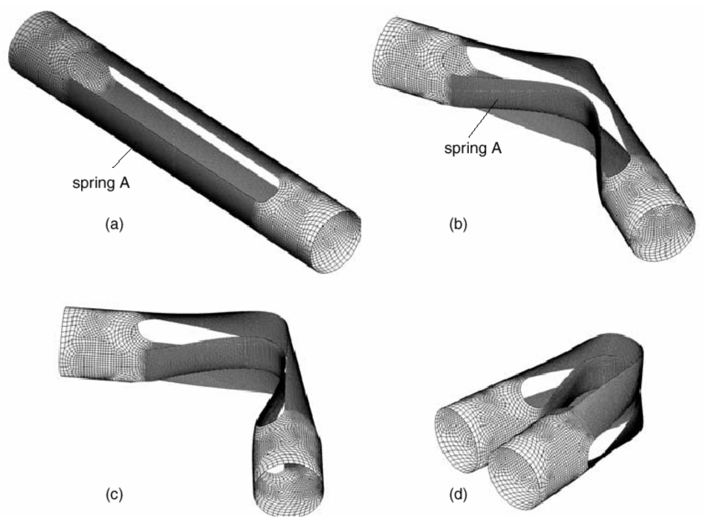


**Figure 9-4: CFRP Elastic/collapsible tube hinge**

Note the relatively small deployment torque generated by this type of hinges and impacts on the HDRM arrangement and deployment configuration. Indeed, all sources of friction and adhesion shall be avoided or minimised if any. Note also the reliability after 7+2 years of storage and related degradations of the selected material properties.

### 9.4.3 Synchronisation and stiffening mechanisms

The deployment sequence is synchronised by a proper arrangement and actuation time sequence of the Hold Down and Release Mechanisms as well as by using dedicated synchronisation mechanisms called “manchets”. “Manchets” are based on the same principle as the one used for the Max Planck Institute CONSERT antenna on the Rosetta spacecraft orbiter (Figure 9-5 and Figure 9-6).

Synchronisation mechanisms are fitted on two of the three elastic hinges of the main arm. Their main functions are to reduce kinetic energy/inertial loads during the deployment and to provide higher stiffness and better stability to the main arm once deployed. The main arm carries most of the structural loads and provides the highest contribution to the overall structure stiffness.

The main arm bars are folded parallel to each other like a concertina, and kept in place by the “manchets”. When the main arm deploys, the “manchets” are pushed back to release one after the other each of the three bars composing the main arms. The latching of each bar element in its final position releases the deployment of the neighbouring elements and so on.

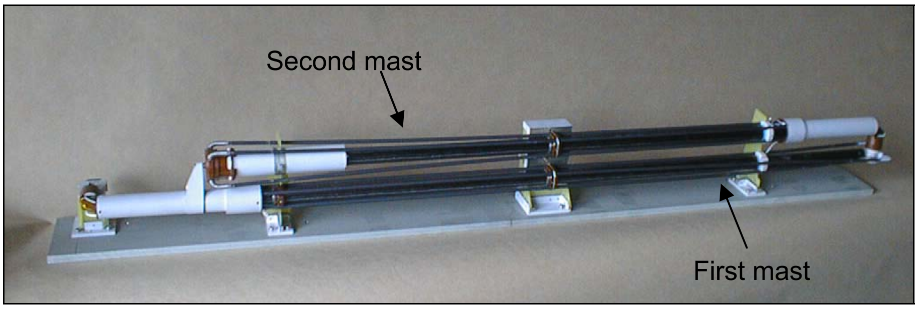


**Figure 9-5: CONSERT Antenna (Max Planck Institute)**

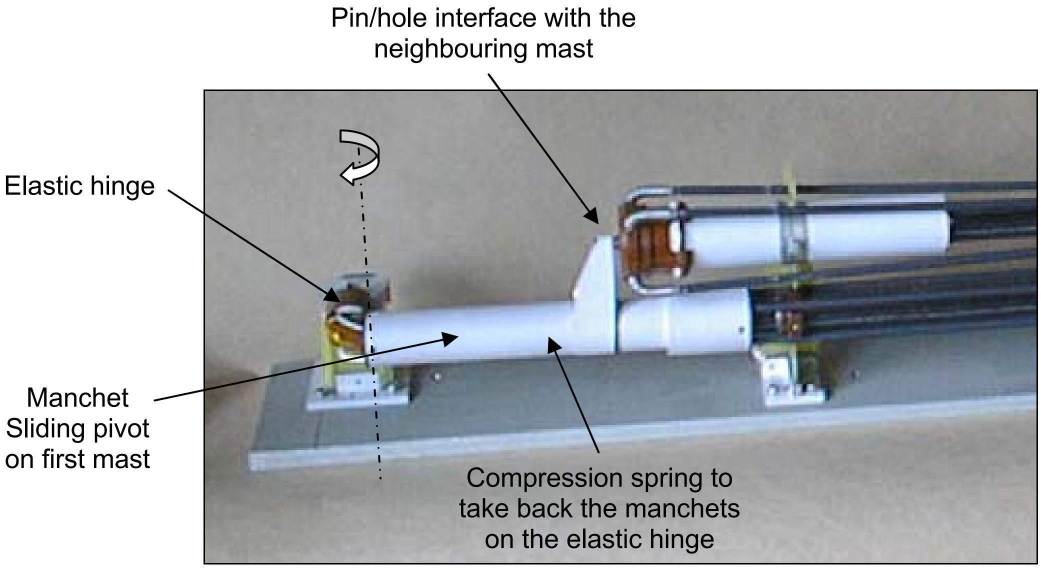


**Figure 9-6 : CONSERT antenna – 'Manchet' description (Max Planck Institute)**

### 9.4.4 Hold-Down and Release Mechanisms

In the stowed configuration, the folded bars package shall be held together and to the spacecraft using a specific Hold-Down and Release Mechanism (HDRM) arrangement (Figure 9-9). This arrangement shall be capable of restraining and releasing 29 bar elements after 7+2 years storage.

The main functions and design objectives related to the HDRM design are to:

- Support the structure during launch
- Synchronise the deployment sequence for risks of collision and allowable inertial loads
- Minimise number of supports according to launch load & structure stability
- Minimise number of actuators
- Minimise number of elements
- Avoid risk of adhesion between contact areas
- Avoid degradation of electrically conductive deposition (if any)
- Minimise friction during deployment

Each of the bars is fitted with two inserts for the antenna elements and with one insert for the main arm elements. In the stowed configuration, all bar elements are pressed against each other and supported and guided by the inserts. To avoid any risk of adhesion, dedicated spring mechanisms like flexible blades shall be implemented with well-controlled tribological properties.

All bars elements are folded parallel to each other like a concertina, against the sides of the main arm tubes for the antenna RF elements and, against dedicated support brackets attached to the platform for the main arm tubes. Figure 9-7 and Figure 9-8 show the arrangement and the preliminary envelope of the antenna in stowed configuration:

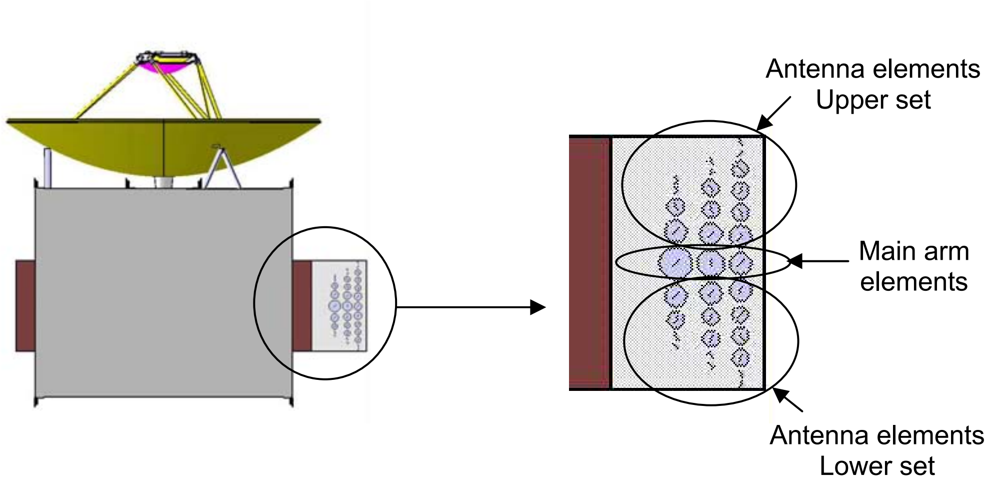


**Figure 9-7: Stowed configuration arrangement**

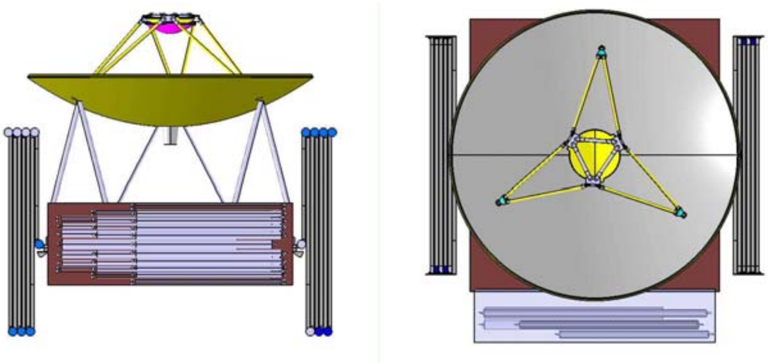

**Figure 9-8: Stowed configuration envelope**

Note that a certain clearance (>0.2m) shall be considered between the spacecraft side panel and the antenna in stowed configuration to avoid any risk of collision with the reflector antenna on top of the spacecraft.

The package shall be restrained with three Hold-Down and Release units: two for the antenna elements and one for the main arm. The main arm HDRM consists of two ropes where one extremity is attached to the external main arm element insert and the other to a specific bracket fixed on the spacecraft wall from where they are tightened to preload the main arm bar elements stack. The antenna elements HDRMs consist of two units located at 25% and 75% of the bars length. They are composed of a rotating cover articulated at one extremity (spacecraft) by a hinge fitted with a return torsion spring. On the other extremity, a rope is attached so that when tensioned, the cover presses the antenna element bars stacks onto dedicated support brackets from where they are tightened.

The release of the main arm elements and the antenna elements are achieved by cutting the ropes made of Kevlar fibres using thermal knives (for example, from Dutch Space), one per HDRM units. Figure 9-9 shows the selected principle for HDRMs arrangement:

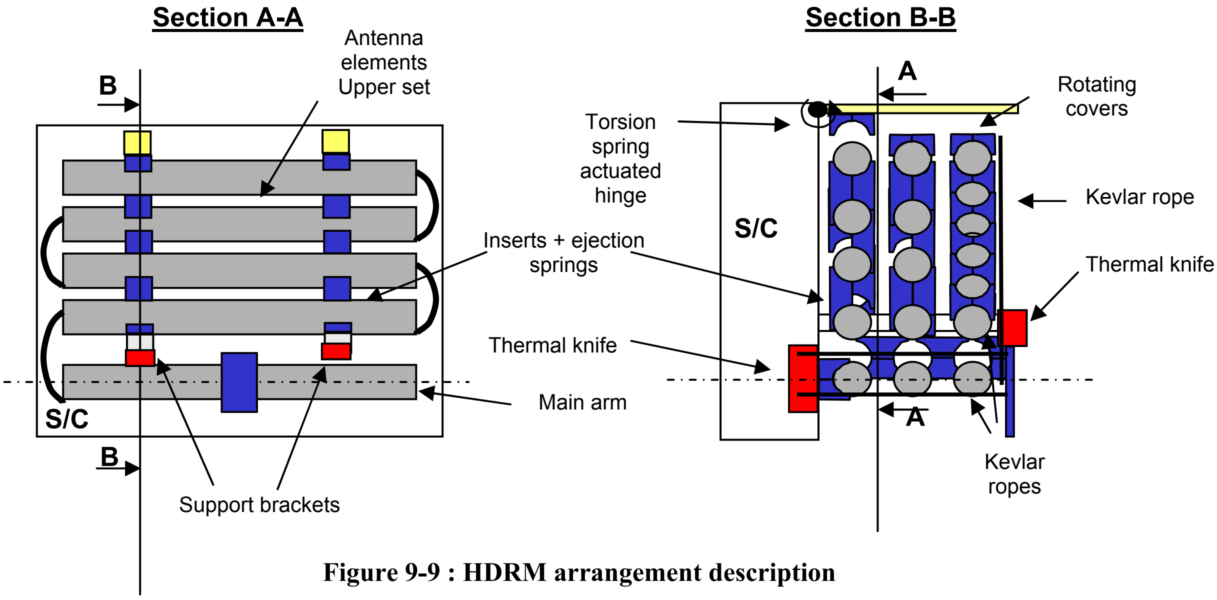


**Figure 9-9 : HDRM arrangement description**

From initiation of the thermal knives, the release can be expected to occur within 600 seconds. The HDRM arrangement is partially redundant. The HDRM arrangement shall be optimised according to the structure behaviour in folded configuration under launch environments.

## 9.5 Stiffness, strength and stability analyses

One of the critical activities of the mechanical and structural design of the antenna is the optimisation of the mass with regard to the first allowable eigen-frequency and, with regard to the maximal allowable load according to the structural stability of the designed structure. These two parameters will define the minimal achievable mass.

### 9.5.1 Stiffness

The aim of the stiffness analysis is to evaluate what is the minimal achievable mass to be compliant with the first deployed eigen-frequency as specified at system level, that is, > 0.1 Hz.

The hypothesis is that:

- No hinge stiffness is considered
- No margins are applied
- Optimised cross-section distribution

Given the high level of uncertainties related to the hypotheses, it appears reasonable to fix conservatively to 1 Hz the first deployed eigen-frequency. The obtained performances are:

- Deployed mass: 2.7 (structure) + 1.74 kg (hinges + mechanisms + inserts…).
- Mode 1: 1.1 Hz – Torsion around main arm axis (X)
- Mode 2: 1.6 Hz – Flapping out of plane (ZX)
- Mode 3: 1.8 Hz – Dipoles elements flapping out of plane (ZX).

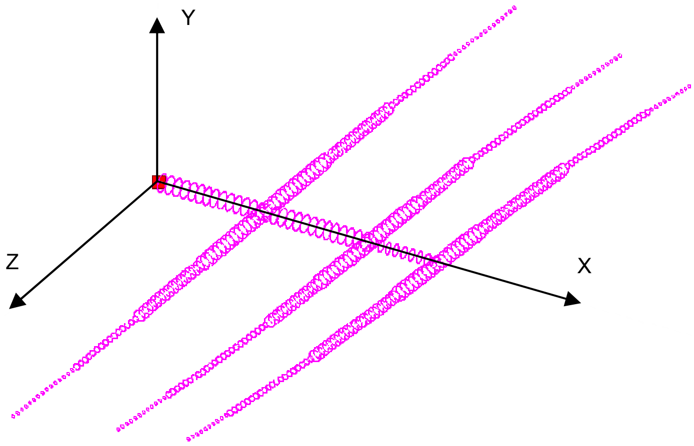


(Cross sections scale not representative)

**Figure 9-10: Simplified finite elements model**

In Figure 9-10, the cross-section scales are not representative. By experience and given the high level of uncertainties resulting from the hypothesis, it appears more realistic to consider that the first achievable deployed eigen-frequency will be > 0.5 Hz including all uncertainties.

### 9.5.2 Strength

The aim of the strength analysis is to evaluate the capabilities of the structure to sustain specified in-orbit loads. It will be focused on the evaluation of the safety margin at the interface between the antenna main arm and the spacecraft where maximal loads are most likely to be carried.

The hypothesis is that:

- Maximum accelerations are: 0.2g / 0.4 rad./s$^2$
- Maximum thrusters load is: 22 N x 8 ⇒ 0.026 g with spacecraft mass of 670 kg ⇒ covered by maximum accelerations
- Safety factor is: 1.5
- Maximum strength is: Tensile/compression = 100 Mpa; Shear = 50 Mpa
- Tube cross-section is: ϕ35mm – Thickness 1 mm.

The results are:

- Maximum moment at spacecraft interface: 15 N.m
- Maximum force at spacecraft interface: 8 N
- Safety Margins: Tensile/compression >10
  Shear >7

### 9.5.3 Structural stability

The purpose of the stability analysis is to assess if the structure will buckle (Global and local buckling modes to be considered) or collapse under both in-orbit or deployment loads due to high kinetic energy/ inertial loads and latching shocks involved.

Such assessment would require refined analyses that cannot be performed in the frame of this study. Nevertheless, the selection of the bar elements cross-sections over the size of the antenna,

properties of elastic hinges and the use of synchronisation mechanisms ("manchets") has been made so that the risk of instabilities is reduced to the maximal extent.
Refined analyses will define:

- Maximal allowable in-orbit loads
- Maximal allowable deployment kinetic energy
- The need of synchronisation mechanisms
- Possible mass reduction

According to the results of the strength analysis, the safety margin with regard to buckling loads can be expected to be greater than 2.

### 9.5.4 Deployed shape stability

This section evaluates the maximal distortions with regard to an ideal antenna shape/pattern that can be expected to mainly arise from hinge deployment inaccuracies.

The hypothesis is that:

- Hinges' accuracy and stability is: $0.1^o$
- Worst case considering that all hinges are contributing
- Very conservative calculation do not consider a statistical approach
- No deformation occurs due to thermal distortion of hinges or thermal gradient within structural members

The results are that:

- Maximal tip to tip deflection is: 0.32 m
- Maximal out-of-plane deflection between two consecutive dipole tips belonging to the same Yagi array is: 0.12 m.

In addition, once deployed the antenna will be very sensitive to external dynamic loads as the structural frame shows a very small amount of structural damping. The mission planning must take into account that, to maintain the planarity requirements, the deployed antenna must not be excited to any large degree. To ascertain the amount of out-of-plane instability a detailed FEM analysis will be required coupled with the forcing functions and mission or orbit time line details. AOCS-induced loads at the level of the antenna shall be tailored in accordance with antenna flexibility characteristics and maximal allowable distortion for optimal antenna performances.

## 9.6 Deployment configuration/sequence

One of the critical issues of the ELRR is the deployment phase. The deployment sequence has been defined so that complexity is reduced and reliability increased with the following results:

- Risks of collision minimised to the maximal extent
- Minimisation of deployment sequence orders
- Deployment sequence controlled by HDRM actuation
- Self-deployment of the antenna once released by using self-actuated hinges
- Self-latching of the deployed elements once deployed by using self-latching hinges
- Self-synchronisation of main arm deployment only to reduce generated kinetic energy and inertial loads
- Deployment status given according to the antenna operation feedback

The deployment of the individual bars is performed in a synchronised manner under control of first HDRMs and secondly "manchets". All bars are interlinked with each other so that the deployment kinetics is limited to well-defined planes for the antenna elements and that risks of collision are reduced to the maximal extent. Nevertheless, within each plane, the deployment kinematics has to be considered as being random, except for the main arm.

A high number of hinges are involved in the deployment with stiffness and damping properties which are theoretically identical but in practice rather different. This leads to high uncertainties in the deployment kinematics. The following Figure 9-11 present, step by step, the selected deployment sequence:

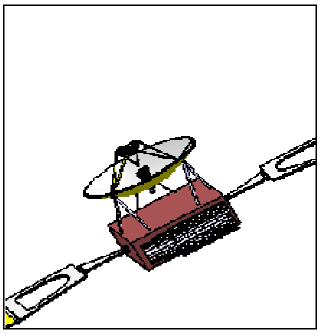

**Step 1: Actuation of the first two HDRM actuators associated to antenna elements (Reflectors, drivers and directors)**

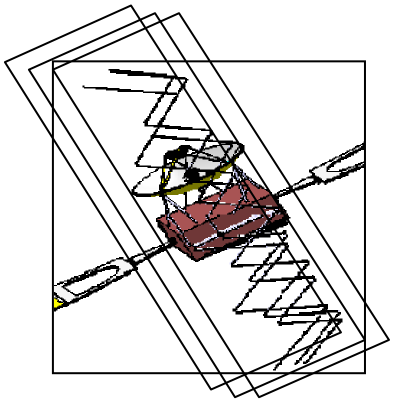

**Step 2: Deployment of upper and lower sets of antenna elements. Deployment inside three parallel planes**

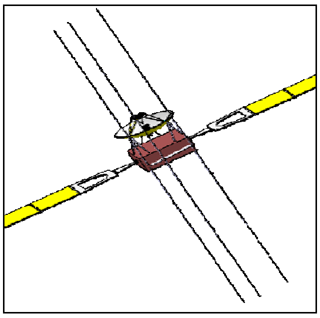

**Step 3: End of deployment of upper and lower sets of antenna elements. All associated hinges latched**

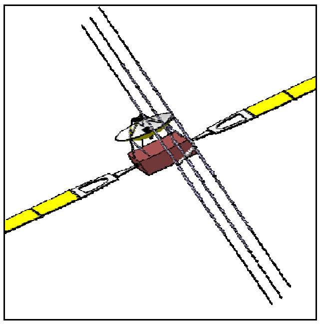

**Step 4: Actuation of the third HDRM actuator and deployment of the first main arm**

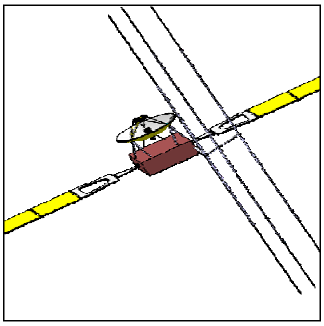

**Step 5: First main arm element latched and stiffened. Releasing of second main arm element**

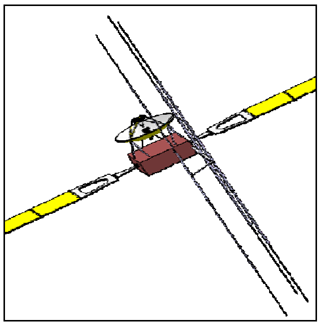

**Step 6: Second main arm element latched and stiffened. Releasing of third main arm element**

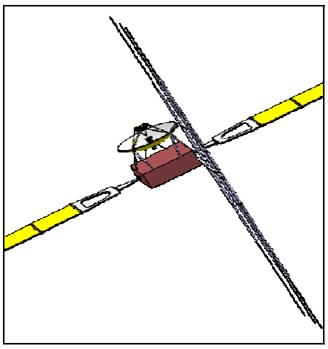

**Step 7: Third main arm element latched and stiffened. End of deployment**

**Figure 9-11: Radar antenna deployment sequence**

## 9.7 Options

The complexity of the considered design baseline can be reduced slightly by:

- Decreasing the length of the first main arm bar element down to 0.3 m (according to specification). The first main arm bar element would then be fixed perpendicular to the spacecraft panel and the two sets (upper and lower) of antenna reflectors elements would be attached to these elements. This would result in removing one synchronisation mechanism, one hinge and one bar to be deployed.
- Additionally, and considering the selected deployment sequence, the number of bars that form the antenna elements can be decreased by increasing the length of the individual bar elements. That would result in a reduced number of hinges also.
- Performing refined analyses to study in detail the behaviour the antenna in folded configuration to identify the optimal arrangement for the HDRM.

Thermal knives can be replaced by wire cutters (for example supplied by PyroAlliance) if Kevlar ropes are not compatible with the ELRR mission-specified environment and more particularly with radiations. This would result in higher mass.

## 9.8 Critical issues and development needs

### 9.8.1 Mass drivers

- The deployed mass can be reduced but the limits are:
  - Structure instabilities with regard to orbit loads
  - Structure instabilities with regard to deployment dynamics
  - Level of integration of hinges with elements of the structural frame
- The HDRM's mass could be reduced by refined launch loads analyses

### 9.8.2 Development critical issues

During the progress of this study, the following criticalities related to the mechanical and structural design activities have been identified and are to be anticipated for further developments:

- AOCS-generated loads according to antenna structure instability limits during deployment and once deployed
- Deployment simulations representativeness / Sensitivity studies
- Deployment kinematics and dynamics uncertainties
- Deployment reliability after 2 + 7 years storage
- Deployment control and regulation, repeatability/hysteresis
- Deployed planarity, shape accuracy and stability
- Back-driving, latching shock and back-buckling.
- Characterisation/validation during ground tests, 1-g to 0-g and air to vacuum effects
- High-performance materials needed
- Materials (structure, mechanisms, wiring) sensitivity to radiation / Cryogenic environment
- Low structural damping / high flexibility once deployed
- Number of hinges which reduces overall stiffness
- Non-linear hinge properties/very low folded stiffness/no folded holding torque
- Electrical conductivity continuity and isolation
- Conductive coating for antenna RF performances

- Wire routing / Resistive torque

### 9.8.3 Specific development needs / investigations

- Structural stability with regard to in-orbit loads for possible early deployment
- Antenna shape accuracy and distortions with regard to deployment accuracy and in-orbit loads (AOCS + thermo-elastic)
- Sensitivity of selected material (FRPs) to high radiation levels to be characterised
- FRPs having high-strength performances in a cryogenic environment and tolerating several (>500) thermal cycles without significant failure or performances degradations
- CMC (SiC/SiC) and beryllium alloys to be investigated as potential material candidates
- Optimisation of HDRM arrangement with regard to launch loads
- Representative mathematical models for deployment simulations
- Elastic/collapsible hinges characterisation test campaigns
- Assess results of the MARSIS deployment problem investigations.

### 9.8.4 ELRR design requirements

Table 9-5 shows requirements resulting from the mechanical and structural design activities, which have to be considered at system level as ELRR accommodation constraints:

| | ***Value*** | ***Remarks*** |
|---|---|---|
| ***Stowed envelope*** | **1.34 x 0.47 x 0.3** | - |
| ***Max. orbit loads*** | **TBD** | According to antenna structural stability and allowable deployed shape distortions |
| ***Temperature*** | **-70oC < T < +90oC** | Tailored by HDRM actuators operating and survival temperatures |
| ***Spacecraft interfaces*** | - | According to HDRM arrangement |

**Table 9-5: ELRR design requirements**

## 9.9 Conclusions

Table 9-6 shows the results of the ELRR mechanical and structural design activities:

| | |
|---|---|
| Mass:<br>Deployed<br><br>Fixed on spacecraft | <br>Structure: 2.70 kg<br>Mechanisms: 1.74 kg<br>Mechanisms: 1.45 kg<br>**Total: 5.89 kg – no margins** |
| Power consumption | 15W during 120 seconds not simultaneously x 3 |
| First deployed Eigen mode | > 0.5 Hz |
| Deployment time | < 600 s |
| Maximal out of plane deflection | +/- 0.16 m wrt average plane |
| Minimal safety margin | > 2 (Buckling) |
| Criticalities | Deployed stiffness and structural stability wrt mass |

**Table 9-6: ELRR mechanical and structural design results**

# 10 THERMAL

The objective of this chapter is to identify the thermal constraints related to the design of the Europa radar within the JEO/JRS mission and to review the possible thermal accommodation compatible with the antenna performance and interfaces requirements.

## 10.1 Requirements and design drivers

Constraints from mission phases:

- The high radiative flux due to the relative proximity of the Sun (0.72 AU) during the Venus fly-by generates thermal constraints on the illuminated surfaces of the spacecraft. Preferential shadowing of critical elements is sought with a possible design driver for the spacecraft configuration and elements, depending on the pointing strategy selected during this phase. The criticality of the stowed Yagi antenna and requirement for a protective cover is open.
- Combination of low solar irradiance and eclipses at Europa generates a cold environment, which is a possible design driver for external appendages like the antenna.
- JEO will experiment eclipses by Jupiter and Europa and varying thermal loads. The low thermal capacitance of the antenna will induce a high rate of temperature change and possibly be the source of constraints (thermal stress, thermal shock) depending on the cycling frequency and amplitude.

| |
|---|
| TH01 – The thermal design of the antenna shall be compatible with hot and cold case as defined by the mission scenario and by the status of the antenna (that is deployed or stowed configuration).<br>TH02 – The design of the antenna shall be compatible with the thermal cycling while orbiting Europa. |

Constraints at the interface:

- The low resources of the JEO spacecraft in terms of power at Jupiter distance call for thermal insulation between the appendages like the Yagi antenna and the spacecraft enclosure. In the opposite way, during hot cases, no heat transfer shall be allowed toward the spacecraft.

| |
|---|
| TH03 – The interface between antenna and spacecraft shall offer sufficient thermal resistance. |

Constraints related to the antenna design and performance are:

- The antenna is an assembly of a different material and functions that perform within a certain temperature range. This is the case in particular for the release mechanisms before deployment. If necessary, heating provision shall be identified and requested to the system.
- The mechanical performance (strength, structural integrity) of the antenna assembly is temperature dependant. In particular, brittleness is a possible design driver for the antenna materials in the low temperature range.
- The antenna RF performance is related to its dimensional stability. The parallelism of the directors shall not experience excessive bending, and the relative dimensions between directors, driver and reflector shall be maintained.
- Performance of the antenna is related to a sufficient electrical conductivity of the dipoles assembly and sufficient electrical resistivity between dipoles.

| |
|---|
| TH04 – For all phases of the mission, the antenna elements' thermal status shall remain within their thermal requirements (non-operating and/or operating temperature limits).<br>TH05 – For all phases of the mission, the antenna elements shall remain safe with respect to the experienced temperature range and thermally stable for the mission duration.<br>TH06 – The thermal design shall not allow thermal distortion.<br>TH07 – The thermal design shall comply with the RF electrical requirements. |

## 10.2 Assumptions and baseline

The antenna elements and configuration have the following characteristics:

- The antenna array is a 3 x 3 Yagi configuration with three similar Yagi of three dipoles (reflector, driver and director). All dipoles are CFRP tubes (aluminium is an alternative).
- The dipoles are mounted on a cantilevered beam (CFRP) and are mechanically connected to each other by isolating elements (GFRP rods).
- For storage and deployment reasons, a number of elastic hinges (CuBe2) break down the dipoles (26 in total) and the mast (3). Thermal knives (2) are used to release the mechanical assembly and synchronisation mechanisms to slow and control the related torques.

The antenna geometry has the following characteristics:

- The antenna has dimensions of 10 x 3.2 m in deployed configuration, with a first dipole distant of 1.2 m to the spacecraft interface, 1.2 m to the driver and 2 m to the director.
- Each dipole is about 3 m long, with a diameter of 10 mm.

The antenna coatings has the following characteristics:

- The dipoles are aluminium coated with sufficient thickness to guarantee electrical conductance.
- White Plasmocer (PTS Jena, Germany) is proposed as thermal coating of the antenna materials to control the temperature when illuminated. Its stable thermo-optical properties versus time and versus all type of radiation are adequate to a Jupiter mission.
- Plasmocer being applicable also with titanium, a thin layer (~10 μm) of this metal is used on the GFRP. Equivalent electrical resistance of the GFRP rod remains unaffected.

As regards the antenna thermal insulation, to limit the heat flow to/from the spacecraft below 5W, Vetronite is used as thermal washers between the interface and the antenna brackets. With a total surface of transfer of about 16.3 cm$^2$, the required thickness is 1.6 cm and the mass 31 g.

The expected temperature limits and criticality are:

- The thermal knives proposed present operating limits of –70 to 90C, and non-operating limits between –165 to 100C
- Other temperature limits are related to the materials integrity. Materials exhibit in general brittle behaviour at low temperature. With that respect, the compatibility of CFRP and GFRP with the AOCS and thermal loads shall be investigated.

## 10.3 Thermal predictions

### 10.3.1 Europa orbit

The thermal environment applicable to JEO when orbiting Europa has the following characteristics:

- Thermal influence of Jupiter on JEO is negligible with a reflected light less than 0.24 W/m$^2$ and infrared radiation less than 0.28 W/m$^2$
- Thermal influence of the other moons on JEO is negligible
- The environmental heat sources applicable to JEO during operation are restricted to the Sun and Europa, with the following values:
  - Sun irradiance at 5.2 AU is 50.7 W/m$^2$
  - Europa albedo is 0.64 and its mean temperature 103K

In the Europa thermal model:

- The low thermal capacitance of the Yagi antenna makes its thermal behaviour very responsive to Europa thermal distribution, particularly considering the low altitude (h). Depending on the solar right ascension (Ωs) and spacecraft true anomaly, the planet temperature in JEO field of view can vary up to a ratio of 3 (corresponding at spacecraft level to an energy ratio up to 80).
- On the basis of existing photometric data RD[22], RD[23], composition of the surface (ice), the basic profile of (Figure 10-1) is assumed.

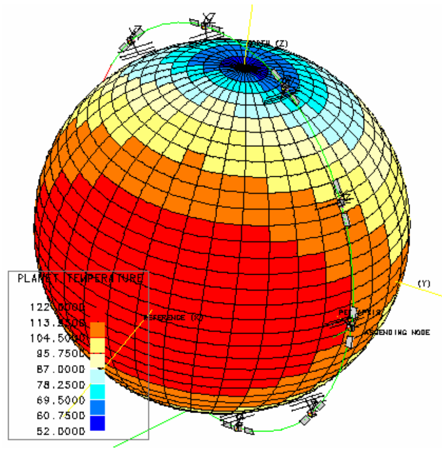


**Figure 10-1: Europa temperature mapping (Kelvin) and orbiting JEO (Ωs = 60°, h= 200km)**

As regards the JEO / Yagi antenna pointing strategy, the existing baseline RD[4] page 57-58, authorises two different pointing orientations depending on the science performed: a radar science with the Yagi antenna nadir pointed and a non-radar science with the Yagi antenna zenith pointed. This second mode includes a steering manoeuvre around nadir to improve solar array performance. Thermal loads on the antenna are derived from the two pointing modes of Figure 10-2 and Figure 10-3.

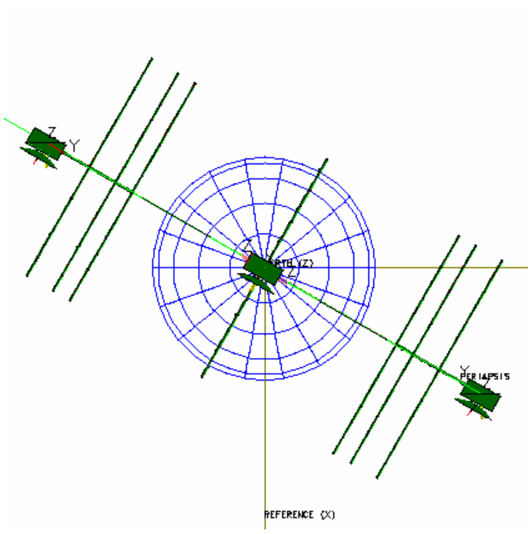


Figure 10-2 : Radar science

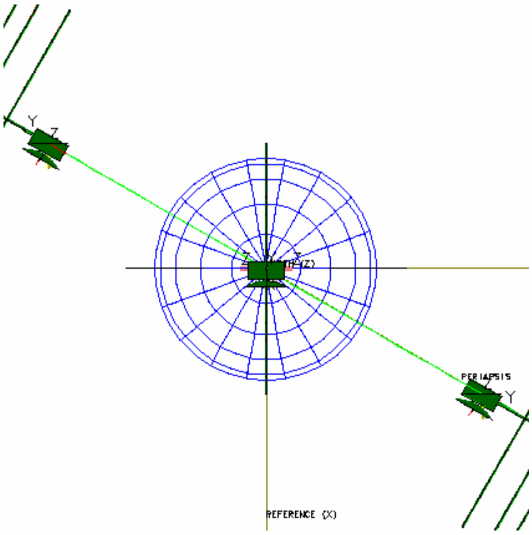


Figure 10-3 : Non-radar science

In the Yagi antenna thermal model:

- On the basis of the assumptions in section 10.2, the Yagi antenna is geometrically modelled (Figure 10-4) and related thermo-optical properties assigned. The spacecraft elements in view of the antenna are represented (solar arrays, HG antenna, main body with dimensions and properties extracted from RD[4].
- The thermal capacitances of the antenna elements are assumed nulls.

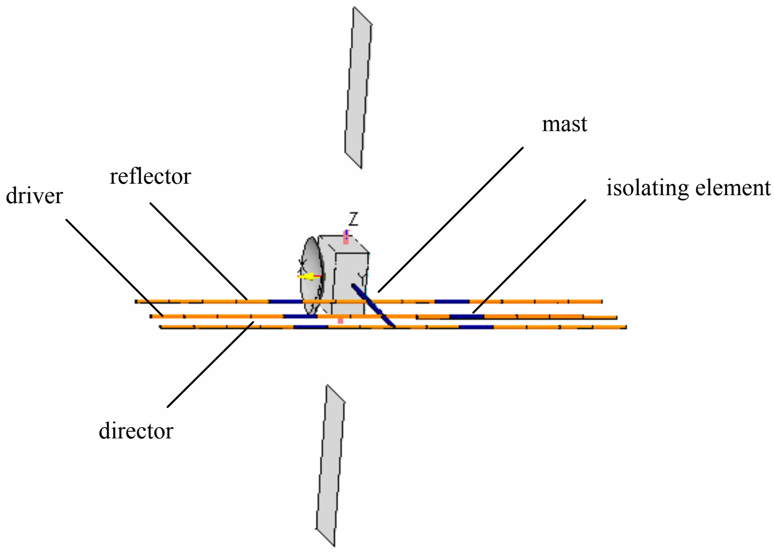


**Figure 10-4: Yagi antenna geometrical model**

For the Yagi antenna predictions:

- Thermal loads on the antenna are derived for each mode (radar science – left figures and non radar science – right figures) at an altitude of 200 km.
- The temperatures of the antenna elements at equilibrium are indicated in Figure 10-5 and Figure 10-6, and the temperature gradients in Figure 10-7 to Figure 10-10 for a complete orbit.

Temperature minima occur when insolation is minimised either when the planet masks Sun rays (during eclipse in radar science and non-radar science, corresponding to the sharp temperature decrease in Figure 10-5 and Figure 10-6 or when the Sun rays impinge a spacecraft surface with a low Incidence. This is the case in non-radar science when the antenna dipoles are colinear with the sun vector, this due to the steering manoeuvre as implemented by the contractor. In this latest case, this decrease of insolation on the dipoles is combined with the Europa north pole radiative influence (see Figure 10-1 the planet mapping and in Figure 10-3 the spacecraft attitude mode with a Sun direction parallel to "reference (X)"). Figure 10-6 shows this steady temperature decrease that leads to the dipoles' temperature minima.

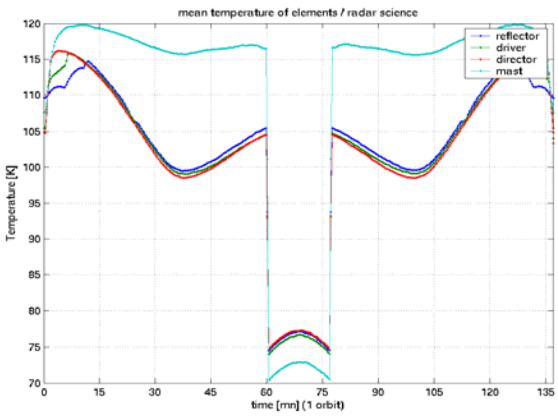


Figure 10-5: Temperatures of the antenna (radar science)

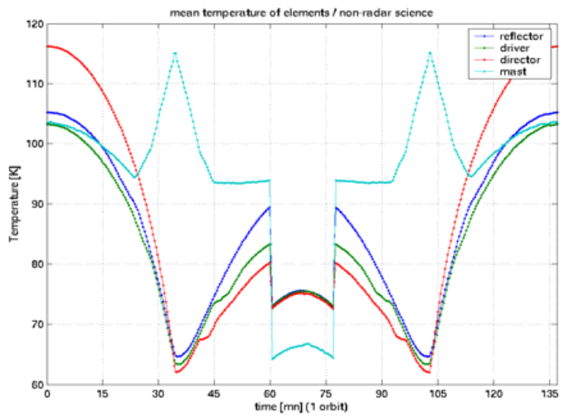


Figure 10-6: Temperatures of the antenna (non radar science)

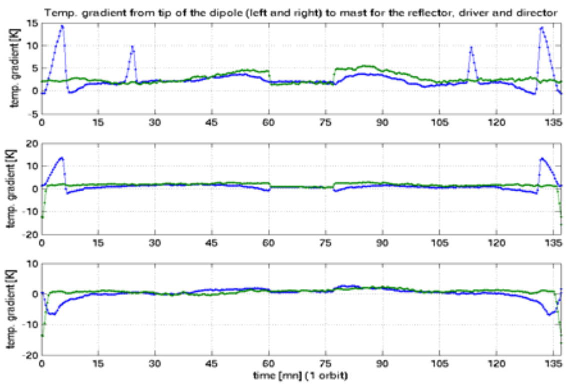


Figure 10-7 : Temperature gradients (radar science)

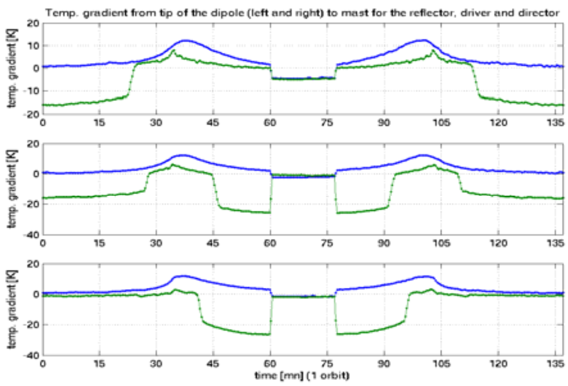


Figure 10-8 : Temperature gradients (non-radar science)

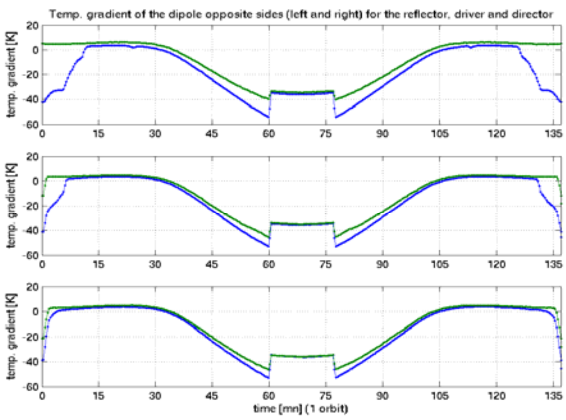


Figure 10-9 : Temperature gradients (radar science)

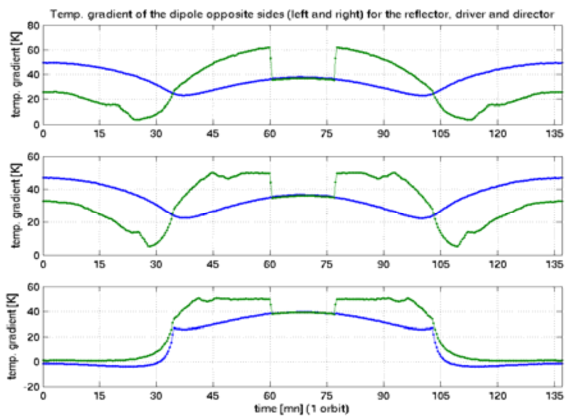


Figure 10-10 : Temperature gradients (radar science)

- The coldest case for the antenna dipoles does not occur during eclipse but during the mode ‘non-radar science’ when passing above the North Pole. The dipoles’ axes are then aligned with the Sun direction (pointing “ref. X” in Figure 10-3) with full view to the lowest planetary temperature and deep space.
- The coldest case for the antenna elements is somewhat different than the spacecraft one and occurs in the mode “non-radar science” for the dipoles when passing above the North Pole. The dipoles’ axes are then aligned with the Sun direction (pointing “ref. X” in Figure 10-3) with full view to the lowest planetary temperature and deep space.
- For the other elements (mast), the coldest case can be found during the eclipse induced by Jupiter. With a low inertia, although subjected to the spacecraft’s influence, the temperature level is expected to be close to the one reached during Europa eclipse (Figure 10-5 and Figure 10-6) but with a duration of 2.9 hrs instead of 0.29 hrs.
- The worst amplitude between Europa hot and cold case is about 50K on the director (farthest from the spacecraft), repeated 640 cycles. The criticality regarding the CFRP and GFRP matrix is open.
- The thermal gradients expected are indicated in Figure 10-7 to Figure 10-10:
  - Maximum longitudinal temperature gradient occurs in the mode “non-radar science” and does not exceed 30K.
  - Maximum transverse temperature gradient is less than 60K (very conservative value due to the absence of transverse thermal conduction – not modelled due to the uncertainty on the thickness, material).

As regards sensitivity to orbital and thermal parameters:

- To check the sensitivity of the antenna temperature to certain parameters, a simplified model (analytic) is used: a uniform planet temperature and a single dipole in space. The solar and planetary radiations (albedo, view factor versus altitude) on a cylinder are estimated using RD[24].
- Figure 10-11 through Figure 10-13 indicate the temperature sensitivity to certain thermal and orbital properties for a different true anomaly (nu=0 and 360 degrees are the ascending node) in Europa orbit and at Venus distance to Sun (Figure 10-14).

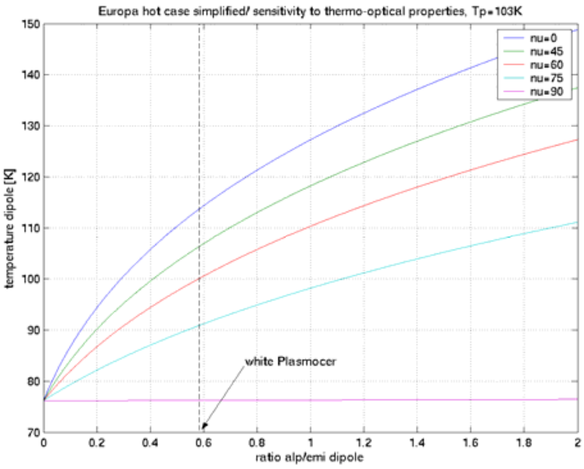


Figure 10-11: Temperature versus thermo-optical properties (Europa)

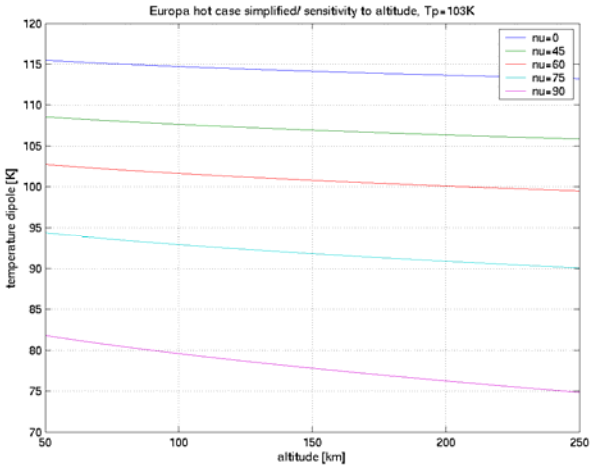


Figure 10-12: Temperature versus temperature planet (Europa)

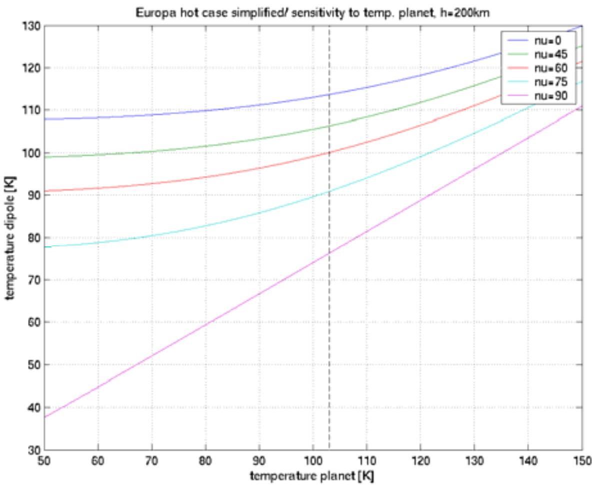


Figure 10-13: Temperature versus temperature planet (Europa)

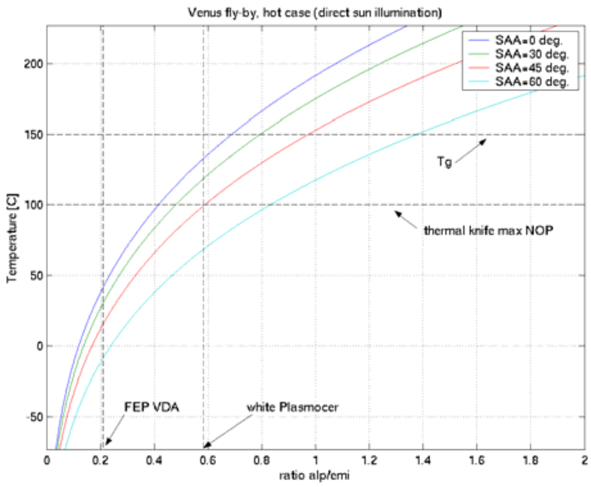


Figure 10-14: Temperature (Venus fly-by)

- The simplified model gives acceptable predictions (Figure 10-11 versus Figure 10-5 and Figure 10-6).
- A low solar absorption coating will decrease the amplitude of the cycling and the related stress on the matrix. White Plasmocer is convenient to such an application (Figure 10-11). Tailoring of the thermo-optical properties is partly possible with the implementation of foreign oxides.
- The temperature variation versus altitude is globally negligible (with respect to the 150 km option).
- The temperature variation of the moon modulates the amplitude of the cycling (Figure 10-13). The low temperature reached in the curve nu=90 (~40K) is due to a higher field

of view (uniform planet temperature in the simplified model) compared to Figure 10-5 and Figure 10-6 (~75K) where the 52K is local (Figure 10-1).

- The minimum operational temperature of the thermal knife (203K) is guaranteed by resistive heating before actuation. Less than 1W is required to bring the temperature from 75K to 203K (equivalent to a 65 W/m$^2$). Appropriate timing (nu=0) or orientation (facing Sun) can be also selected to benefit from a higher thermal environment.

### 10.3.2 Venus fly-by

The baseline selected in RD[4] (option 4 p. 55) authorises an illumination on the face +/- Z during the modes 1 and 2 (see Figure 10-15) to illuminate JRS solar arrays when communicating. This would allow the stowed radar to be illuminated to a certain extent.

In both modes, a rotation around the antenna axis seems possible, but will depend finally on the configuration (JRS electronics, instruments, valves) and related criticality.

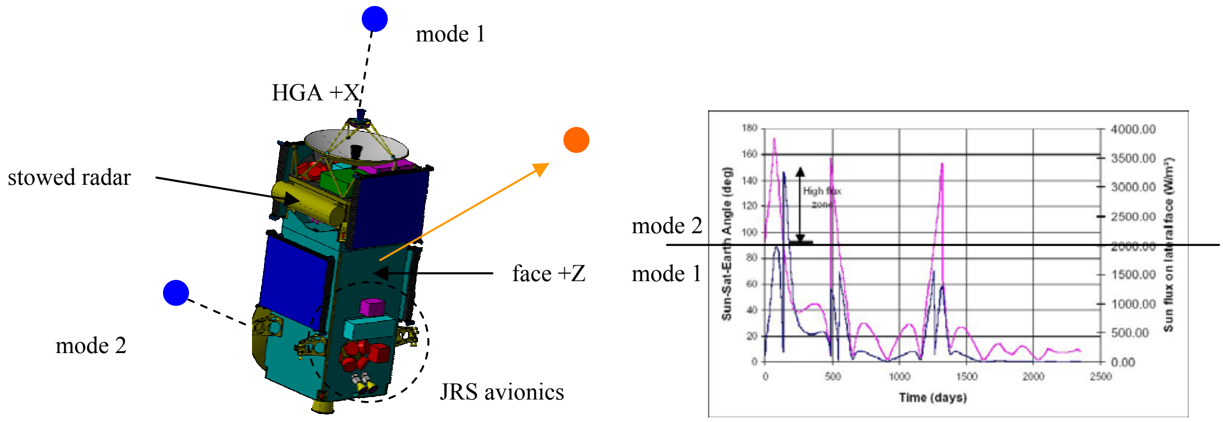


**Figure 10-15 : Spacecraft ± Z face illumination**

Figure 10-14 indicates the expected temperature for different Sun incidence on a flat surface:

- Acceptable temperatures can be met on the thermal knives using either a low incidence (SAA>45°) or a more performant solar reflector. An aluminised FEP can be used locally on the exposed thermal knives surfaces.
- If composites with polymer matrix are used (epoxy, cyanates), the glass transition temperature (with adequate margin) shall not be exceeded. A white Plasmocer coating is sufficient in most of the cases to maintain the dipoles temperature below this limit.

The composite was identified as not critical (probable Tg value not exceeded) but constraints shall be brought on sensitive elements, such as the thermal knives. These are presently seen as the most critical components. The temperature requirement could be met either by appropriate Sun angle or coating, but this shall be further checked with respect to the configuration/design of this element. Shadowing or proper control of the Sun incidence should be the simplest answer, but its implementation has to be validated at system level.

## 10.4 Budget

| | |
|---|---|
| Mass | • Thermal washers: Vetronite, 16 mm thick, 0.03 kg total<br>• Ceramic coating (WP) between 3 and 45 μm thick, mass negligible |
| Power | Thermal knives: < 1W of heating before actuation |

**Table 10-10-1: Mass and power budget**

| **ELRR Expected Temperature Range** | |
|---|---|
| Europa Orbit (Cold case) | 62/120K |
| Venus Fly-by (Hot case) | < 100K (under appropriate configuration) |

**Table 10-10-2: Temperature range for hot and cold case**

## 10.5 Critical issues and conclusions

- The required combination of low CTE, high stiffness and lightweight can be met using composites.
- Composites might face critical issue regarding:
  - The structural integrity of the matrix at low temperature under repeated loads (thermal cycling mainly, AOCS)
  - CTE Mismatch between matrix and fibres that shall remain proportional between room to service temperature (tensile stresses leading to micro cracks.
- An alternative to composites is to use metals, but with a question mark on the required mass budget. Aluminium alloys, in general, increase their mechanical performance at low temperature (~30% at 77K on the yield strength, ~40% at 77K on the ultimate tensile strength, ~10% at 77K on the E modulus) so that a sizing for in-orbit loads should be less demanding in term of mass (depending on the sizing criteria). As regards launch loads, latching of the stowed elements may be considered (compare Rosetta design) which will ease the requirements.
- Metals however do not compete well with composites when low CTE is required, even if a certain decrease is observed in the cryogenic range. The choice depends finally on the tolerance acceptable on the antenna design. If composites are preferred:
  - Bending initiated by different thermal sources (spacecraft, Sun and Europa) on the antenna assembly has to be further checked. Transverse CTE depends on the matrix characteristics and show in general somewhat decreasing values with temperature. Use of a high dimensional matrix like cyanate is advisable offering a stable and very low CTE versus decreasing temperature
  - The compressive strength between tip to mast initiated by thermal gradients is not seen as critical, because of the low CTE value available with tailoring of the fibre direction.
- Passive thermal control only is considered providing the low resources allocated to the antenna. Low absorptance to solar radiation is sought:
  - To minimise the maximal temperature during hot cases when close to the Sun
  - To minimise the amplitude of the cycling when orbiting Europa. Thermal stability should be a design driver if composites are maintained. In that frame, white Plasmocer is selected for its long-term stability
- The Venus fly-by is critical to the antenna thermal knives if illuminated within a high solar aspect angle. A certain tolerance to the spacecraft attitude apparently exists and

could be used to avoid direct sun illumination. The alternative could be the implementation of a sunshade or use of a FEP tape on its exposed surfaces. However, the Venus fly-by is not critical to the other antenna elements if coated with white Plasmocer.

- Heating of the thermal knives is required before activation.
- With a polar orbit, the Europa temperature variation induces by itself a thermal cycling on the antenna.

As regards further development:

- The subsolar temperature of Europa might be revisited with a higher value. The consequence would be a slightly larger amplitude of the thermal cycling.
- Thermal (preliminary and conservative figures have only been provided herein) and thermo-elastic behaviour of the antenna can be assessed when selection of materials and sizing is confirmed.
- Further investigation can be done on the integrity of candidate materials at cryogenic range.

# 11 SIMULATION AND VISUALISATION

## 11.1 Introduction

A simulation of the satellite coverage was performed using Eurosim as a simulation tool and a 2D mapping tool to represent instrument coverage of the surface.

## 11.2 Simulation requirements

These initial requirements were identified for simulation:

- To establish the shortest time for the radar to achieve global coverage assuming 100% radar operations at full available power from Europa orbit.
- To determine the time to achieve global coverage assuming radar operations duty cycles of 90%, 80%, 70%, and 60% and so on down to 10%.

## 11.3 Assumptions

For the simulation a simple orbit propagator for the satellite was used that takes the Kepler elements computed over time that were provided by the Mission Analysis domain. A simple model of the orbit of Europa with a period of approximately 3.5 days was also used. The radar FOV was computed accordingly to the altitude to cover 10 km of the surface of the moon.

## 11.4 Simulation results

The simulation results indicate that 100% radar coverage with a 100% duty cycle is already very hard to obtain during the reference mission. These are some of the values obtained for altitudes of 200, 150 and 125 km:

- 200 km 2.86° FOV
  - 10 days: Total 28.5% - One Pass 25%
  - 20 days: Total 49% - One Pass 36 %
- 150 km 3.82° FOV
  - 10 days: Total 30% - One Pass 26% FOV
  - 20 days: Total 52% - One Pass 39%
- 125 km 4.58° FOV
  - 10 days: Total 30% - One Pass 26%
  - 20 days: Total 48.5% - One Pass 33%

In this case, “Total” means the percentage of total area that has been covered by the radar and “One Pass” is the area that only has been covered once by the radar.

The following figures, Figure 11-1 through Figure 11-4, show 2D-maps of the radar coverage for a 200 km orbit.

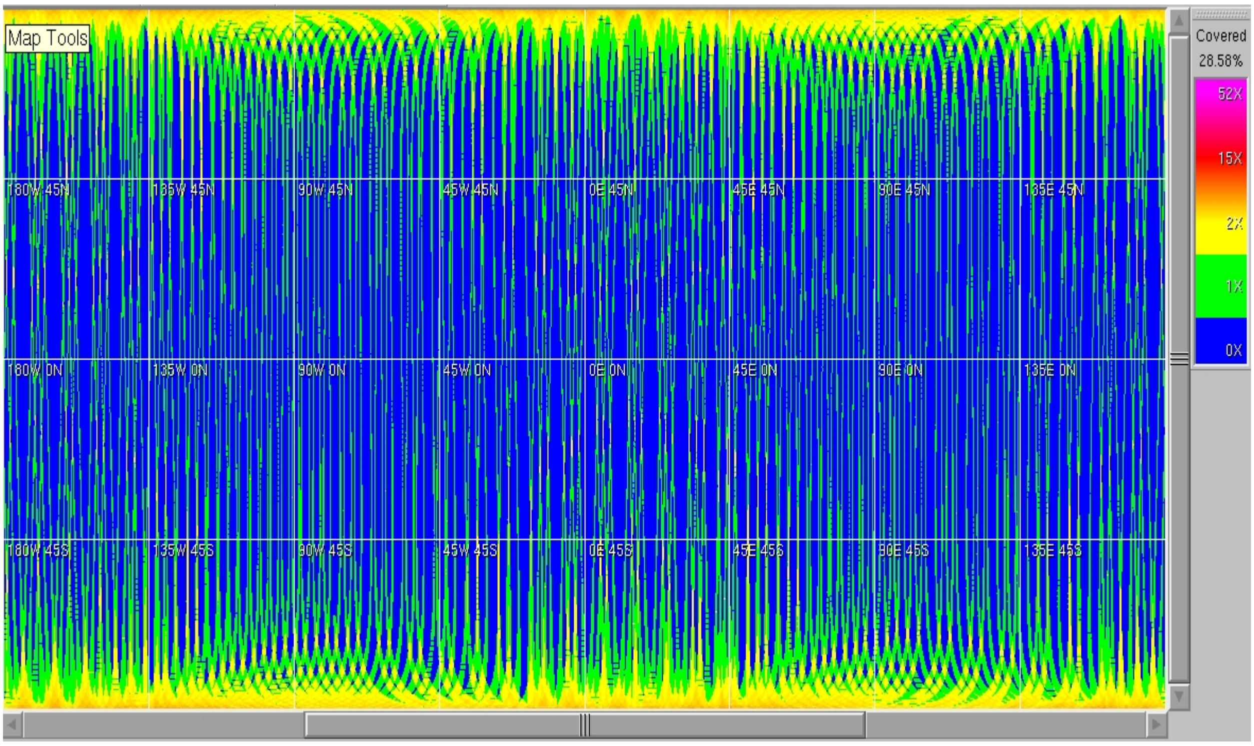


**Figure 11-1: 10-day coverage**

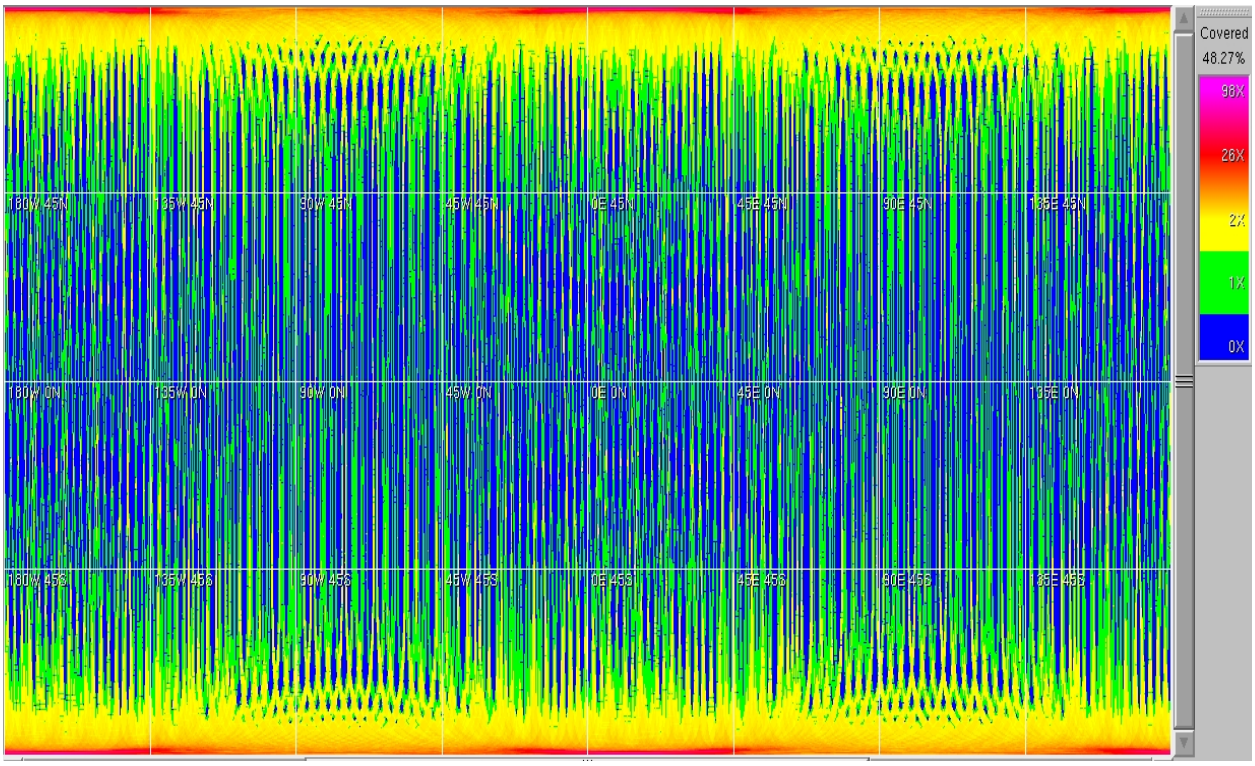


**Figure 11-2: 20-day coverage**

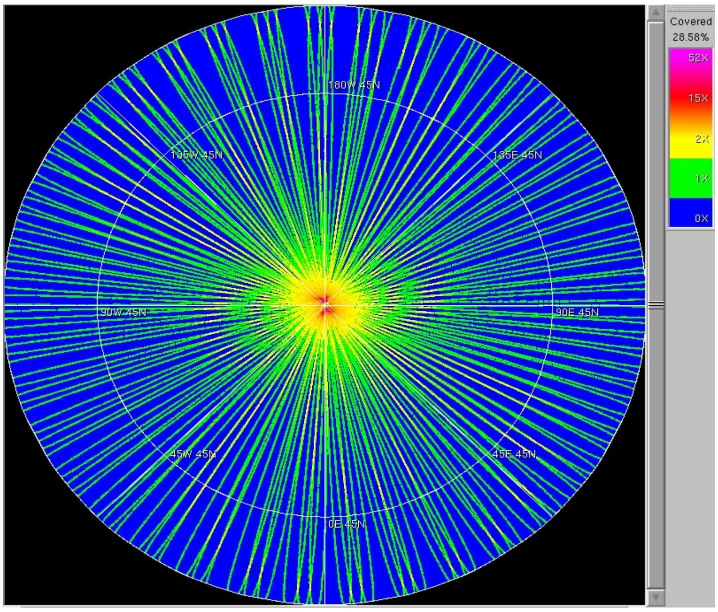


**Figure 11-3: 10-day polar coverage**

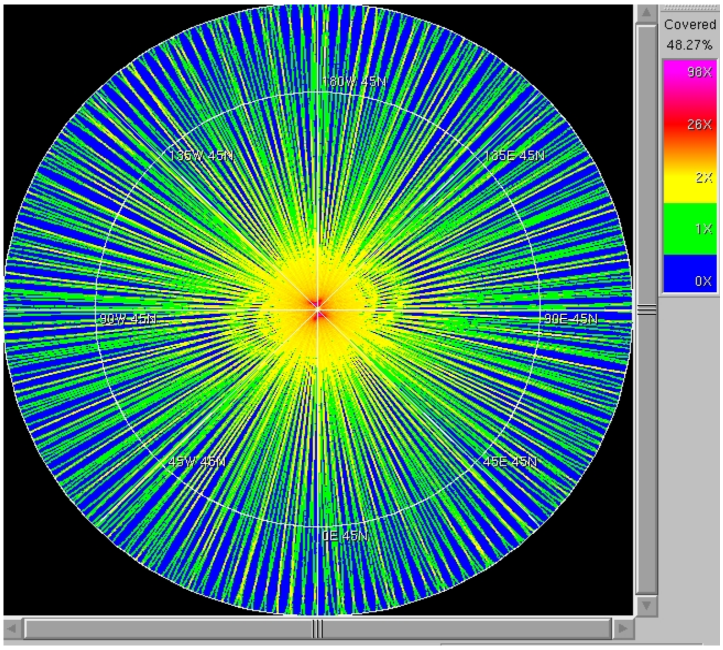


**Figure 11-4: 20-day polar coverage**

# 12 PLATFORM DESIGN REVIEW

## 12.1 Platform systems

### 12.1.1 Design review

The objective of this study is to design a Europa radar compliant with the low resources in terms of mass, power, data rate, data storage provided by the Jupiter Europa Orbiter (JEO) platform and the configuration of the spacecraft. A key design driver is the location of the antenna and the volume available for the antenna in stowed configuration. The JEO platform design was performed by EADS-Astrium in the frame of the Jovian Minisat Explorer (JME) (RD[3]).

The purpose of this chapter is to review this design and identify the interface and resources available for the antenna and describe the antenna design trades respecting these criteria.

### 12.1.2 Requirements and design drivers

The JEO platform design RD[4] drives the system requirements for the antenna:

- Launch in the 2010-2020 timeframe with Soyuz-Fregat 2-1b (Soyuz-S fairing)
- A transfer duration of six years and a Jovian system tour of one year prior to operations
- An operational Europa circular polar orbit at 200 km altitude with a Sun angle tangential to orbit plane of 60°
- A lifetime of 66 days (science phase around Europa limited by orbit perturbation and radiation dose)
- 3-axis stabilised spacecraft
- A mass allocation for the payload of 30 kg of which 10 kg retained for the radar
- A power allocation of 25W
- A data rate of 40 kbps

The design drivers for the system are:

- The high radiation environment
- The platform constraints (low resources, configuration)
- The mechanisms of deployment
- Nadir-pointing payload
- AOCS design regarding the pointing requirements and the required distribution of the payload on two opposite sides of the JEO satellite.

### 12.1.3 JEO design baseline

The JEO spacecraft is part of the Jovian Minisat Explorer mission composed of two spacecraft: JEO and Jovian Relay Spacecraft (JRS). JEO is lifetime and power limited, making transmission of all data impossible in the 66 days lifetime (science phase duration). Therefore a relay spacecraft is required that is close enough to receive all data gathered by JEO. JRS will then transmit all data to Earth within a year, while gathering data on the Jovian system.
The review is limited to JEO since it is the platform providing the resources to the payload. Figure 12-1 and Table 12-1 show the characteristics of the JEO baseline configuration:

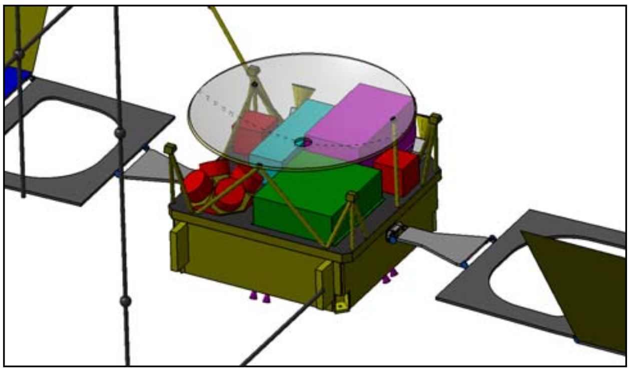

**Figure 12-1: JEO baseline configuration**

| JEO Bus | Without Margin | Margins % | Margins kg | Totals kg | % of Total |
|---|---|---|---|---|---|
| Structure | 64.3 kg | 10.0 | 6.4 | 70.7 | 11.13 |
| Thermal Control | 4.8 kg | 20.0 | 1.0 | 5.8 | 0.91 |
| Mechanisms | 18.3 kg | 6.6 | 1.2 | 19.6 | 3.08 |
| Communications | 22.3 kg | 11.1 | 2.5 | 24.8 | 3.90 |
| Data Handling | 12.0 kg | 20.0 | 2.4 | 14.4 | 2.27 |
| AOCS | 10.0 kg | 9.8 | 1.0 | 11.0 | 1.73 |
| Propulsion | 43.4 kg | 6.0 | 2.6 | 45.9 | 7.23 |
| Power | 75.4 kg | 11.3 | 8.6 | 83.9 | 13.21 |
| Harness | 11.2 kg | 10.0 | 1.1 | 12.3 | 1.94 |
| Radiation | 27.0 kg | 0.0 | 0.0 | 27.0 | 4.25 |
| Total Dry (excl.adapter) | 288.8 kg | | | 315.5 | 49.64 |
| System Margin (excl.adapter) | | 20.0 % | | 63.1 | |
| Total Dry with Margin (excl.adapter) | | | | 378.6 | 59.56 |
| Propellant | 196.0 kg | | 61 | 257.0 | 40.44 |
| Total Launch Mass | | | | 635.6 | |

**Table 12-1: JEO platform mass budget**

Table 12-1 shows the mass budget of the JEO platform (JEO spacecraft without the payload). The JEO platform dry mass is about 379 kg and the propellant mass is 257 kg (including propellant for the AOCS and residuals). The total platform dry mass is about 636 kg. By adding the 30 kg of mass allocation for the payload RD[5], the JEO mass in launch configuration increases to 666 kg.

For power generation, a 14.7 $m^2$ solar generator (divided in 2 x 5 solar cell panels) and 29 $m^2$ of concentrator panels provide 232W EOL.

In terms of dimensions, JEO can be assimilated as a box with the following dimensions:

- Length: 1340 mm
- Width: 1340 mm
- Height: 900 mm.

For the payload accommodation, only two sides are available (see Figure 12-1); since among the six sides, one is used by the high-gain antenna (HGA), two by the two solar generators and one for the interface with JRS in the composite configuration (during launch and cruise phase).

As the ELRR (radar) and the rest of the payload will operate separately (due to low-power allocation) and for FOV and configuration aspects, the radar and the rest of the payload will be located on two different sides of the satellite. Considering the JEO platform configuration, the payload will be distributed on the two opposite sides available on the spacecraft. This means the spacecraft will have to operate a 180° manoeuvre (use of reaction wheels) to pass from radar operation to the rest of the payload operation.

### 12.1.4 Baseline design summary

Considering the science objectives and the instrument requirements and following instrument design trades, it was decided to take as baseline for the radar a 3 x 3 elements Yagi type of antenna operating at 50 MHz. The size associated to this frequency (and wavelength) in deployed configuration is: 10 m x 2 m. The surface available to fold the antenna is one side of the JEO platform with the following dimensions: 1340 mm x 470 mm.

Different Yagi antenna architectures were proposed to support the 3 x 3 elements and allowing a stowed configuration compatible with the surface available. For mechanisms complexity during the deployment sequence, an architecture using a minimum number of elements and a low risk deployment sequence was selected. This architecture is composed of one main arm supporting three bars each composed of three conductive dipoles (red parts in Figure 12-2) separated by non-conductive parts. The architecture and material properties were selected to optimise the structural mass, to reduce the mechanism's mass and complexity and have a first eigen-frequency compatible with AOCS and structure subsystems. A distance of 1.2 m from the spacecraft (see Figure 12-2) was required.

The dimensions of the antenna in stowed configuration are: 1340 mm x 470 mm x 300 mm.

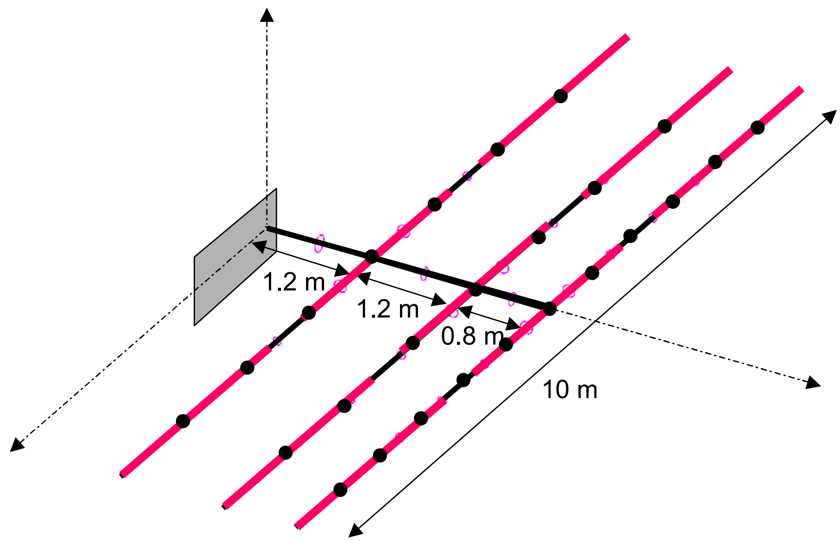


**Figure 12-2: Antenna in deployed configuration**

Different materials are proposed for the antenna:

- Aluminium/Beryllium alloy (current baseline)
- CFRP + coating
- Aluminium
- Titanium

The non-conductive material separating the dipoles has to be defined in future work.

Table 12-2 shows the architecture trade-off for the antenna for the resulting two options following antenna design and architecture trades (see below). It provides the main design parameters for the baseline and the option 1 as well as for the Europa Radar Sounder that was designed by NASA/JPL RD[6].

| | Baseline | Option 1 | Europa Radar Sounder (NASA/JPL) [4] |
|---|---|---|---|
| Deployed antenna | 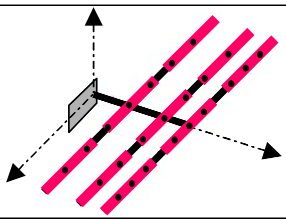 | 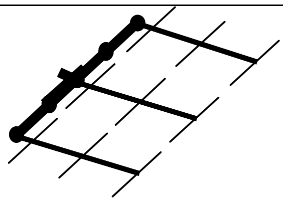 | 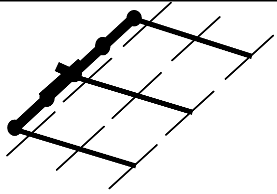 |
| Technology | Bars/hinges | Bars/hinges | |
| Deployed mass (kg) | Structure: 2.70<br>Mechanisms: 1.74 | Structure: 3.2<br>Mechanisms: 2.2 | Structure: 4<br>(Dipoles in Titanium) |
| Mass fixed on spacecraft (kg) | Mechanisms: 1.45 | Mechanisms: up to 3 | Mounting brackets: 0.4 kg |
| First eigen frequency | 1.1 Hz | 1.4 Hz | ~ 1 Hz |

**Table 12-2: Antenna architecture trade-off**

Compared to the option 1, the baseline offers a lower deployment complexity and a reduced risk of collision (deployment in 2 planes). The structural and mechanisms masses were also reduced. The main drawback associated with this design is the need to separate the dipoles by non-conductive elements (need to identify a material non-conductive, resistant to high level of radiation and with appropriate mechanical properties). The architecture of Option 1 was not selected as baseline due to the high number of elements to deploy and the risk of collision during the deployment.

Others technologies to deploy the antenna were reviewed (see Chapter 9, Mechanisms):

- Membrane: not selected due to high mass of mechanisms associated
- Ropes: not selected due to the relatively high mass of mechanisms associated
- Inflatable technology: rejected due to high mass associated considering the low mass allocation
- Telescopic bars: not considered because of the complexity of deployment (2D) and the very high number of components

For comparison, Table 12-2 shows the design of the Europa Radar Sounder performed by NASA/JPL. In this case, the radar is a 3 x 3 Yagi antenna operating at 50 MHz with the following size in deployed configuration: 10 m x 2.6 m. This design provides a good element of comparison since the objectives and design parameters are similar to the CDF ones. The main difference in terms of mass budget is coming from the mechanisms part of the antenna where the mass of mechanisms is 0.4 kg for the Europa Radar Sounder and 3.19 kg for ELRR. This is primarily due to the larger spacecraft body size of the NASA Europa Orbiter Mission enabling a design with fewer antenna mechanisms.

### 12.1.5 Budgets

Table 12-3 shows the mass budget for the radar including design margins. The system margin is 20%. The total mass with margin reaches 11.45 kg, that is 1.45 kg above the mass target of 10 kg.
The structural mass without margin represents 2.7 kg. The material composing the structure still has to be defined and CFRP is baseline, however, Aluminium/beryllium alloy and ceramics are also included. The elements are hollow tubes with 1 mm thickness.

| | | | | | |
|---|---|---|---|---|---|
| | Target Spacecraft Mass at Launch | | | 10.0 kg | |
| | ABOVE MASS TARGET BY: | | | (1.35) kg | |
| ELRR (P/L | Without Margin | Margins % | Margins kg | Totals kg | % of Total |
| Structure | 2.70 kg | 10.0 | 0.3 | 2.97 | 25.28 |
| Thermal Control | 0.03 kg | 5.0 | 0.0 | 0.03 | 0.29 |
| Mechanisms | 3.19 kg | 16.5 | 0.5 | 3.72 | 32.78 |
| RFSystems | 2.35 kg | 20.0 | 0.5 | 2.82 | 24.85 |
| Total Mass | 8.27 kg | | | 9.54 | 83.26 |
| System Margin | | 20.0 % | | 1.91 | |
| Total Mass with Margin | | | | 11.45 | 100 |

**Table 12-3: Antenna mass budget**

Table 12-4 shows the mass budget for the others instruments composing the JEO payload RD[5]. These instruments are located on the opposite side of the JEO spacecraft comparing to the radar (Payload 2). The total mass of these seven instruments is 12.6 kg to which is added the mass of electronics associated (1.5 kg) and the radiation shielding mass (mass estimated to 20% of the instrument mass that is 2.5 kg). It reaches finally 16.6 kg without system margin.

| Functional subsystem | nr | Mass per unit (kg) | Total Mass with margin (kg) |
|---|---|---|---|
| **Instruments** | | | **12.6** |
| Stereo Camera (EuS-Cam) | 1 | 0.60 | 0.60 |
| Near Infrared Mapping Spectrometer (EuVN-IMS) | 1 | 2.00 | 2.00 |
| Radiometer (EuRad) | 1 | 2.00 | 2.00 |
| Laser Altimeter (EuLat) | 1 | 2.00 | 2.00 |
| Magnetometer (EuMAG) | 1 | 1.40 | 1.40 |
| γ-ray Spectrometer (EuGS) | 1 | 3.10 | 3.10 |
| Radiation Environment Monitor (EuREM) | 1 | 1.50 | 1.50 |
| **Electronics** | | | **1.5** |
| **Shielding** | | | **2.5** |

**Table 12-4: Payload 2 mass budget**

Table 12-5 summarises the total payload mass budget adding the mass of the rest of the payload to the ELRR mass.

| | | | |
|---|---|---|---|
| | Target Spacecraft Mass at Launch | 30 kg | |
| | ABOVE MASS TARGET BY: | -1.39 kg | |
| Wet masses: | Dry mass | System Margin used % | Mass with margin kg |
| ELRR (Payload 1) | 9.54 kg | 20.0 | 11.45 |
| Payload 2 | 16.6 kg | 20.0 | 19.94 |
| Total Payload without Margin | 26.14 kg | | |
| Total Payload with Margin | | | 31.39 kg |

**Table 12-5: Total payload mass budget**

### 12.1.6 Critical issues and conclusions

A preliminary instrument design has been performed using Astrium JEO design as the platform for the radar. A baseline ELRR design was conducted considering the low-resources requirements and the JEO configuration constraints in terms of location.

Although optimisation of structural mass was performed, the final total mass of the antenna is 11.45 kg, that is, 1.45 kg above the mass target of 10 kg. This is mainly due to the complexity to deploy the antenna that has to be stowed in the surface available on the platform (increasing the number of elements composing the antenna). The mechanisms become in that case a mass driver (33% of the radar mass).

The critical issues associated to this baseline design are:

- The deployment of the antenna and risk of collision associated
- To define reliable materials for the antenna (stiffness, high-radiation resistive) and the part separating the dipoles (non-conductive, high-radiation resistive) and the radiation tolerance of the electronics components
- AOCS technological issue to provide accurate and reliable Nadir and attitude pointing control in a high-radiation environment

## 12.2 AOCS

### 12.2.1 Introduction

The AOCS segment of the Instrument Design Activity (IDA) of the Europa Low Resource Radar (ELRR) focused on the specific requirements to support the implementation of the Radar Antenna payload on the Jupiter Europa Orbiter (JEO) spacecraft.

The primary objective was to analyse and assess the effects of the AOCS support for the ELRR payload mission requirements established by the baseline EADS-Astrium JME system design (RD[3], RD[4]) These system constraints were further analysed and developed from the JME initial system definition, specifically to assess the impact on the AOCS on the radar antenna detailed design of the CDF-IDA study.

Refining the antenna design through an iterative process, a mature design was established in terms of the mechanical structure and RF performance aspects. It was then necessary to ensure the AOCS could support the slewing, pointing and stability control requirements of the antenna payload instrument implementation.

The specific nature of the JEO mission imposes severe environmental constraints on all spacecraft subsystems. In particular the low temperatures and low power resources due to the large distance from the Sun (5.5 AU) and the high-radiation environment caused by the charged particle interaction with the Jovian magnetic field. The powerful magnetic field of Jupiter concentrates charged particles from the Sun around the planet. This mechanism is responsible for causing the highest charged particle radiation flux measured anywhere in the Solar System, particularly at the radius of the Europa moon orbit.

### 12.2.2 JEO – radar antenna design impact on the AOCS

The proposed radar antenna design has been implemented using a three-element, three-Yagi array. A central supporting rod to holds the antenna's three array elements. The frequency of operation is 50 MHz and the resulting design takes into account many factors including mass, storage dimension, beamwidth, spacecraft altitude, frequency resolution, transmitted power, noise temperature, surface clutter and other constraints.

The tip-to-tip length of each antenna element is 10.2 metres and proposed to be made of aluminium-beryllium alloy tubing. The Yagi array consists of a reflector, driver and director elements. The mode-1 torsional (or axial rotation) eigen-frequency of the antenna has been calculated at 1.1 Hz. The mode-2 out-of-plane oscillation of the complete antenna has an eigen-frequency at 1.6 Hz, and the mode-3 out-of-plane oscillation of the individual elements have an eigen-frequency at 1.8 Hz. The antenna displacements are shown in Figure 12-3 as generated from the antenna structural design analysis (Chapter 7, Antennas).

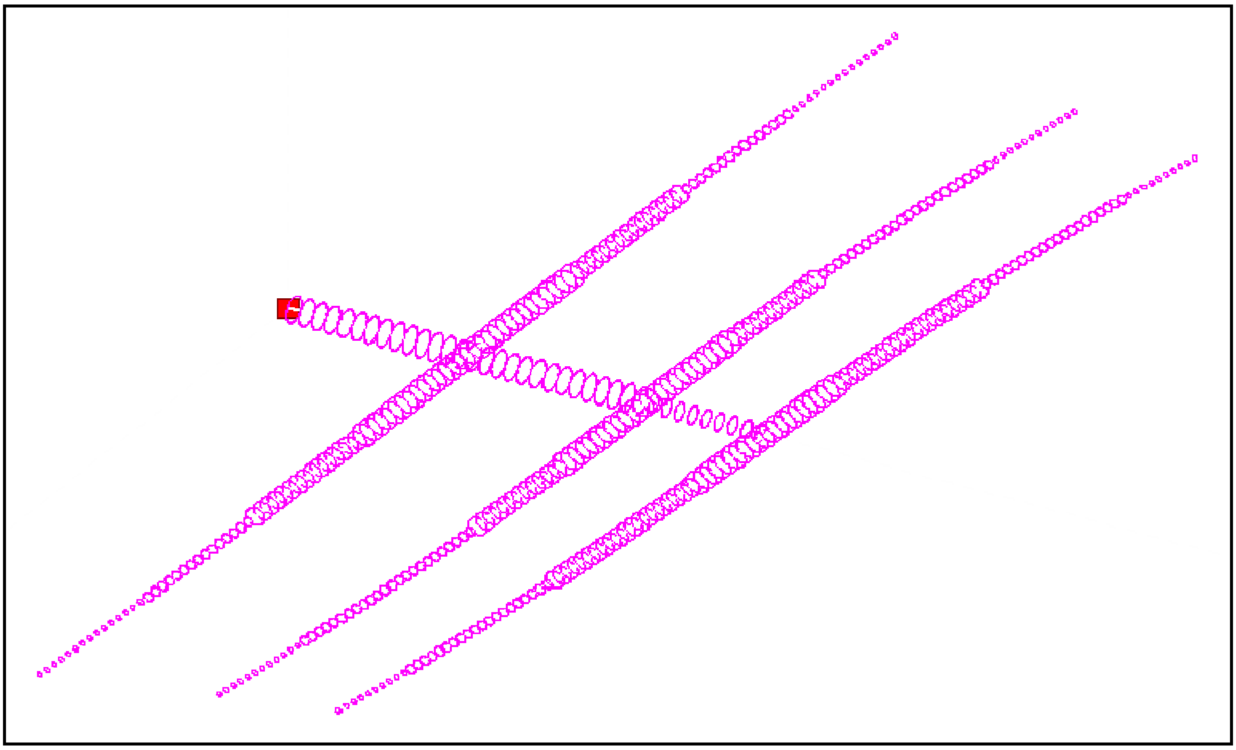

**Figure 12-3: Radar Antenna displacements associated with antenna eigen-frequency analysis**

It is necessary to ensure the AOCS does not "drive" or excite any instabilities in the antenna structure as a consequence of actuator control commanding. The eigen-frequency response of the antenna is strongly correlated to the structural mass that currently exceeds by 1.45 kg the preferred mass requirement of 10 kg. Reducing the mass of the antenna will reduce further the eigen-mode frequencies.

In AOCS terms it is certainly possible to reduce the eigen-frequency of the antenna structure to a value as low as 0.1 Hz, by antenna mass reduction, without seriously impacting the AOCS slew performance or control stability. Reducing radar antenna mass causes instability concerns to be raised with respect to the antenna structure itself, but in terms of the AOCS there is significant margin available for antenna mass reduction.

Earlier antenna designs proposed using materials with CFRP + coating, aluminium and titanium with three separate three-element Yagi array antennas. This structure had a lower eigen-frequency of 0.2 Hz. For the purposes of the AOCS slew performance analysis an absolute "worst case" figure of 0.1 Hz (10 s period) has been taken as the lowest antenna eigen-frequency, assuming there shall be an antenna mass reduction exercise in the future.

Large angle (180º) slews are necessary during the JEO scientific mission phase around Europa. These slews will rotate the radar antenna mounted on one spacecraft panel 180º to an opposite spacecraft panel where the optical instruments are mounted to view the Europa surface. Two axis slews of less than 180º are also required to rotate the JEO fixed HGA to point at Earth to receive up-link telecommands or to rotate the MGA to acquire the JRS spacecraft for science data telemetry downlink.

To avoid exciting flexible mode eigen-frequencies of the radar antenna, the applied reaction wheel (RWL) torque is profiled to avoid generating multiple dynamic frequency components. A "profiled" reaction wheel slew with a ½ period sinusoid acceleration ramp up and then down has the benefit of only one predominant dynamic frequency component defined by the commanded sinusoid period.

The first low frequency "pole" of the AOCS controller closed loop transfer function may be chosen to be a decade in frequency lower than the lowest mechanical eigen-frequency of the radar antenna. It is likely the solar arrays will be of greater concern in this respect as their greater dimensions and inertia will have lower eigen-frequency components than the Yagi radar antenna.

The reaction wheels selected by the EADS Astrium system engineering activity are the Dynacon microwheel 1000. This RWL unit has a maximum total angular momentum storage capacity of 1 Nms at 10 000 rpm and a maximum reaction torque of 30 mNm

$$\theta_{SCslew} = \frac{1}{2}\ddot{\theta}_{SC} \quad t^2$$

$$N_{wheel} = I_{wheel}\dot{\omega}_{wheel} = I_{SC}\ddot{\theta}_{SC}$$

The above equations give the spacecraft 180º slew period as 770 seconds, for a maximum torque from the Dynacon wheel, assuming a spacecraft body inertia about the axis of rotation as I = 200 kgm$^2$. The slew period includes the sinusoidal acceleration and deceleration time of 100 seconds, which is one decade in frequency (20 dB attenuation) away from the worst-case eigen-frequency mode of the radar antenna.

Finally, the spacecraft dynamic slew characteristics demonstrate that the radar antenna structural properties have no significant impact on the JEO AOCS performance, stability or design and vice-versa.

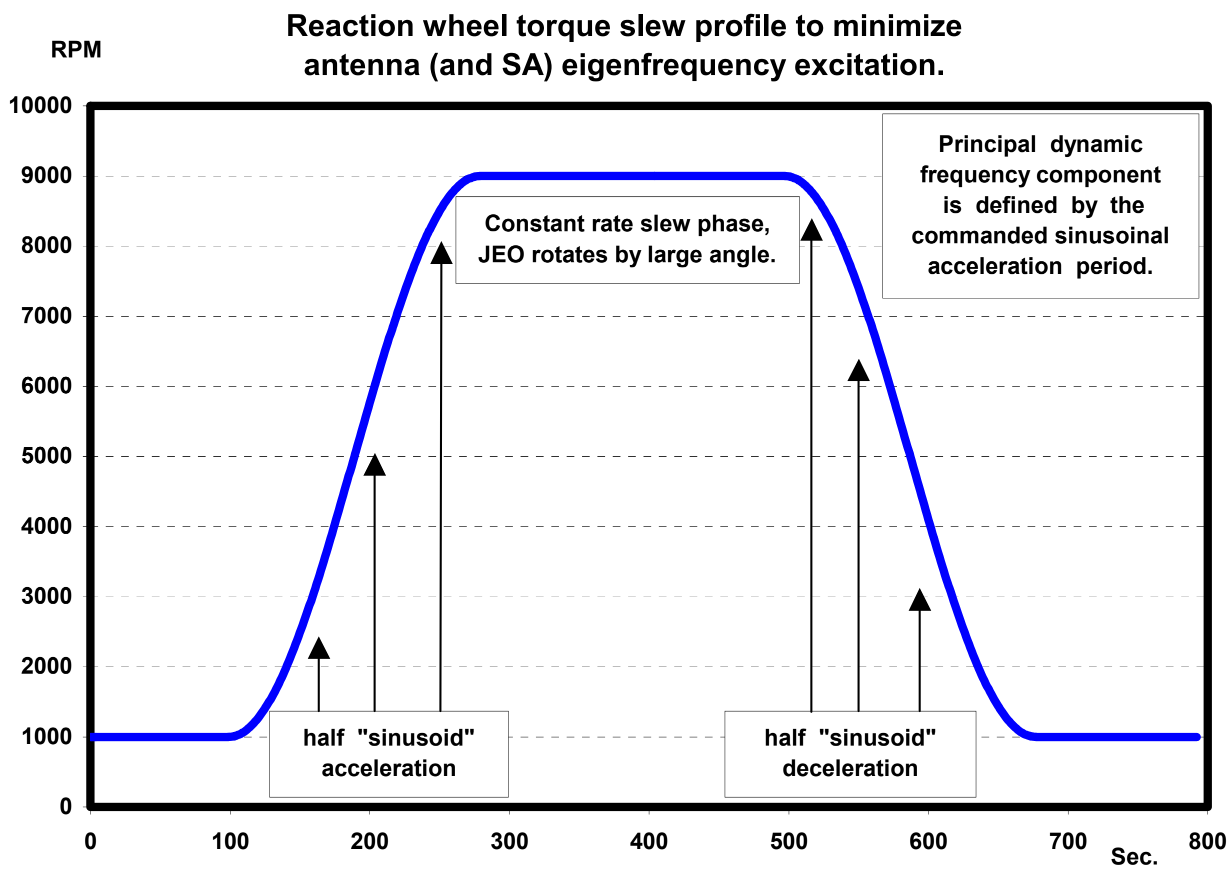


**Figure 12-4: Example of a reaction wheel torque slew profile**

### 12.2.3 RCS-based control modes

JEO RCS-based actuator control modes will need to specify RCS duty-cycles to explicitly avoid excitation of the eigen-frequency modes of flexible spacecraft structures. RCS actuation pulse firings impart relatively high impulse torques that may excite eigen-frequency oscillations in the Yagi antenna or the solar panels if not carefully specified. It is a simple task to implement this requirement in the AOCS mode control software without penalty to the controller stability or performance.

As previously mentioned, orbit maintenance is not part of the JEO baseline mission, however, reaction wheel angular momentum unloading is still a functional requirement during the JEO scientific mission phase. It is also sensible design practice to foresee the possibility to introduce at a later stage an orbit maintenance mode as a future mission requirement. It should also be considered to accommodate a possible mission contingency.

### 12.2.4 Antenna deployment

The complex dynamics imposed by the deployment of large flexible structures like the JEO radar antenna impose complex control requirements on the AOCS. The deployment sequences are once only events that generally last for only a few minutes and are never repeated for the whole mission. Maintaining active control during these very short mission events ironically may consume more design and analysis effort than a mode used for several years of the spacecraft's operational life.

The most effective strategy during complex flexible structural deployments in AOCS terms is to simply do nothing. This means temporarily inhibiting AOCS active control during the antenna or solar array deployments, until the complex dynamics have ended (decayed). Control is then re-enabled taking into account the effect of the "new" spacecraft inertia matrix after the change in the mass properties as a consequence of new antenna position.

During the detailed design phase of the antenna structure, the design of the deployment mechanism, envelope, kinetics and synchronisation shall take into account the AOCS will be disabled during deployment. The spacecraft body may be treated as a simple "reaction-less" inertial mass connected to the antenna. This significantly simplifies the AOCS and antenna deployment design strategies.

The Europa orbiter radar has a complex two-plane synchronised multi-element mechanical deployment using locking elastic hinges that will take about 400 seconds (Figure 12-5 generated by the Mechanisms domain). In the worst case the spacecraft's Sun-pointing may be lost for a few minutes. After complete deployment, an AOCS Sun reacquisition sequence and normal mode attitude pointing recovery logic may be initiated to re-establish AOCS control.

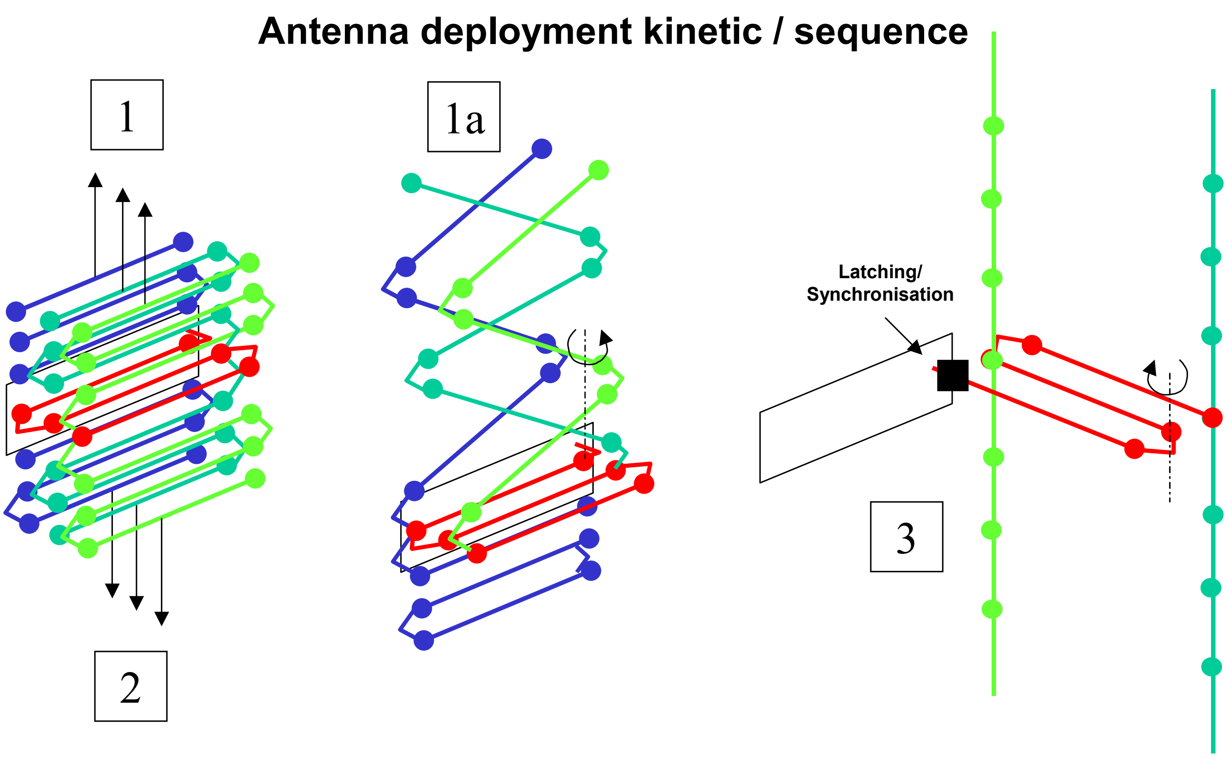


**Figure 12-5: Complex deployment dynamics of multi-element JEO Yagi radar antenna**

### 12.2.5 Antenna nadir-pointing requirement

The primary JEO scientific payload requirement is to detect, locate and measure the radar echo generated by an ice/ocean "interface" to 20 km below the Europa surface. To correctly model and simulate the electromagnetic surface interaction and response from the radar signal a precise and accurate knowledge of the nadir pointing of the radar to the subsurface satellite point is necessary.

Attenuation and perturbations of the RF signal caused by off-nadir pointing has considerable impact on the accuracy of the radar results. The radar cross-section from off-nadir surface echo reflections will be confused as Europa surface slope signals and will result in errors to the small-perturbation-model of the radar signals.

To minimise the effect of off-nadir angle errors, surface clutter (noise) and signals attenuation effects there is a need for accurate Nadir determination from the JEO AOCS. The overall performance of the radar instrument payload is affected by the knowledge of the Nadir pointing accuracy and control. This has the ultimately effect of influencing the radar's ability to measure the structure of the Europa ice crust.

Radar instrument design analysis (see Chapter 5, Instrument System Design) confirms that for a low altitude orbit of 125 km the beamwidth, clutter, penetration and signal/noise performances are not significantly affected with up to +/-5º variation about the X,Y or Z spacecraft axes. It is possible to consider operating the complete science phase of the JEO Europa mission using only inertial data propagated for 66 days. This would require a bias drift of less than 0.2 arc minutes/hour to keep within the +/-5º requirement for 66 days. This is certainly possible with current HRG technology.

### 12.2.6 Effect of Europa radiation environment on AOCS

The charged particle total ionising dose (TID) for the JEO Europa orbiter spacecraft has been specified at 4 Mrad(Si) with equivalent 1 MeV fluence of 3.06E+15 e-/$cm^2$. This aggregate dose specification indicates the total radiation energy absorbed per unit volume of silicon with 4mm of aluminium shielding. This figure amounts to more than 40 times the absorbed radiation of a 15-year geostationary mission.

Analysis shows that the JEO spacecraft will absorb about 50% of the total ionising radiation en-route during the 7 year cruise phase and the remaining 50% dose during the 66 days science mission phase in orbit around Europa. This is equivalent to more than 1 krad/hr during the JEO scientific orbital mission phase.

It is necessary to design and implement an AOCS that can perform in this extremely high radiation environment and satisfy all JEO mission requirements. The proposed design by the EADS-Astrium report requires initial attitude determination to be performed by startracker optical sensors. The CDF-IDA study has identified possible weaknesses in the proposed JEO attitude determination strategy relying on using startrackers in the high-radiation environment of Europa.

Using a startracker to provide the initial inertial attitude reference for attitude control ephemerid propagation or nadir reconstruction is satisfactory only if a startracker can operate reliably in the extremely high Europa-Jovian radiation environment.

Currently, no startracker exists that has been qualified to operate in a 4 Mrad radiation environment specified for the JEO mission. This is an extremely demanding requirement for any CCD or APS (silicon)-based technology for this magnitude of radiation. Shielding cannot prevent radiation entering the startracker optical axis onto the CCD and cannot prevent high-energy events.

A reflecting front-end optical path (mirrors) may be a solution but imposes field-of-view limitations and a significant technology development effort. High levels of radiation are also known to darken optical glass. These problems will need to be addressed before a startracker can be considered for this mission.

Direct measurement of the radar antenna nadir using conventional limb sensor technology should then be considered. Here again environmental constraints of Europa impose technology development problems. Existing Earth limb sensor technology operates by sensing the infrared radiation emitted by the molecular vibration of the carbon dioxide ($CO_2$) gas molecule (14 µm wavelength) in the Earth's atmosphere. This technique has the advantage that the Earth's infrared $CO_2$ radiance profile is the same in daylight as night, as the $CO_2$ molecular vibration emission is not dependant on sunlight illumination.

Europa does not have (sufficient) $CO_2$ in its atmosphere to allow conventional Earth-based limb sensor technology to be exploited. The large angle (12.5º) subtended by the disc of Jupiter "masking" the limb of Europa during the JEO orbit, will also present operational difficulties. This will complicate the Europa edge detection functionality significantly. A new edge detection technology would need to be developed for Europa.

A Europa Orbiter analysis report written by NASA confirms the CDF-IDA's concerns: ***"****The Stellar Reference Unit (SRU) is expected to have significant image degradation in high flux environments such as this"* and *"The Europa Orbiter will depend on gyros alone for attitude information upon Europa Orbit Insertion, because the optical sensors may not meet performance requirements in the worst case temporal variations in the natural space environment that surrounds the Jovian moon****"***, RD[25].

Analysis of inertial measurement technology shows that Hemispherical Resonant Gyro (HRG) units may operate to required specifications in high Jovian radiation environments about Europa. These units will also satisfy the low-power, high-reliability, long-life and low-mass constraints necessary to satisfy the JEO mission requirements. Once a reliable initial attitude reference has been established, attitude propagation by an inertial platform will not present the same difficulties experienced by current startracker technology.

It has therefore been identified that the high-radiation environment around Europa presents considerable technology challenges particularly for silicon-based optical sensors used by the AOCS.

### 12.2.7 JEO – Europa orbit characteristics

The baseline orbit for the JEO spacecraft was defined as a circular, 200 km altitude, 90º inclination orbit with a 60º tangential solar aspect angle. Based on these inputs, Figure 12-6 through Figure 12-10 were generated by ESOC RD[26], and advised by the CDF study mission analysis domain. They summarise the environmental consequence of the selected orbit geometry for the AOCS.

An important mission requirement was for no orbit maintenance after JEO-EOI (Europa Orbit Insertion) around Europa. The spacecraft scientific mission phase is to be performed without station-keeping ΔV orbit control. The mission lifetime will then be defined by the natural orbital decay of the spacecraft determined by local environmental effects. The instrument electronics and solar array lifetimes limited from the severe radiation around Europa and full radar coverage being achieved within two months makes orbit maintenance unnecessary.

Refinement of the radar antenna design and RF/signal operational requirements (including: beamwidth, noise temperature, clutter, signal-noise ratio) demonstrated that a lower orbit of 125 km would have significant advantages. Coincidently this is also the case for the AOCS.

Strong gravitational tidal forces from Jupiter together with a large J2 gravitational potential term (from Europa) causes a maximum orbit duration without correction at an altitude of 125 km. Normally higher altitudes would guarantee longer orbital duration, however the powerful gravitational effects of Jupiter rapidly perturbs orbit eccentricity and causes a more rapid orbital decay above 125 km. This effect also breaks down at altitudes below 125 km where the Europa J2 gravitational harmonic term predominates and eccentricity is again more rapidly perturbed.

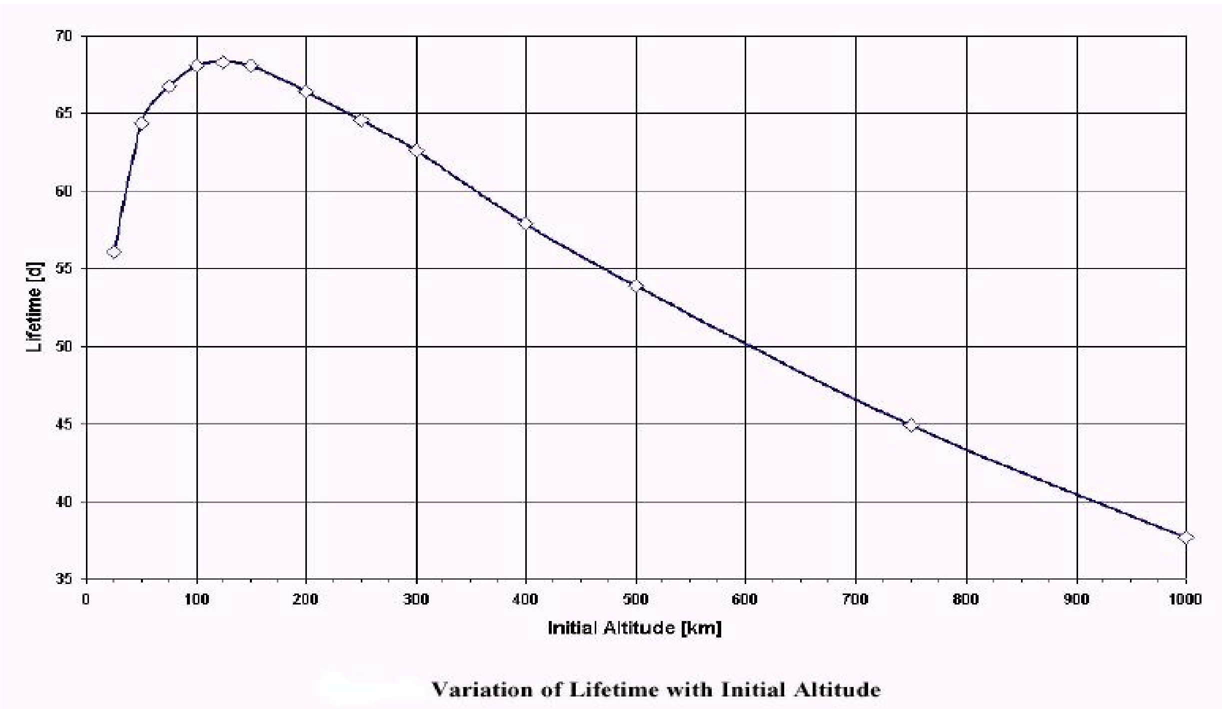


**Figure 12-6: JEO mission span without RCS orbit maintenance for circular Europa orbit insertion**

Mission analysis of the Jovian-Europa system shows that the JEO mission lifetime is very sensitive to the initial eccentricity of the JEO orbit insertion. There also appears to be an unusual local maximum to the mission lifetime if a JEO-EOI can be achieved with an initial orbit eccentricity of 9.0E-04. This appears to almost double the lifetime of the mission, but this effect is not fully understood and requires further explanation. Nevertheless, accurate circular orbit injection is a prerequisite for extending an un-maintained JEO orbiting mission.

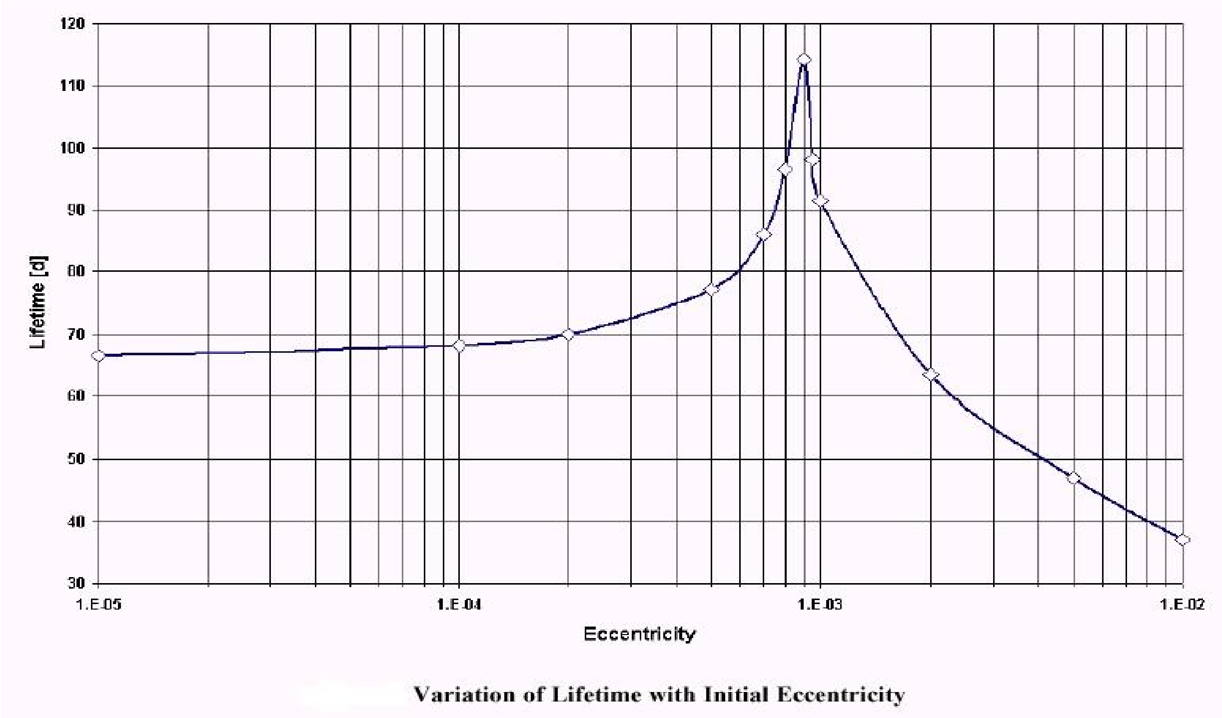


**Figure 12-7: Sensitivity of mission duration based on initial JEO orbit insertion eccentricity**

The 200 km orbit was used as the initial baseline for the mission analysis. It can be seen that once accurate circular orbit insertion has been achieved, orbit decay is relentless and rapid. This figure emphasises the need for accurate, circular JEO-EOI to guarantee mission duration.

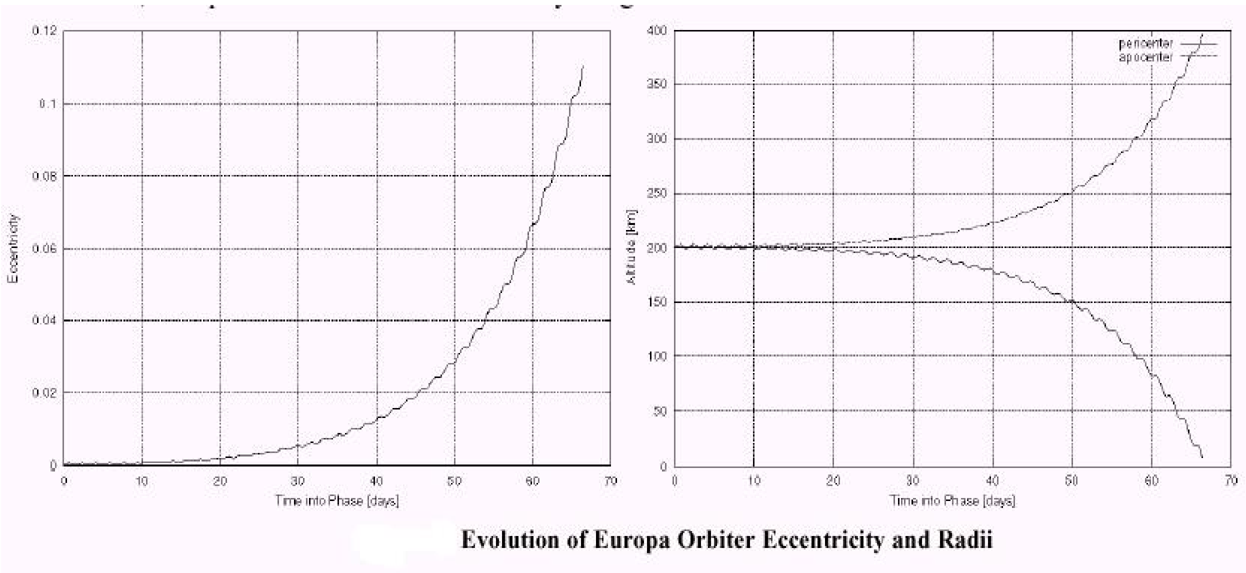


**Figure 12-8: JEO orbital decay timeline for Europa orbit insertion at 200 km**

The JEO mission could be prolonged if a "non-polar" orbit is chosen, but this would compromise full radar surface coverage. Simulation shows that full coverage with at least 7 passes over each point on the Europa surface could be achieved for a circular orbit at 125 km altitude with 90º inclination (see Chapter 11, Simulation and Visualisation). Mission prolongation by reduced orbit inclination is not a necessary mission requirement.

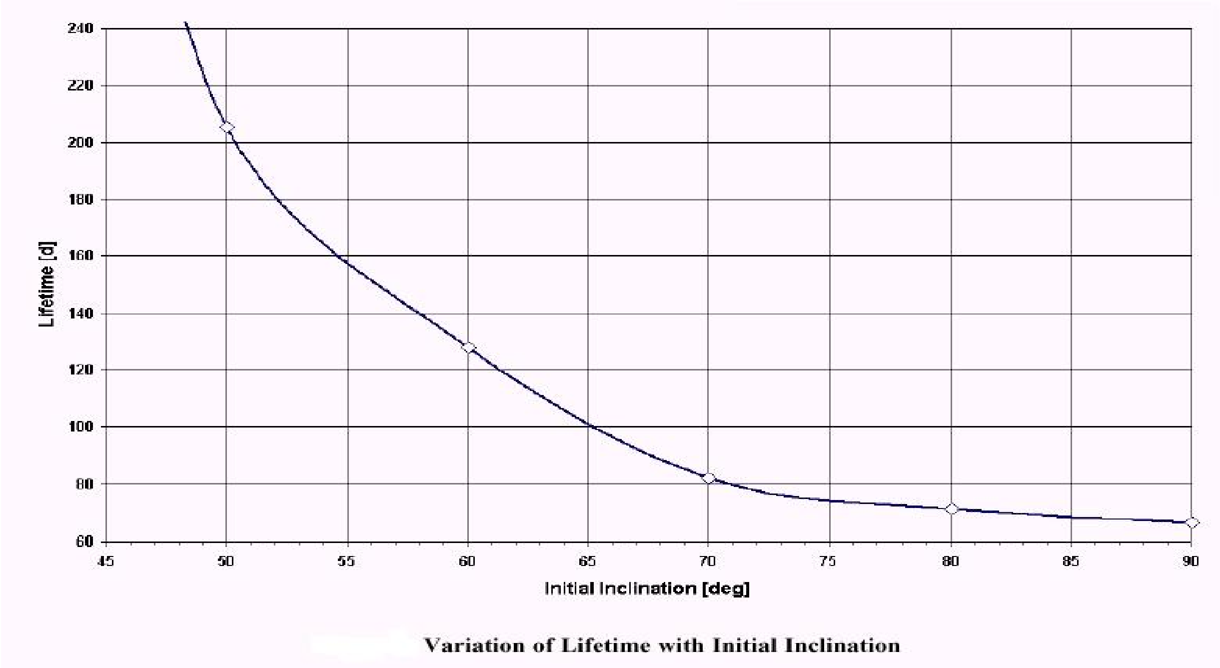


**Figure 12-9: JEO orbital decay timeline based on initial orbit inclination**

The argument of the ascending node for the JEO-EOI does not significantly affect the mission lifetime. The baseline orbit has a 60º inclination to the Sun, chosen to minimise eclipse duration. These last 0.28 hours every 2.24 hours caused by Europa, and 2.9 hours every 3.5 days caused by Jupiter.

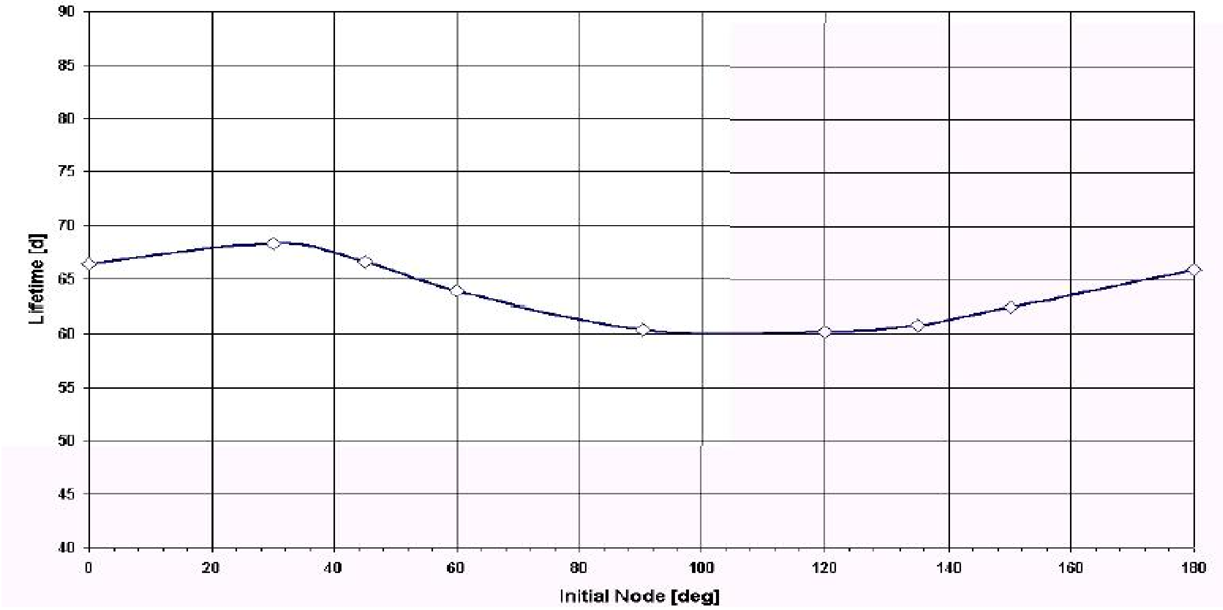


Variation of Lifetime with Initial Node

**Figure 12-10: JEO orbit lifetime based on initial ascending node of JEO at 200 km orbit insertion**

## 12.3 Power constraints: orbital altitude selection trade

### 12.3.1 Introduction

The current EADS design of the JEO mission does not provide sufficient power for the mounted radar. The power required for the radar increases with the altitude of the spacecraft. Unfortunately, the selection of a lower altitude has several consequences, including a loss of the power available on the bus (Figure 12-11). The goal of this study was to assess this loss of power and to compare it with the evolution of the power required for the radar.

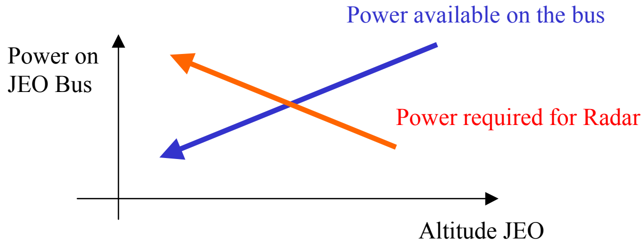


**Figure 12-11: Evolution of the power required for the radar on the resources available**

### 12.3.2 Inputs and assumptions

This study is based on the documents illustrating the mission (RD[3], RD[4]). The design has clearly evolved between these two reference documents. In case of conflict, the data are issued from the most recent document (RD[4]).

The description and the performances of the power subsystem are not completely provided in this reference so it is impossible to make a proper power budget. Nevertheless, another possible approach is to estimate the differences compared to the established baseline.

### 12.3.3 Mission inputs

In the selected mission, the spacecraft, when orbiting around Europa, has an initial circular orbit of 200 km. The proximity of Jupiter is the main rationale of the fast modification of this orbit: after 66 days, the spacecraft is expected to crash on the surface.

Figure 12-12 shows this variation of the lifetime as a function of the initial latitude RD[26]. To avoid cases with too short mission durations, orbits with an initial altitude below 50 km are rejected.

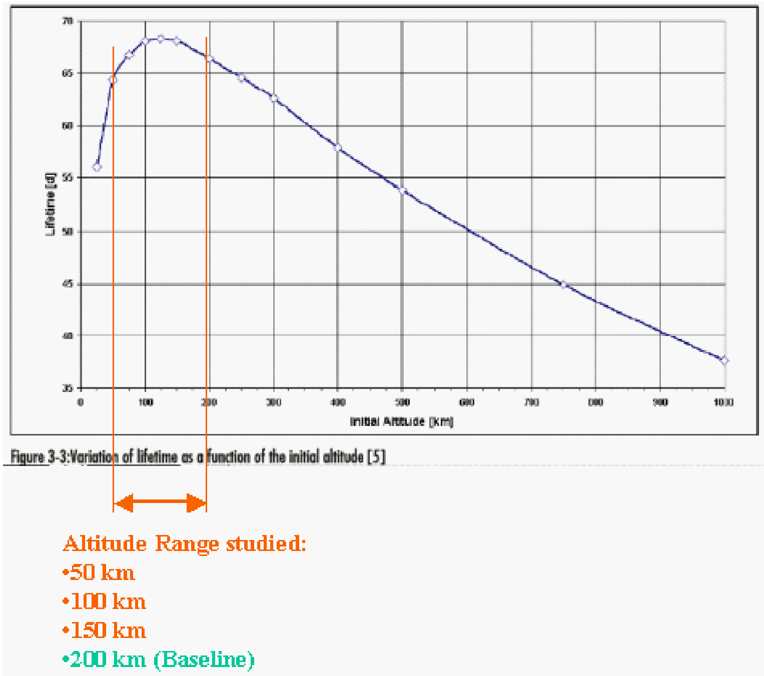


**Figure 12-12: Variation of lifetime as a function of the initial altitude**

The proposed circular orbit of the JEO around Europa has a Sun incidence of 60 degrees. This value is issued from a trade between, on one side, the power requirement (limitation of the time in eclipse) and on the other side, the visibility of the camera (avoidance of the partial shadowing of the ground visible area). The main parameter that influences the power available on the bus is the eclipse duration (see Figure 12-13). The JEO has to endure the eclipses from Europa and also the eclipses from Jupiter (see parameters in Figure 12-14).

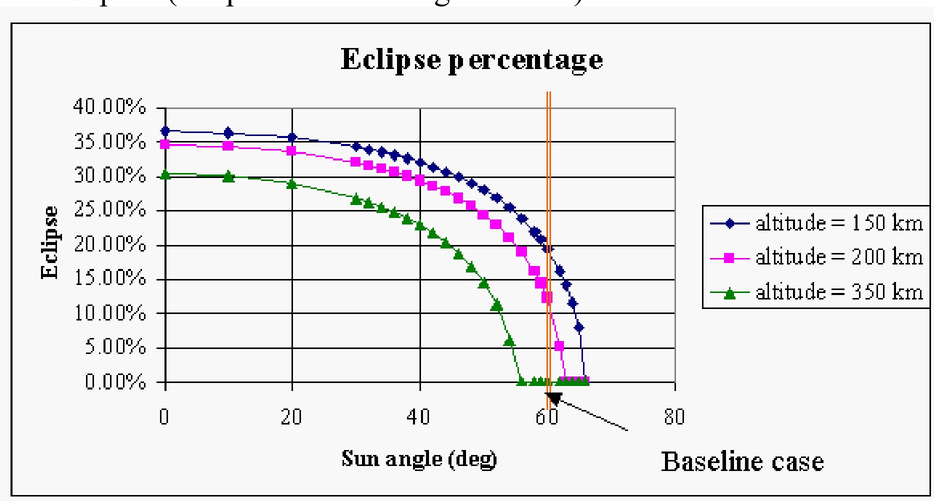


**Figure 12-13: Europa's eclipse percentage for different altitudes and Sun angles**

| Altitude Range studied: | Satellite Parameters | | Europa Parameters | |
|---|---|---|---|---|
| | orbit duration (BOL) | eclipse duration (BOL) | Jupiter eclipse duration | Orbit Duration |
| | h | h | h | h |
| •50 km | 1.96 | 0.67 | 2.90 | 85.23 |
| •100 km | 2.05 | 0.55 | 2.90 | 85.23 |
| •150 km | 2.15 | 0.43 | 2.90 | 85.23 |
| •200 km (Baseline) | 2.24 | 0.28 | 2.90 | 85.23 |

Figure 12-14: Europa's and Jupiter's eclipses seen by the JEO for different altitudes

### 12.3.4 Power inputs

The power budget of the JEO RD[4] is shown in Figure 12-15:

| | Description | MARGIN | Current JEO Consumptions (W) including margins | | | | | | | | | | Assumptions |
|---|---|---|---|---|---|---|---|---|---|---|---|---|---|
| | | | Cruise | | Transfer | EOI | Science 1 | | Science 2 | | Commu with JBS | | |
| | | | without comms | with comms | | | With Sun | Eclipse | With Sun | Eclipse | With Sun | Eclipse | |
| | Duration | | 15 min | | 15 min | 75 min | | | | | | 90 min | |
| RF | X/Ka-band TRSP 1 | 5% | 0.0 | 13.5 | 13.5 | 5.3 | 5.3 | 5.3 | 5.3 | 5.3 | 13.5 | 13.5 | Motorola SDST data sheet |
| | X/Ka-band TRSP 2 | 5% | 0.0 | 5.3 | 5.3 | 5.3 | 5.3 | 5.3 | 5.3 | 5.3 | 5.3 | 5.3 | |
| | Down converter 1 | 10% | 0.0 | 0.0 | 0.0 | 0.0 | 0.0 | 0.0 | 0.0 | 0.0 | 8.8 | 8.8 | Estimated from Payload C-band downconverter |
| | Down converter 2 | 10% | 0.0 | 0.0 | 0.0 | 0.0 | 0.0 | 0.0 | 0.0 | 0.0 | 0.0 | 0.0 | |
| | Ka-band SSPA 1 | 10% | 0.0 | 12.8 | 12.8 | 0.0 | 0.0 | 0.0 | 0.0 | 0.0 | 12.8 | 12.8 | 30% efficiency estimated for 3.5W RF power |
| | Ka-band SSPA 2 | 10% | 0.0 | 0.0 | 0.0 | 0.0 | 0.0 | 0.0 | 0.0 | 0.0 | 0.0 | 0.0 | |
| | USO 1 | 20% | 0.0 | 0.0 | 5.4 | 0.0 | 0.0 | 0.0 | 0.0 | 0.0 | 5.4 | 5.4 | TESAT infos |
| | USO 2 | 20% | 0.0 | 0.0 | 0.0 | 0.0 | 0.0 | 0.0 | 0.0 | 0.0 | 0.0 | 0.0 | |
| Data Handling | OBMU | 20% | 28.8 | 28.8 | 28.8 | 28.1 | 28.8 | 28.8 | 28.8 | 28.8 | 28.8 | 28.8 | Bepi Colombo HICDS / estimated for SB |
| Power | PCDU | 10% | 9.1 | 9.4 | 9.6 | 9.2 | 9.5 | 9.5 | 9.5 | 9.5 | 9.5 | 9.5 | Estimated from Myriades |
| | Battery charging | 0% | 0.0 | 0.0 | 0.0 | 0.0 | 52.5 | 0.0 | 52.5 | 0.0 | 52.5 | 0.0 | Calculated |
| | SADA | 10% | 0.0 | 10.1 | 10.1 | 0.0 | 10.1 | 10.1 | 10.1 | 10.1 | 0.0 | 0.0 | SNECMA information |
| ACS | STR1 | 20% | 0.0 | 0.0 | 4.6 | 4.6 | 4.6 | 4.6 | 4.6 | 4.6 | 4.6 | 4.6 | Bepi Colombo |
| | STR2 | 20% | 0.0 | 0.0 | 0.0 | 0.0 | 0.0 | 0.0 | 0.0 | 0.0 | 0.0 | 0.0 | |
| | IMU 1 (BOL) | 10% | 0.0 | 0.0 | 5.5 | 5.5 | 5.5 | 5.5 | 5.5 | 5.5 | 5.5 | 5.5 | Bepi Colombo |
| | IMU 2 (BOL) | 10% | 0.0 | 0.0 | 0.0 | 5.5 | 0.0 | 0.0 | 0.0 | 0.0 | 0.0 | 0.0 | |
| | ION Thrusters | 20% | 0.0 | 0.0 | 0.0 | 9.6 | 0.0 | 0.0 | 0.0 | 0.0 | 0.0 | 0.0 | AREFI |
| | RWA 1 | 10% | 0.0 | 0.0 | 4.4 | 0.0 | 4.4 | 4.4 | 4.4 | 4.4 | 4.4 | 4.4 | Dynacon microwheel 1000 |
| | RWA 2 | 10% | 0.0 | 0.0 | 4.4 | 0.0 | 4.4 | 4.4 | 4.4 | 4.4 | 4.4 | 4.4 | |
| | RWA 3 | 10% | 0.0 | 0.0 | 4.4 | 0.0 | 4.4 | 4.4 | 4.4 | 4.4 | 4.4 | 4.4 | |
| | RWA 4 | 10% | 0.0 | 0.0 | 0.0 | 0.0 | 0.0 | 0.0 | 0.0 | 0.0 | 0.0 | 0.0 | |
| Harness | | 0% | 1.7 | 2.8 | 3.7 | 1.9 | 5.1 | 3.5 | 5.1 | 3.5 | 5.1 | 3.6 | 3% of total consumption |
| | **Total Bus** | | **59.6** | **82.8** | **112.5** | **75.6** | **139.8** | **85.8** | **139.8** | **85.7** | **165.1** | **111.0** | |
| Thermal Control | | 20% | 28.3 | 28.3 | 28.3 | 0.0 | 28.3 | 28.3 | 28.3 | 28.3 | 28.3 | 28.3 | 13.6W for propulsion + 10W for heating |
| Payload | DPU/CPS | 0% | 0.0 | 0.0 | 2.0 | 0.0 | 2.0 | 2.0 | 2.0 | 2.0 | 0.0 | 0.0 | Cruise |
| | Ground penetrat. radar | 0% | 0.0 | 0.0 | 0.0 | 0.0 | 20.0 | 20.0 | 0.0 | 0.0 | 0.0 | 0.0 | |
| | Stereo Camera | 0% | 0.0 | 0.0 | 0.0 | 0.0 | 0.0 | 0.0 | 1.0 | 0.0 | 0.0 | 0.0 | |
| | Visible-Near IR Spectro | 0% | 0.0 | 0.0 | 0.0 | 0.0 | 0.0 | 0.0 | 1.0 | 1.0 | 0.0 | 0.0 | |
| | LIDAR | 0% | 0.0 | 0.0 | 0.0 | 0.0 | 0.0 | 0.0 | 5.0 | 5.0 | 0.0 | 0.0 | |
| | Europa radiometer | 0% | 0.0 | 0.0 | 0.0 | 0.0 | 0.0 | 0.0 | 2.0 | 2.0 | 0.0 | 0.0 | |
| | X-ray spectrometer | 0% | 0.0 | 0.0 | 0.0 | 0.0 | 0.0 | 0.0 | 5.0 | 5.0 | 0.0 | 0.0 | |
| | gamma and neut. spectro | 0% | 0.0 | 0.0 | 0.0 | 0.0 | 0.0 | 0.0 | 3.0 | 3.0 | 0.0 | 0.0 | |
| | Magnetometer | 0% | 0.0 | 0.0 | 0.0 | 0.0 | 0.0 | 0.0 | 0.5 | 0.5 | 0.0 | 0.0 | |
| | radiation monitor | 0% | 0.0 | 0.0 | 2.0 | 0.0 | 0.0 | 0.0 | 2.0 | 2.0 | 0.0 | 0.0 | |
| **Total power without system margin** | | | **67.9** | **111.1** | **144.8** | **75.6** | **190.2** | **136.1** | **189.6** | **134.5** | **193.4** | **139.3** | |
| **Total power with 20%system margin** | | | **81.5** | **133.3** | **173.8** | **90.7** | **228.2** | **163.3** | **227.6** | **161.4** | **232.1** | **167.2** | |

Figure 12-15: JEO power budget

The power subsystem is assumed to be sized for a complete revolution around Jupiter (3.55 days) by staying in Science Mode 1: the energy balance is achieved on the bus for this duration. As regards the recharge of the battery, an average value of 52W on the bus is taken into account for this computation (RD[4]).

This value is not compatible with the data from Figure 12-15. Hence, the computation of the power loss with the altitude of the spacecraft has been calculated in the two cases.

### 12.3.5 Power architecture inputs

Referring to the JEO documentation RD[4], the power system topology is based on a Maximum Power Point Tracker (MPPT) design.

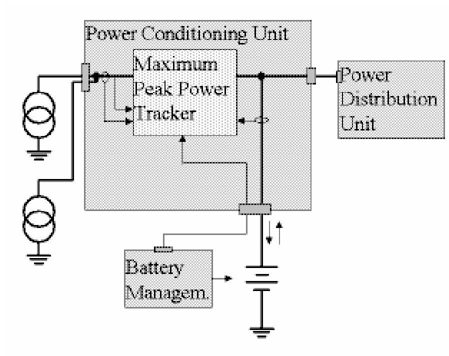


**Figure 12-16: MPPT unregulated (battery bus) architecture**

The selection between a MPPT architecture with an unregulated bus (Figure 12-16) and a MPPT architecture with a regulated bus (add of battery regulators) has not been traded yet. However, the JEO design has been computed by assuming the following losses for the battery regulators:

- Battery Charge Regulators (BCRs): 90%
- Battery Discharge Regulators(BDRs): 90%

On top of these losses, a battery round-trip Wh-efficiency of 90% has also been considered.

To cover both possible design options, the power loss evolution on the bus has been assessed for the two types of MPPT architectures: unregulated and regulated.

### 12.3.6 Results

As described in section 12.3.5, the power loss on the JEO bus for different orbit altitudes compared to the baseline has been computed for both a MPPT regulated and a MPPT unregulated bus with power inputs issued from, on the one side, the power budget and on the other side, the power required for the recharge of the battery.

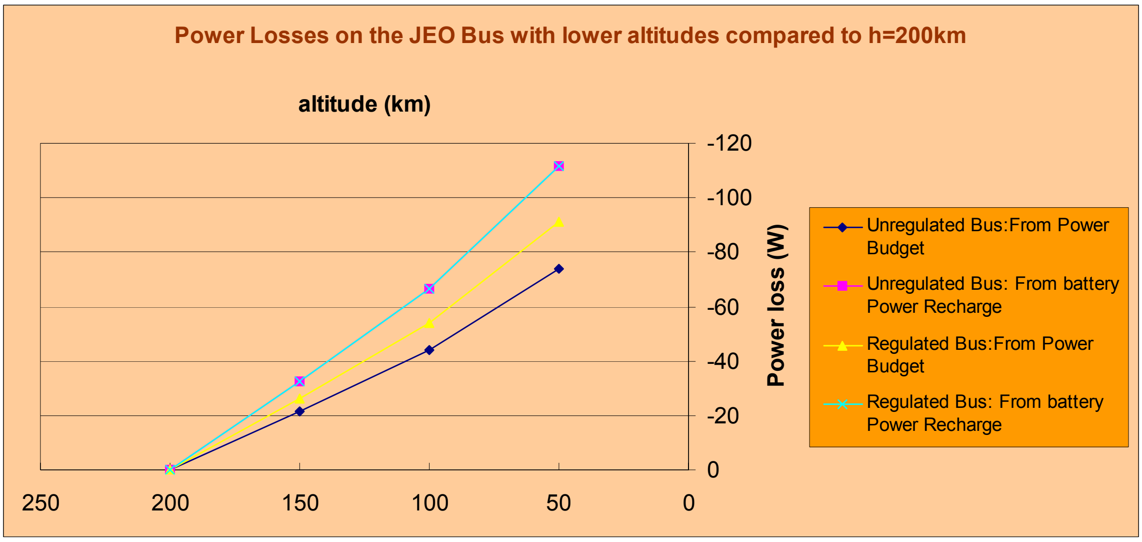


**Figure 12-17: Power losses on JEO bus for lower altitudes compared to baseline h=200 km**

The four power loss estimations are slightly different. However, even in the best case, for an attitude of 150 km, the power loss is higher than the power allocated to the radar (20W).

To summarise, the option to decrease the altitude of the initial circular orbit of the spacecraft around Europa is not feasible with the current design of the spacecraft. To solve the lack of power available for the radar, others solutions may be to:

- Increase the Sun angle of the orbit (to trade with the camera field of view requirements)
- Increase the size of the solar panels (to trade with the volume and mass limitations of the launcher)
- Keep the JEO solar arrays folded during cruise for limiting the radiation degradations (to trade with the risk of a deployment mechanism failure)
- Decrease the working time of the payload by compensating with the battery module (to trade with the mission completion).

## 12.4 Telecommunications

### 12.4.1 Assumptions and trades

#### 12.4.1.1 Pointing mechanism trade-off for JEO

This trade-off has been done to optimise data transfer from JEO to JRS. Three options are taken into account for the JEO HGA antenna: no pointing mechanism (fixed antenna configuration), 1 DOF pointing mechanism and 2 DOF.

The main purpose of this optimisation is to increase radar observation time of Europa. With a 2-DOF pointing mechanism, no change of attitude is necessary to point JEO-HGA to JRS-HGA. Due to the low JEO mission duration, communications time should be minimised. Otherwise, in case of fixed HGA, for each attitude change, time is required and additionally, time is required for data transmission to JRS. The addition of both times is the amount of time lost for science.

Table 12-6 shows the data requirements calculation. In conclusion, an average data rate during each JEO orbit around Europa of 36 kbps needs to be transmitted, including the overhead introduced by the transmission protocol plus a margin.

| | |
|---|---|
| **Radar data rate** | 28 kbps |
| **HK** | 2 kbps |
| **Transmission protocol overhead (14%) +Extra Margin (6%)** | 20% - > 6 kbps |
| **Total** | **36 kbps** |

**Table 12-6: JEO on-board data requirements calculation**

The time for transmitting the TM data from JEO to JRS depends, in a trade-off, mainly on the modulation and used coding (see RD[27] and RD[28]), since power and antenna diameter are given. In Table 12-7 a transmission time estimate per day (24 h) is assumed. These data will be used in Table 12-8 to calculate the lost observation time due to communications. Turbo codes are not recommended for this mission since the decoder complexity on JRS will be high, while with convolutional code it will be low.

| Modulation | Coding | Data rate | Data transmission duration for 24 h generated data. |
|---|---|---|---|
| SPL/PM | Convolutional | 900 kbps | 0.96 h |
| SPL/PM | Turbo code ¼ | 1.58 Mbps | 0.55 h |
| GMSK | Convolutional | 1.8 kbps | 0.48 h |
| Data rates are calculated for a maximum distance JRS-JEO of 400 000 km, transmitted power 3.5W and 1.5 m antennas in JRS and JEO | | | |

**Table 12-7: JEO-JRS data transmission duration for different modulations and coding**

In the case of a no pointing mechanism being present for the JEO HGA, a HGA spacecraft pointing time (change of spacecraft attitude) of 13 minutes is assumed. Therefore 26 minutes are assumed to be lost for that purpose due to pointing (two pointing manoeuvres, pointing JEO-JRS and pointing JEO-Europa surface).

In the trades no data compression techniques have been assumed due to the low efficiency of "no-loss" compression techniques when applied over radar data.

When working efficiently, a transmission protocol overhead of around 14% is assumed. An extra margin of 6%, in addition to 14%, has been applied in Table 12-6.

The mechanism mass budget used in Table 12-8 has been calculated in Table 12-9. In that table, an antenna mass of 10 kg (pessimistic value) has been assumed to calculate the mass of the mechanisms.

| HGA CONFIGURATION | FIXED | 1 AXIS | 2 AXES |
|---|---|---|---|
| **Mechanism Mass** | N/A | 4.5 kg | 5 kg |
| **Mechanism Power consumption** | N/A | 6W<br>4% duty cycle<br>(worst case) | 12W<br>4% duty cycle<br>(worst case) |
| **Operation complexity** | - | 0 | + |
| **JEO Cost** | + | 0 | - |
| **Time lost for science due to comms in percentage (%)** | **No data compression and 0.5 h for pointing:**<br>• 4% (GMSK)<br>• 6% (SPL/PM)<br>• 4.4% (SPL/PM, Turbo Code ¼ ) | Simulations are necessary | Close to 0% |
| **Risk** | - | 0 | + |
| **'+' = a positive aspect, '-' = a negative aspect, '0' = a neutral aspect** | | | |

**Table 12-8: Trade-off between 1 DOF, 2 DOF or no pointing mechanism for JEO HGA**

| | |
|---|---|
| **3 HDRM (antenna support during launch)** | 1 kg x 3 = 3 kg |
| **ADPM** | 0.9 kg for 1 DOF<br>1.4 kg for 2 DOF |
| **Deployment arm** | 0.5 kg |
| **TOTAL** | **5 kg** for *2* DOF<br>**4.5 kg** for *1* DOF. |

**Table 12-9: Mass budget for 1 or 2 DOF steering mechanism**

### 12.4.2 Conclusions

The JEO system baseline has a fixed HGA due to the constrained resources available. It has been shown that such a baseline reduces the radar operations time by between 4 – 6% depending on the modulation and coding used. The additional system resources required for a HGA pointing mechanism range between 4.5 kg/6W and 5 kg/12W for one DOF and two DOF, respectively.

# 13 PROGRAMMATICS

Section removed from web based version.

# 14 TECHNICAL RISK ASSESSMENT

Section removed from web based version.

# 15 COST

Section removed from web based version.

# 16 CONCLUSIONS

The key conclusions, critical areas and recommendations for further work are described in this chapter.

## 16.1 Key conclusions

The key conclusions are as follows:

- Radar sounding of the Europa ice is feasible to a depth penetration of about 13.9 km (resolution of 100 metres at the surface and with 10% degradation by depth) using an 850 kHz bandwidth.
- Based on the very limited datasets accessible within the small duration of the study, the ice model used to assess the radar performance is an average case that underestimates the absorption of the ice and that slightly overestimates the surface clutter (two effects that compensate each other). The effect of moving to other (also realistic) cases was assessed, however, further analysis is recommended that shall focus on the conversion from scientific to observation requirements, based on all the data on Europa available to the community.
- To achieve this depth penetration, an RF transmit power of 375W is required. The instrument is operated only half the time, so twice the power is available during the time of operation, that is, about 50W. The overall power consumption of the instrument including margin in the radar mode is 67.1W including a 20% margin (approximately 56W without margin). The average power consumption is 33.6W with a 20% margin or 26.5W without margin.
- To constrain the instrument power consumption to 25W including all margins continuously, the peak RF transmission power requirement must be reduced by 4.5 dB to 133.75W; this will reduce the performance.
- Increasing the bandwidth to 2.55 MHz increases the penetration depth to 14.4 km.
- Decreasing the orbit altitude to 125 km increases the penetration depth (with similar resolution) to 14.4 km (850 kHz bandwidth) and 14.8 km (2.55 MHz). This also improves insensitivity to roll error. However, decreasing the altitude increases the eclipse time that is outside the system constraints of the current JEO spacecraft power system design and is not baseline.
- Depth penetration extension of the radar is limited to increasing the bandwidth, however this is at the expense of increased data rate and instrument complexity.
- Assuming the feasibility of further improvement in gain through higher power, better efficiency or a larger antenna would result in an improvement of penetration depth at a rate of only 150 m/dB.
- Mechanical design of the 50 MHz triple Yagi, three–element baseline antenna is feasible.
- Key resources confirmed as 11.45 kg, 67.1W, 28 kbps.
- The stowed antenna can be accommodated on the current JEO spacecraft within dimensions of 1340 x 470 x 300 mm.
- The materials selected for the radar antenna are subject to further technology development work, that is, suitable materials that meet the stringent radiation, cryogenic and electrical requirements are not a trivial matter.
- The baseline antenna design (with no risk of deployment collision with the spacecraft) assumes the use of non-conductive elements. The electrical properties of such an antenna is subject to further verification.

- An alternative and conventional antenna design with free space between the elements has been shown to collide with the spacecraft during deployment in preliminary assessments. Further analysis may show such a design to be feasible.
- The JEO spacecraft systems have been shown to be generally compatible with the baseline radar sounder defined during the CDF activity.

## 16.2 Critical areas

Table 16-1 shows the solutions for critical areas:

| Discipline | Issue | Solution |
|---|---|---|
| **Instrument systems** | Depth penetration. | Up to 14.0 km feasible at 200 km altitude. |
| | | Improvement of 150 m/dB if noise temperature and power improved |
| | | Up to 15 km feasible at 125 km. |
| **Wave interactions** | Roughness/ topography of Europa surface. | More detailed analysis of Galileo data. Performance depends on terrain type (surface clutter strength). |
| | Inner structural/dielectric composition of ice crust. Unknown ice composition. | Understanding of ice formation models and further sensitivity analysis. |
| | | Earth based microwave measurements. |
| | Model validity (slopes, inhomogeneous medium). | Dedicated model for simulation of microwave interaction should be developed for echo sounding. |
| | Radio noise. | More research to quantify the spatial extent of emission and performance impact. |
| **Instrument electronics** | Component radiation hardness. Power MOSFET for High Power Amplifier (HPA). MOSFET for Electrical Power Conditioning (EPC). VLSI digital components. | Technology development. |
| | Resources estimates. | Bread-board modelling, development and testing. |
| | Amplifier efficiency. | |
| **Antenna** | Non-conductive material between dipole elements. | Technology research and development. |
| | Low loss coaxial cable for long duration stress. | Long duration life time testing. |
| | | New development of coaxial tube guide. |
| | RF loss of hinges. | Development programme. |
| **Mechanisms** | AOCS generated loads as a function of structure instability limits. | Planned development. |
| | | Slow slewing, avoidance of thruster firings, fundamental eigen-frequency design. |
| | Structural stability during deployment. | Simulations and breadboard testing. |
| | Deployment simulations. | Sensitivity studies. |
| | Ground testing. | 1 g effects analysis and test compensation. |
| | Radiation/cryogenic sensitivity. | Materials selection and development. |
| | Low structural damping/low deployed flexibility. | Design specification and development. |

| Discipline | Issue | Solution |
|---|---|---|
| | Number of hinges reducing stiffness. | Increase stowage volume available. Analysis and development testing. |
| | Deployment reliability after 7 years storage. | Verification planning. |
| | Electrical conductivity continuity. | Development testing and materials selection. |
| | Wire routing/resistive torque. | Design and development monitoring. |
| | Collision with spacecraft HGA. | Guidance/protection implementation. |
| **Configuration** | Stowed volume and collision. | Test and verification. |
| **Thermal** | Venus fly-by high temperatures. | Shadow stowed antenna with S/C body. |
| | | Dedicated Sun shade (system resources). |
| | | Operations/Comms. pointing constraints. |
| | Europa orbit deployment HDRM within temperature limits. | Heating before actuation. |
| | Europa orbit phase. | |
| | High rate temperature change due to low thermal capacitance antenna elements. | Thermal stresses/shock – materials selection. |
| | | Amplitude of cycling minimised by coating selection. |
| | Low resources. | Passive control – materials selction. |
| **AIV** | Antenna deployment. | Development of test procedure and method |
| | Planetary Protection | Stringent procedures including bio-testing and personnel training. |
| | Highly integrated payload suites. | Integration, test and sterilisation (planetary protection) before delivery. |
| | Payload critical technologies. | Completed at phase B start. |
| | Availability of AIV facilities. | Compliant with planetary protection criteria. |
| **Cost** | Beryllium, C-SiC (antenna). | Exotic antenna materials have cost impact. |
| | Strict mass limits. | High engineering effort. |
| | Planetary protection. | Increased costs. |
| **AOCS** | Attitude sensors. | Technology development. |
| | Altitude and orbit lifetime. | Accurate circular orbit insertion. |
| | Slew and pointing requirements. | Easily achieved. |
| **Power** | Increase power available for payload. | Increase orbit Sun angle (camera conflict) |
| | | Increase size of solar arrays (volume limit) |
| | | Keep JEO SAs folded during cruise (risk) |
| | | Decrease payload working time (compensate with battery module) (Mission constraint) |
| **Communications** | 4 – 6% science operations loss. | Use 1 DOF (4.5 kg/6W) or 2 DOF (5 kg/12W) mechanism for spacecraft HGA. |

**Table 16-1: Solutions for critical areas**

# 17 REFERENCES


RD[1] Science Requirements Document for Jupiter Minisat Explorer, SCI-A/2004-069/AA, ESA, 26/4/04.

RD[2] Status Report on the Jupiter Minisat Explorer, SCI-A/2004/TN-085/AA, ESA, 21/5/04.

RD[3] JMO System Concepts Analysis - draft, JMO.NT.0004.T.ASTR, EADS-Astrium, 23/1/04.

RD[4] JMO Technical Assistance – Progress Meeting 3, EADS-Astrium, 18-19/05/04.

RD[5] Jovian Microsat Explorer – Payload Definition Document (PDD), CR-PTRM-JME-PDD, Cosine, 18/2/04.

RD[6] Europa Radar Sounder Instrument Definition, Feasibility Study Report 184, NASA-JPL, 25/6/99.

RD[7] Giese, private communication, 1998.

RD[8] Moore J.C., Models of radar absorption in Europan ice, Icarus 147 (2000) 292-300.

RD[9] Eluszkiewicz J., Dim prospects for radar detection of Europas's ocean, Icarus 170 (2004) 234-236.

RD[10] Galileo Radio Propagation Experiment, http://www.star.stanford.edu/projects/gll/

RD[11] Chyba C. et al., Radar detectability of a subsurface ocean on Europa, Icarus 134 (1998) 292-301.

RD[12] Picardi G. et al., Performance and surface scattering models for the Mars Advanced Radar for Subsurface and Ionosphere Sounding (MARSIS), Planetary and Space Science 52 (2004) 149-156.

RD[13] Ulaby F.T., Moore R.K. and Fung A.K., Microwave Remote Sensing, Artech House, 1982.

RD[14] Brown, G.S., The average impulse response of a rough surface and its applications. IEEE Transactions on Antennas and Propagation, Vol. 25, No. 1, January 1977.

RD[15] Picardi G. et al., MARSIS Design description, science analysis and performance, Internal Report, INFO-COM, 1999.

RD[16] Zarka P., "Les sursauts S de Jupiter", CNRS.

RD[17] Magnetic Fields of Planets, University College, London, http://www.es.ucl.ac.uk/research/planetaryweb/undergraduate/dom/magrev/magtoc.htm.

RD[18] Low frequency array (Radio Telescope), www.lofar.org.

RD[19] Microwave Devices and Radar, David Jenn, US Naval Postgraduate School, 20/7/03, http://www.dcjenn.com/EC4610/VolIV(v4.6).pdf.

RD[20] Numerical Electromagnetics Code (NEC), Lawrence Livermore Laboratories, 1977.

RD[21] Contract ESA/ESTEC 5562/83/NL – Avenant 5 – Evaluation de matériaux composites polymérisés par ionosation à l'environment spatial.

RD[22] Ojakangas, GW and Stevenson DJ (1989). Icarus 81, 220.

RD[23] Europa temperature data, www.johnstonsarchive.net/astro/europa.html.

RD[24] Spacecraft Thermal Control Design Data Handbook, Issue 1, ESA, November 1989, ESA PSS-03 108.

RD[25] Enabling Technology for NASA's Europa Orbiter Mission, NASA-JPL, Konefat E., Litty E., Voigt S., Wright D. American Astronautical Society AAS 01-001, 31/1-4/2/2001.

RD[26] Europa TRM Mission Analysis – The Science Phase, TN No. 34 issue 2, Michel Khan, ESOC, 7/6/04.

RD[27] ECSS-E-50-05A, Radio Frequency And Modulation Standard, published 24 January 2003.

RD[28] CCSDS 101.0-B-6. Telemetry Channel Coding Standard. Blue Book. Issue 6. October 2002.

RD[29] Europa Orbiter Preliminary Planetary Protection Requirements, Outer Planets Programme, NASA, April 1999.

RD[30] Appendix A of NPG 8020.12B, "Planetary Protection Provisions for Robotic Extraterrestrial Missions".

RD[31] ECSS-M-00-03A on Risk Management for Space Projects.

# 18 ACRONYMS

| | |
|---|---|
| ACS | Attitude Control Subsystem |
| AOCS | Attitude and Orbit Control Subsystem |
| ADC | Analogue to Digital Converter |
| ADPM | Antenna Deployment and Pointing Mechanism |
| AIT | Assembly Integration and Test |
| AIV | Assembly Integration and Verification |
| ASIC | Application Specific Integrated Circuit |
| BB | Bread Board |
| BCR | Battery Charge Regulator |
| BDR | Battery Discharge Regulator |
| BOL | Beginning of Life |
| CAD | Computer Aided Design |
| CATIA | Computer-graphics Aided Three dimensional Interactive Application |
| CCD | Charge Coupled Device |
| CCSDS | Consultative Committee for Space Data Systems |
| CDF | Concurrent Design Facility |
| CFRP | Carbon Fibre Reinforced Polymer |
| CMC | Ceramic Matrix Composite |
| CNR | Clutter Noise Ratio |
| CNRS | Centre Nationale de la Recherche Scientifique |
| CONSERT | COmet Nucleus Sounding Experiment by Radiowave Transmission |
| CTE | Coefficient of Thermal Expansion |
| CuBe2 | Copper Beryllium alloy |
| DAC | Digital Analogue Converter |
| DC | Direct Current |
| DDS | Direct Digital Synthesis |
| DEM | Digital Elevation Model |
| DMU | Digital Mock Up |
| DOF | Degree of Freedom |
| DPU | Data Processing Unit |
| EADS | European Aeronautic Defence and Space Company |
| EBB | Electrical Bread Board |
| ECSS | European Cooperation for Space Standardisation |
| EEM | Electrical Engineering Model |
| ELRR | Europa Low Resource Radar |
| EOI | Europa Orbit Insertion |
| EPC | Electrical Power Conditioner |
| EQM | Electrical Qualification Model |
| ESA | European Space Agency |
| ESOC | European Space Operations Centre |
| ESTEC | European Space Research and Technology Centre |
| EuGS | Europa Gamma Ray Spectrometer |
| EuLat | Europa Laser Altimeter |
| EuMAG | Europa Magnetometer |
| EuRad | Europa Radiometer |
| EuREM | Europa Radiation Environment Monitor |
| EuS-Cam | Europa Stereo Camera |
| EuVN-IMS | Europa Near Infrared Mapping Spectrometer |
| FEM | Finite Element Method |
| FEP | Fluoronated Ethylene Propylene (Perfluoroethylenepropylene) |

| | |
|---|---|
| FFT | Fast Fourier Transform |
| FOV | Field of View |
| FPGA | Field Programmable Gate Array |
| FRP | Fibre Reinforced Polymer |
| GaAs | Gallium Arsenide |
| GFRP | Glass Fibre Reinforced Polymer |
| GMSK | Gaussian Minimum Shift Keying |
| HDRM | Hold Down and Release Mechanism |
| HGA | High Gain Antenna |
| HICDS | Highly Integrated Control and Data System |
| HIPS | Highly Integrated Payload Suites |
| HK | House Keeping (data) |
| HPA | High Power Amplifier |
| HRG | Hemispherical Resonate Gyro |
| I/Q | in-phase/quadrature |
| IDA | Instrument Design Activity |
| IEEE | Institute of Electrical and Electronics Engineers |
| JEO | Jupiter Europa Orbiter |
| JME | Jovian Minisat Explorer |
| JMO | Jupiter Microsat Orbiters |
| JPL | Jet Propulsion Laboratory |
| JRS | Jovian Relay Spacecraft |
| LOFAR | Low Frequency Array |
| LNA | Low Noise Amplifier |
| MARSIS | Mars Advanced Radar for Subsurface and Ionospheric Sounding |
| MGA | Medium Gain Antenna |
| MOSFET | Metal Oxide Semiconductor Field Effect Transistor |
| MPPT | Maximum Power Point Tracker |
| NASA | National Aeronautics and Space Administration |
| NEC | Numerical Electromagnetics Code |
| NPG | NASA Policy Guidebook |
| NRCS | Normalised Radar Cross Section |
| OBC | On-Board Control |
| PDD | Payload Definition Document |
| PFM | Proto-Flight Model |
| PLL | Phase Lock Loop |
| PP | Planetary Protection |
| PRF | Pulse Repetition Frequency |
| PTM | Prototypen Technologien Systeme |
| QM | Qualification Model |
| RCS | Reaction Control System |
| RF | Radio Frequency |
| RI | Risk Index |
| RMS | Root Mean Square |
| RWL | Reaction Wheel |
| S/C | Spacecraft |
| S/W | Software |
| SA | Solar Array |
| SAA | Solar Aspect Angle |
| SAR | Synthetic Aperture Radar |
| SCI-A | Directorate of Science – Science Payload and Advanced Concepts Office |
| SCR | Signal-to-Clutter Ratio |
| SiC | Silicon Carbide |

| | |
|---|---|
| SMCS | Scalable Multi-channel Communication Subsystem |
| SNR | Signal-to-Noise Ratio |
| SPL/PM | Split Phase Level/Phase Modulation |
| SPM | Small Perturbation Model |
| SpW | SpaceWire |
| SQNR | Signal to Quantisation Noise Ratio |
| SRU | Stellar Reference Unit |
| SSMM | Solid State Mass Memory |
| SSPA | Solid State Power Amplifier |
| STM | Structural Model |
| STR | Star Tracker |
| TBC | To Be Confirmed |
| TBD | To Be Defined |
| TID | Total Ionising Dose |
| TM | Telemetry |
| TRS | Technology Reference Study |
| UHM | Ultra High Modulus |
| VGA | Variable Gain Amplifier |
| VHF | Very High Frequency |
| VLSI | Very Large Scale Integration |
| XO | Crystal Oscillator |